PLASTIC DEFORMATION AT MODERATE TEMPERATURES OF 6XXX-SERIES ALUMINIUM ALLOYS.

by

Knut Iver Aastorp

A thesis submitted to
The Norwegian University of Science and Technology (NTNU)
in partial fulfilment of the requirements for the degree of

Doktor Ingeniør

Trondheim
February 2002

URN:NBN:no-2108

URN:NBN:no-2108

ACKNOWLEDGEMENTS

This work has been carried out at the Norwegian University of Science and Technology, Department of Materials Technology and Electrochemistry. Professor Nils Ryum has been my supervisor since the start in January 1997. I gratefully acknowledge his advice, encouragement and interest in my work!

I also wish to thank the members of the steering committee. They have all contributed with interesting discussions and valuable guidance. Dr. Ola Jensrud and Dr. Anders Søreng at Raufoss Technology are also responsible for the financial support. From SINTEF (The Foundation for Scientific and Industrial research at the Norwegian University of Science and Technology), Dr. Otto Lohne and Dr. Ketill Pedersen have participated. As Dr. Ketill Pedersen's projects have been closely related to my work, I would like to emphasize his encouragement and contributions!

My dear wife Grete is the one person who should be given special attention in this chapter! With no offence to the other people mentioned on this page, she has never quit supporting me during my effort to fulfill my work! Her encouragement, applied pressure(..), patience, support, re-heated dinners and babysitting are highly appreciated!!

- *Your effort is inestimable –Thanks a lot, dear !!!* ♡

Moreover, special thanks should be given to Mr. Pål Ulseth (SINTEF) and Mr. Tore Jørgensen (NTNU) for all their technical help, Ms. Ingrid Gamst Page and Mr. Harald Gether for fruitful conversations, my room-mate Dr. Arve Johansen, Dr. Øyvind Frigaard, Dr. Børge Forbord, Dr. Jo Fenstad, Mr. Bjarne Salberg, Mr. Shahriar Abtahi, Dr. Tanja Pettersen, Dr. Bjørn Rønning, Dr. Sverre Gulbrandsen-Dahl, Professor Jarle Hjelen and Dr. Odd Lauritzen for interesting discussions and support.

Furthermore, thanks to all the kind and helpful people at Raufoss Technology ASA, NTNU, SINTEF, and finally to my colleagues at CorrOcean ASA who have been patient and helpful during the last stage of this work.

Trondheim, 06.02.2002
Knut Iver Aastorp

Torodd and Elise, - Daddy is coming home! J

URN:NBN:no-2108

TABLE OF CONTENTS

URN:NBN:no-2108

ABSTRACT

The present work has been carried out in order to investigate Al-Mg-Si alloys that are deformed at moderate temperatures. These temperatures are in the range between 200°C and 300°C. Also some experiments are performed at room temperature. Two deformation modes have been applied in the experiments: Material deformation by compression testing and by forward extrusion.

The investigated alloys are AA6063, AA6082 and an alloy that is named ''Alloy R'' in this work. The latter alloy is the industrial alloy AA6082 without the Mn-addition (0.56wt%Mn in the AA6082). The ''R'' denotes the recrystallized microstructure in the material after hot forming operations.

The investigations show the effect of changing the temperature in the given temperature interval on the stress-strain relationship for each alloy. From the compression testing, it is found that none of the alloys AA6063 or Alloy ''R'' reaches a steady state condition as true strain approaches 0.8 for deformation temperatures between 200°C and 250°C. At compression testing performed at 300°C, the alloy ''R'' reaches a steady state condition at a true strain equal to 0.4.

As true stress-true strain relationship has been investigated for the ''Alloy R'' and the AA6063 at comparable deformation parameters, it is shown that the alloy ''R'', with the highest Si-content, requires the highest true stress for a given true strain value (AA6063: 0.45wt%Si, Alloy ''R'': 0.87wt%Si).

From the compression testing, the effect of Mn on the material properties in the AA6082-alloy has been determined. For the Alloy ''R'' and the AA6082, the true stress reaches the same value after a certain amount of deformation. As deformation temperature increases, this common value of true stress corresponds to a decrease in true strain.

The AA6082 and the Alloy ''R'' are also compared in experiments performed in forward extrusion. One observes that for the same deformation temperature and at identical die diameters, the ram force is identical. It is worth noticing that these alloys did not show the same relationship during the compression testing at low values of true strain (<0.8). On a microscopic scale, one concludes that Mn has no significant effect on the stress- strain

URN:NBN:no-2108

relationship for the applied deformation parameters in the forward extrusion equipment.

Hardness measurements indicate that the age hardening potential in the extruded test specimen decreases as the deformation temperature increases. The hardness data is similar for both the AA6082 and the Alloy R, thus indicating that the Mn content has no significant effect on the strength of the material.

The deformed material has been annealed in order to investigate the recrystallization process in the AA6082 and the Alloy ''R''. The recrystallized grain size in the Alloy ''R'' is significant larger than in the AA6082 at comparable deformation parameters after annealing at 530°C for 15 minutes. This result is due to the effect of Mn-containing dispersoids in the AA6082. The recrystallized grain size in the Alloy ''R'' seems to be unaffected by the deformation temperature after annealing for 15 minutes. The observation of the AA6082 is quite different. A small increase in grain size is observed for both reduction ratios as the deformation temperature is elevated from 20°C to 200°C and further to 250°C. At extrusion temperatures of 300°C the recrystallized grains are significant larger. Annealing experiments performed at 430°C on the AA6082 indicates that a change in the deformation temperature from 200°C to 250°C does not affect the amount of stored energy in the material significantly.

The Forge2 programme has been used to perform numeric simulations of the forward extrusion experiments. From this the temperature distribution, strain rate variation and true strain development in the test piece has been investigated. As the simulated true strain values are compared to the grain size in the annealed material, the recrystallized grain size is related to the amount of stored energy in the material in a very convincing way. It is also shown that the recrystallized grain diameter is related to the amount stored energy as the grain diameter is investigated in the radial and the extrusion direction separately.

URN:NBN:no-2108

1 INTRODUCTION

The background for this project is the search for extended knowledge about forming of age hardenable aluminium alloys at moderate temperatures. As cold forging of complex parts for the car industry is both time consuming and expensive, the originator and financiers of this thesis wants to see if it we can combine benefits from both cold and hot forming into the same process by doing the forming at moderate temperatures.

What makes the cold forging process especially time-consuming is the need for intermediate soft annealing and surface treatment (lubrication) during production of parts of complex geometry. As can be seen from *Figure 1.1*, the main difference between the two deformation methods is removal of

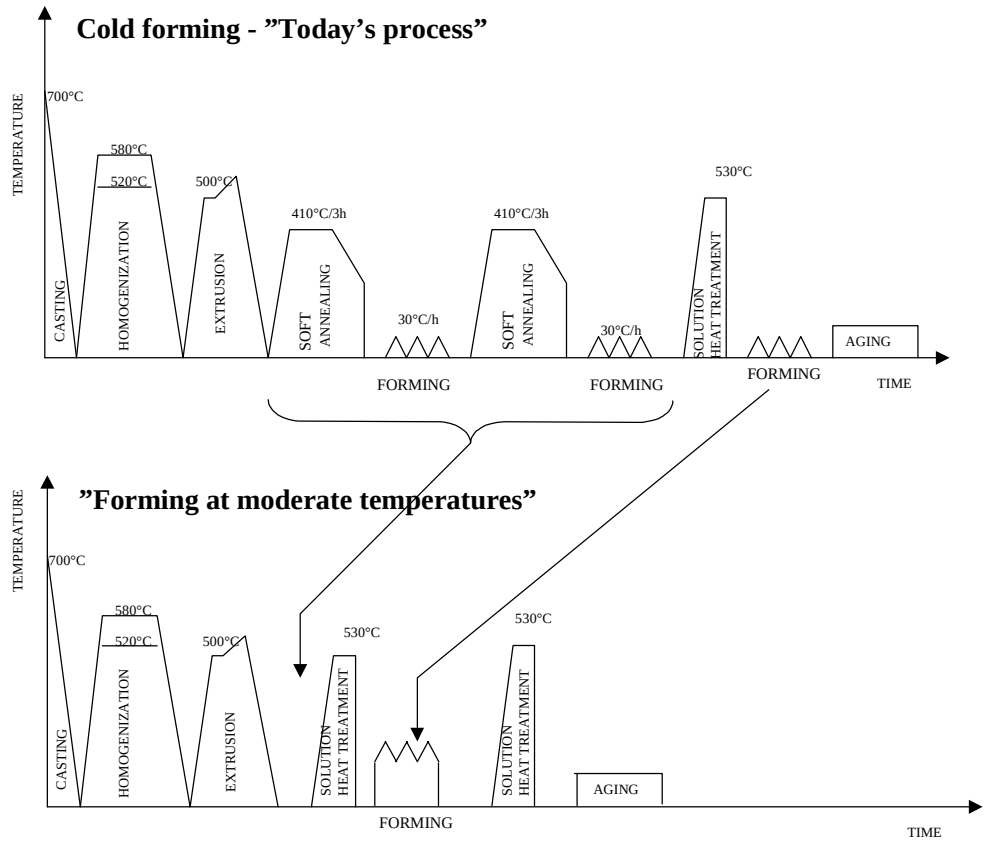

Figure 1.1 *Time saving benefits from forming at moderate temperatures.*

heat treatment and lubrication in the forming process. When temperature is increased during the deformation, yield stress is lowered and formability is increased. However, hardening mechanisms in age hardenable aluminium alloys are complicated, as the improved mechanical properties are a result from the combination of precipitation hardening and deformation hardening.

The definition of moderate temperatures in the work carried out in this project is 200°C to 300°C. This temperature interval is chosen due to preliminary results from a SINTEF-project that had been going on for a short while on subjects closely related to the topics covered here. SINTEF's research indicated that forming of AA6082 in the W-temper at approximately 250°C demanded the same force as cold forging of material in O-temper. There were also results indicating that the mechanical properties of the material deformed at 250°C would be in the same range as mechanical properties in the material that was cold formed. However, experimental work is also carried out at room temperature. These tests will act as a reference to changes that take place in the microstructure at low temperatures.

This thesis covers several metallurgical aspects connected to the forming process at moderate temperatures. Even though it is divided into three parts, these parts are closely linked to each other. The configuration of chapter 3 – ‘‘Results’’, might be summarised as follows: In Part I the material is deformed and mechanical properties are determined. From these tests, the microstructure in the material is investigated in Part II, and the same material is recrystallized in part III. A combination of the observations from Part I and Part II gives the basis for the understanding of recrystallization behaviour in the material as a function of variations in deformation parameters at moderate temperatures. Numeric simulations in Forge 2 are meant to give indications on how the variation in deformation parameters influenced on the material during forming. An illustration of how the work in this thesis is carried out is also given in *Figure 1.2*.

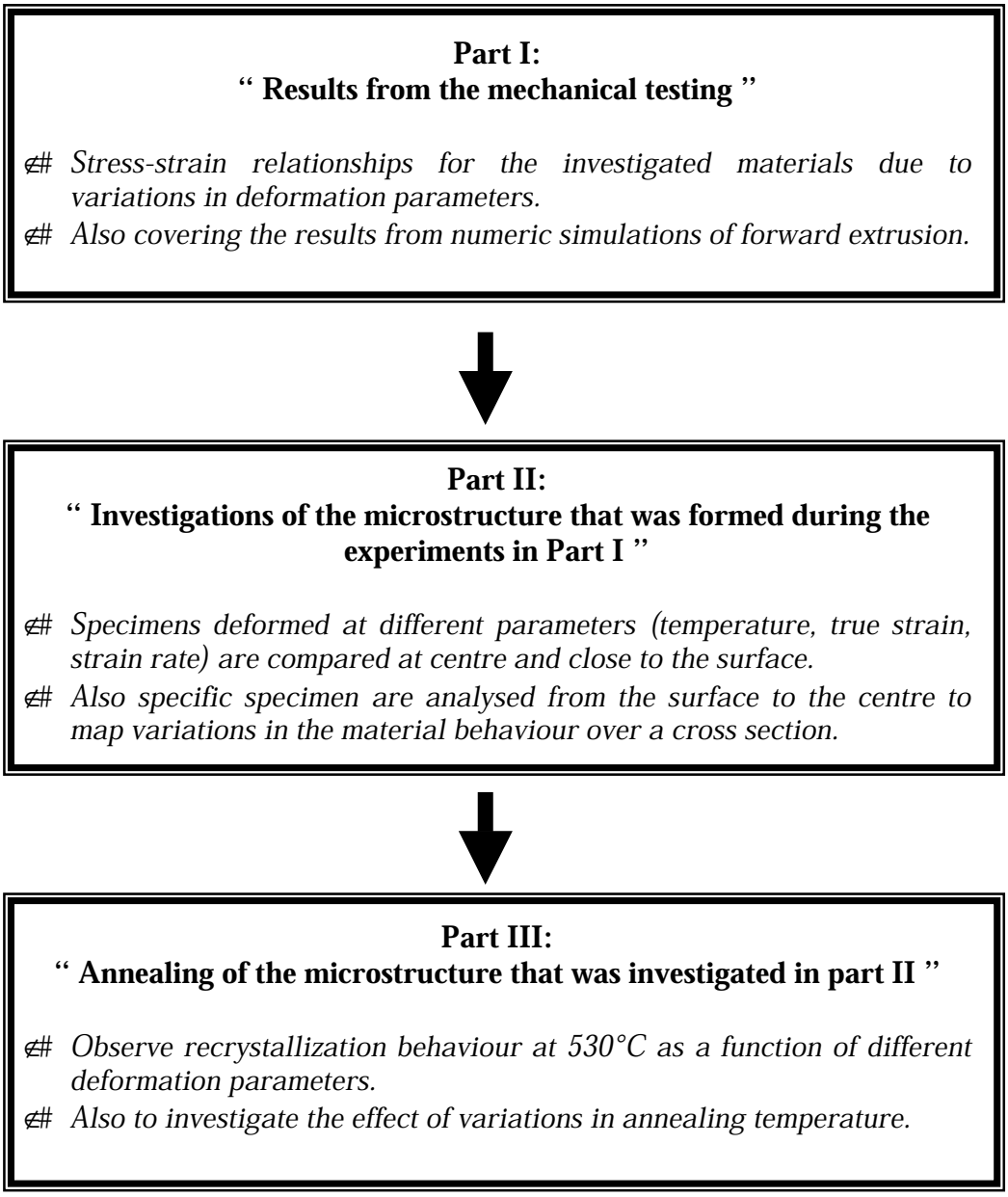

Figure 1.2 *The configuration of the thesis.*

URN:NBN:no-2108

2. Theoretical background

This chapter will introduce well-known theories that can be related to the experimental work in the thesis. Some references to investigations published during the last years are included in an attempt to establish an updated knowledge on the chosen subjects. The underlying chapters will guide the reader through different forming operations at different temperatures in the range from cold to hot deformation and describe the changes that take place in the microstructure during the forming process. Further, the influence and nature of precipitates in the 6xxx-series alloys and aspects concerning recrystallization and texture are described. Finally, an introduction to the construction and theories of the numeric simulation programme Forge2D is given.

As the definition of deformation temperature is essential in this work, it is important to be aware of the fact that both the term “elevated temperature” and the term “moderate temperature” is used to describe the same temperature interval. The experimental work is mainly carried out in the temperature interval from 200°C to 300°C, and therefore temperatures in this region is most often considered when temperatures are described as “elevated temperatures” or “moderate temperatures”.

Temper designations that are used to describe the mechanical and microstructural characteristics of the material are “O”, “W” and T4:

O : Annealed, recrystallized. The softest temper of wrought alloy products.

W: The unstable condition following solution heat treatment.

T4: Solution heat treated and naturally aged to a substantially stable condition. No cold working after heat treatment.
Metals Handbook (1961)

2.1 Cold forming:

Plastic forming by cold forging is a production process where high strength aluminium alloys can be produced with close tolerances. It might have

several additional advantages including simplified tooling and improved concentricity. The process is therefore particularly suitable for parts with narrow geometrical tolerances, smooth surface finish, and for near net shape products. Often, combinations of forward and backward forging make the process route in order to create products of complex geometry.

When parts for advanced technological use are produced, the need of several consecutive forming operations becomes of importance. Due to strain hardening in the material, the need of soft annealing between the forming operations is required. Also lubrication is very important in cold forging. Sticking between the tool and the work piece must be avoided. As for the soft annealing, the lubrication process must be performed several times to secure no friction at every production stages. This might lead to a time-consuming and expensive production route of the part. A typical cold forging process is shown in ***Figure 2.1.1***.

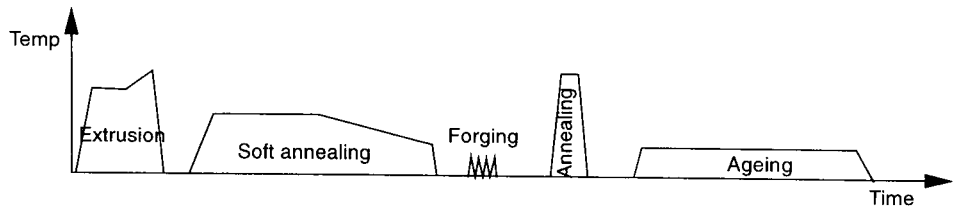

Figure 2.1.1 *A sketch of a cold forging process of a material in O-temper. Jensrud, O., Pedersen, K (1998)*

In cold work production, the work piece is inserted into the container at room temperature. However, during the deformation process, the temperature can increase to above 100°C as a result of local geometrical and frictional conditions. This means that what is called cold forging, actual is forging with an increase in temperature during the forming process. Anyway, due to the subsequent solution heat treatment, this increase in temperature is not considered to have influence on the mechanical properties of the final product.

URN:NBN:no-2108

2.2 Warm forming (forming at moderate temperatures)

In the past years, several papers have been published on the cold forming process and the hot forming process, or even at combinations of hot and cold forming in the production of steel parts. Anyway, increasing attention has been given to aluminium alloys, and the opportunity to perform the forming operations at moderate (warm) temperatures. The main motivation for this is to reduce the number of heat treatment steps, as soft annealing is both time-consuming and expensive. Jensrud, and Pedersen (1998) has investigated some aspects concerning forming of the AA6082 at moderate temperatures. *Figure 2.2.1* shows the true stress relationship to increasing true strain in a compression test at different deformation temperatures. One observation is that when increasing the deformation temperature of AA6082 in the W-temper from 225°C and 300°C, a reduction in the true stress of 100 MPa is obtained. They also point out that deformation of material in the W temper at 250°C, gives approximately the same stress strain relationship as deformation of the soft annealed material (O-temper) at room temperature.

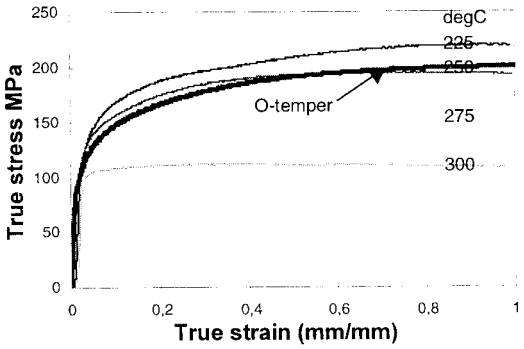

Figure 2.2.1 *True stress-strain curves for compression of AA6082 at elevated temperatures. The bold line is O-temper deformed at room temperature. Jensrud, and Pedersen (1998)*

URN:NBN:no-2108

Also backward forging tests performed by Jensrud and Pedersen (1998) show the same tendency as shown in *Figure 2.2.1*. In this test, the material forged at moderate temperatures even show a reduction in forging load. Also the peak force from cold forging is almost removed by warm forging. These results are shown in *Figure 2.2.2*.

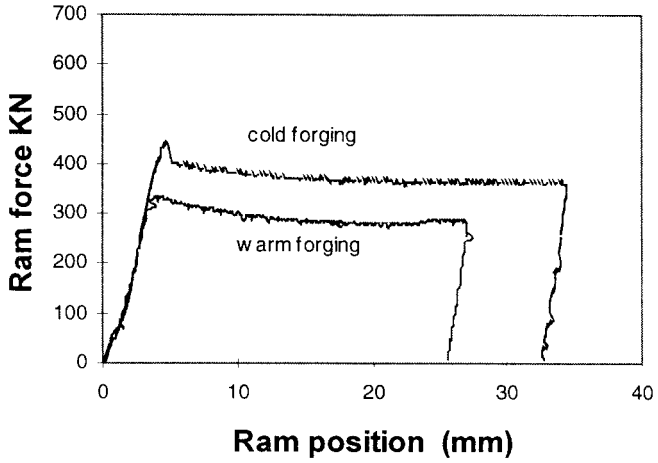

Figure 2.2.2 *Force vs. ram position for backward extrusion of tubes with an outer diameter of 29 mm and wall thickness of 1 mm. Cold forging of material in the O-temper, warm forging of material in the W-temper. Jensrud and Pedersen (1998)*

It is also shown that by using a forging temperature of 250°C, a reduction in the forging loads is obtained without any reduction in hardness of the final product. The maximum hardness is the same at low strains as at moderately higher strains, but at strains of approximately 1.0, there is negligible effect from age hardening at maximum hardness as shown in *Figure 2.2.3*.

URN:NBN:no-2108

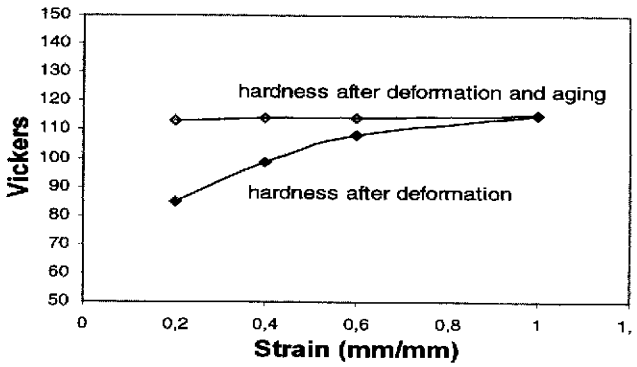

Figure 2.2.3 *The Vickers hardness versus strain after deformation and subsequent ageing at 225°C for30 minutes. Jensrud and Pedersen (1998)*

2.3 Hot forming (extrusion).

The conventional temperature of transition from cold to hot forming is approximately $0.5T_m$. In *Figure 2.3.1* the effects of work hardening and dynamic recovery on the form of the high temperature stress-strain curve are shown.

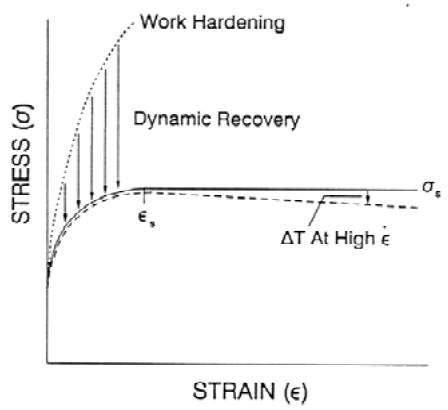

Figure 2.3.1 ***Schematic diagram showing t****he effects of work hardening and dynamic recovery on the form of the high temperature stress strain curve. Sellars, C.M. (1991)*

The term hot extrusion is used to describe a forming operation in which a billet is pushed through a die at elevated temperatures. The main advantage of this process compared to e.g. rolling or bar drawing, is that practically any cross-sectional shape can be produced. The most important process parameter is the deformation temperature. This temperature is normally above the recrystallization temperature of the material. The upper temperature limit is usually the solidus temperature of the alloy. Other important parameters are the speed of the press v, the reduction ration of the cross-sectional areas of the billet and the product, R (equation 2-1). This ratio can also be expressed in terms of the true strain (equation 2-2).

$$R = \left(\frac{Billet \cdot cross \cdot \sec tional \cdot area}{\Pr oduct \cdot cross \cdot \sec tional \cdot area} \right) = \left(\frac{A_0}{A_1} \right) \qquad \textbf{(Equation 2-1)}$$

$$\varepsilon = \ln\left(\frac{A_0}{A_1} \right) = \ln\left(\frac{r_0^{\,2}}{r_1^{\,2}} \right) \qquad \textbf{(Equation 2-2)}$$

Classification of the hot extrusion processes is similar to the classification of the cold extrusion process. This is based on the material flow direction compared to the press direction, and the shape of the product. Typical descriptions are solid/hollow extrusion (direct extrusion of solid/hollow sections), solid/hollow backward extrusion and solid/hollow side extrusion. Lange (1985).

Lang and Castle have investigated the influence of copper, manganese and chromium additions on the extrudability of AlMgSi-alloys. Additions of both Cu and Mn increased the initial load during extrusion, while additions of Cr had a more significant effect in the same way. However, Cr additions increased the frictional load and lead to a poorer surface finish even at low extrusion speed, while alloys with Cu- and Mn addition had a good surface finish at high extrusion temperatures. The experiments also showed that alloying with 0.11wt% Mn to AA6063, gave a recrystallized structure after extrusion, but as this amount was increased to 0.30wt%, the Mn-containing dispersoids prevented recrystallization effectively. The same effect was found when adding the same amounts of Cr to the alloy. A non-recrystallized microstructure after extrusion was observed in the alloy after additions of 0.30wt% Cr.

URN:NBN:no-2108

Latkowski and Stec (1984) investigated the effect of extrusion temperature and manganese content on structure and mechanical properties of the AlMgSiMn alloy after precipitation hardening. It was found that the smaller subgrain size is connected with an increase in the manganese content. When extruding at increasing temperatures, the subgrain size increased too. An increase in the extrusion temperature in all Mn-containing alloys resulted in a decrease in the yield strength. Homogenisation causes a decrease in all values mentioned above. The lower the rate of deformation is, the larger subgrains are established as a result of dynamic recovery. Also the yield strength is decreased. Additions that form dispersoids (Al_6Mn, Al_3Cr etc) increase the temperature for recrystallization, and promote the formation of unrecrystallized structure. The dispersoids also retains the unrecrystallized structure during subsequent heat treatment. The velocity of nucleation and grain growth is delayed by the small dispersoids, but when the size exceeds approximately 300Å, they were observed to accelerate recrystallization. Particles of the second phase prevent grain boundary from moving. During homogenisation, the precipitates grow larger, and the distance between them increases. Also the dispersoids move into the subgrains thus high dislocation density is observed inside grains after homogenisation. Extrusion tests that were performed by Latkowski and Stec (1984), show that the addition of manganese increased the strength after heat treatment over a wide range of extrusion temperatures. Homogenisation reduces this extrusion temperature interval.

2.4 The formation of deformed microstructure.

During deformation, a lot of changes that affect the mechanical properties of the material take place. During the next chapters, these changes will be explained with basis in dislocation theory. Recovery reactions and subgrain formation are essential topics.

2.4.1 Dislocations in aluminium

There is little intrinsic resistance to dislocation glide in aluminium, and it would be very soft in the absence of defects such as other dislocations, solutes, second-phase particles and grain boundaries.
Aluminium has high stacking fault energy, and dislocations are not significantly dissociated into partials. Thus dislocations are able to relatively

easy move out of their slip-planes by cross slip and climb even at low deformation temperatures. During deformation, the dislocation density ρ increases. Relations between the velocity of dislocations (v), the dislocation density (ρ) and the strain rate ($\dot{\varepsilon}$), are given in equation 2-3. "b" is the Burgers vector.

$$\dot{\varepsilon} = \rho \cdot b \cdot v \qquad \textbf{(Equation 2-3)}$$

Further, the relationship by the distance moved by dislocations (L) and the strain rate ($\dot{\varepsilon}$), is given in equation 2-4.

$$\dot{\varepsilon} = \rho \cdot b \cdot L \qquad \textbf{(Equation 2-4)}$$

2.4.2 Recovery

Forces that act between dislocations induced recovery. These forces are inversely proportional to the distance between dislocations. The limiting factor in recovery is usually climb of edge dislocations, as cross-slip is usually easier than climbing. The dislocation substructure is determined by interactions between dislocations, e.g. pile-up, annihilation, formation of tilt boundary and twist boundary. Also solute atoms may affect the behaviour of dislocations in Al. Mg segregate to dislocations and pin them. This has significant effect on the development of texture and microstructure, as the recovery process becomes more difficult. Temperature influences the rate of recovery (R) through its effect on climb rates as shown in equation 2-5.

$$R = K \cdot \exp(-\frac{Q}{k \cdot T}) \qquad \textbf{(Equation 2-5)}$$

Q is typically equivalent to the activation energy for self-diffusion in Al (140kJ/mole). K and k are constants and T is temperature in K.

2.4.3 Softening by dynamic recovery only

In aluminium and its alloys, dynamic recovery is typical. From the dynamic recovery reactions, the stress strain curve gets it typical shape as shown in *Figure 2.4.*. As can be seen from this figure, the level of the curve is sensitive to the strain rate ($\dot{\varepsilon}$). At low strain rates, dynamic recovery is

more efficient. As dynamic recovery is a thermally activated process, higher temperature will lower the curve in *Figure 2.4.1*.

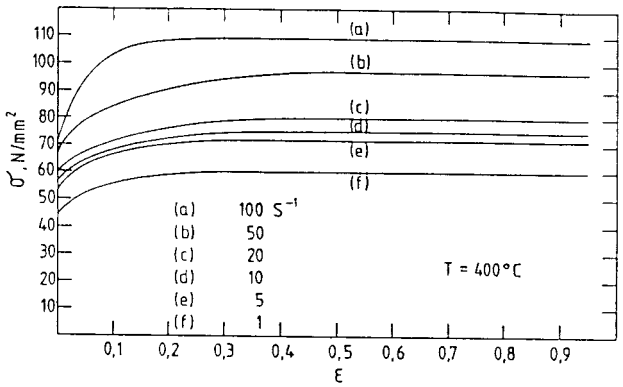

Figure 2.4.1 *Stress strain curves for commercial Al-1%Mg at 400°C. Puchi et al. (1988)*

For alloys where there is no transformation reaction in the investigated temperature interval, the Zener-Hollomon parameter (Z) describes the effect of $\dot{\varepsilon}$ and T on stress and microstructure. In equation 2-6, the definition of the Zener-Hollomon parameter is given, (Sellar (1991))

$$Z = \dot{\varepsilon} \cdot \exp(\frac{Q_{def}}{RT}) \qquad \textbf{(Equation 2-6)}$$

2.4.4 Subgrain formation

The stored energy (E_s) in the microstructure is the driving force for recovery. This stored energy, are expressed as a function of the dislocation density as shown in equation 2-7.

$$E_s = \rho \cdot G \cdot b^2 \qquad \textbf{(Equation 2-7)}$$

If dislocations are arranged in ordered network, their stored energy is lowered. Deformation at higher temperature and at higher strain leads to the formation of subgrain structure with well-defined walls. As strain increases, the subgrain size decreases. The subgrain size reaches a minimum at a true strain of approximately 3-4. This minimum subgrain size depends upon the

alloy composition. For instance, the minimum subgrain size in high purity Al is approximately twice the size of the minimum subgrain size in Al-1%Mn or commercial purity aluminium (Humphreys, 1999). The average boundary misorientations between subgrains, seems to increase with increasing strain, but it appears to saturate at a strain level of about 1 (Furu et al, 1995).

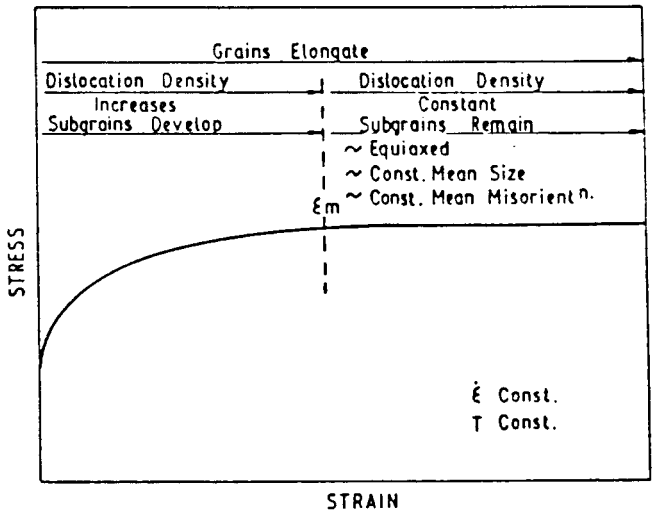

Figure 2.4.2 *Summary of the dynamic micro structural changes in relation to the stress strain curve at constant Z (Sellars, 1986).*

Because the subgrain size depends on the flow stress, it varies with temperature, strain and strain rate, Nes, Dons and Ryum (1982) also pointed out a relationship between the strength of the alloy, the subgrain size and the mean misorientation ɗ between neighbouring subgrains. They found that the flow stress in Al and Al-alloys varies proportional to $(ɗ/d)^{1/2}$. In equation 2-8, the relationship between the flow stress and subgrain size (d) is given

$$\sigma = \sigma_0 + kGBd^{-m} \qquad \textbf{(Equation 2-8)}$$

σ is the flow stress, σ_0 is the frictional stress, k, G and B are constants, m is the strain rate sensitivity.

URN:NBN:no-2108

Effect of second phase particles:
Very small particles, e.g. coherent precipitates, will be sheared by dislocations during plastic deformation. Larger particles (<0.5µm) will form prismatic loops, -or geometrically necessary dislocations. The density of these may be reduced by dynamic recovery. Large, non-deforming particles (>0.5µm) may be surrounded by a deformation zone with the highest misorientation closest to the particle.

2.5 Precipitation reactions in the 6xxx-series aluminium alloys.

Many investigations have been performed in order to establish the precipitation sequence in the 6xxx series aluminium alloys. Also the determination and characteristics of every phase has been given thoroughly studies. In *Figure 2.5.1* the Pseudobinary equilibrium diagram for Al-Mg_2Si is shown.

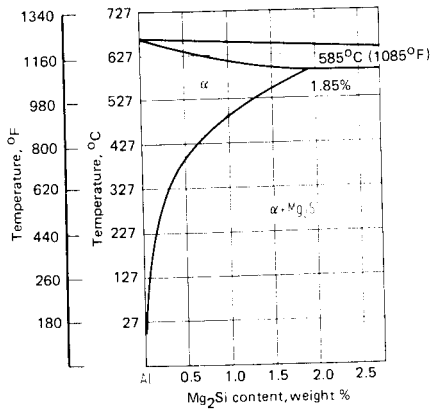

Figure 2.5.1 *Pseudobinary equlibrium diagram for Al-Mg_2Si. Altenpohl, D. (1965)*

In *Figure 2.5.2*, the temperature range "1" is the preferred range for Mg_2Si precipitation and must be traversed rapidly during cooling of the extrusion. Mg_2Si precipitation is suppressed during cooling if the cooling curves are to the left of the solid parabolic curve. The age hardening process are traced by 2 to 5: Coarse Mg_2Si precipitates (2), Tendency for increasing strength (3), Fine Mg_2Si precipitates (4), no ageing (5) and 100% age hardening (6).

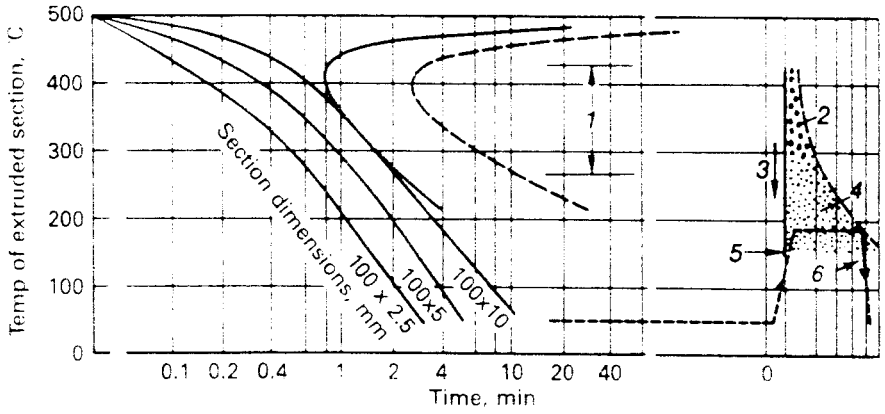

Figure 2.5.2 *Time-precipitation diagram for AlMgSi0.5, Laue (1981)*

2.5.1 Small particles (Mn-dispersoids)

Lodgaard and Ryum (2000) investigated the precipitation of dispersoids containing Mn and/or Cr in Al-Mg-Si Alloys. They found that during heating from 20°C to 580°C at a heat rate of 3K/min, an intermetallic phase, referred to as the "u-phase" nucleated on the ß'-phase needles. The phase was rich in Mn and/or Cr, and by further increase in heating temperature (above 400°C), dispersoids containing Mn and Mn+Cr nucleated heterogeneously on the "u-phase" precipitates before these precipitates dissolved.

Summary of existing knowledge on the effect of Mn, Cr and Zr additions on recrystallization after extrusion in AlMgSi-alloys:
Controlled additions of small amounts of transition elements such as Mn, Cr, and Zr are used extensively to modify the microstructure and properties of aluminium alloys. The tendency of these elements to be present in supersaturated solution after rapidly solidification is of great importance and leads to precipitation of inter-metallic compounds (dispersoids) during homogenisation.

The dispersoids will have an inhibiting effect on recrystallization as long as the diameter is between approximately 5µm to 200µm, and the inter-particle spacing does not exceed 1µm. As AA6082 is homogenised at 580°C, the

URN:NBN:no-2108

dispersoids only prevents recrystallization moderately good. Therefore, after extrusion, one often observes that the outer layer of the extruded product consists of a coarse grain structure. If cooling is too slow after extrusion, another unwanted effect might occur. Then the dispersoids may act as nucleation sites for non-hardenable Mg_2Si particles. This is referred to as quench sensitivity. The amount of Mn is usually kept between 0.1% and 1.0%. Increasing the Mn content to above 0.5% will increase the size of the dispersoids but the amount will probably be less than doubled. Tundal et al. (1994). The purpose of homogenisation is to level out segregations of Si and Mg and to spheroidize the primary particles and to form dispersoids. Homogenisation temperature is a compromise of spheroidizing at higher temperatures to decrease deformation resistance and to precipitate dispersoids in order to prevent recrystallization at lover homogenisation temperature, Lohne and Dons (1983).
Reiso (1986) has shown that additions of Mn might have a significant influence on the deformation resistance and the maximum extrusion speed.
The break through pressure, which may be regarded as the deformation resistance, was measured for three alloys with Mn content from 0wt% to 0.52%. Three different homogenisation temperatures were chosen. Regarding the breakthrough pressure, these investigations showed that when homogenising at 580°C the Mn content did not have a significant effect. At lower homogenisation temperatures the influence of the Mn content increased as the pressure rose. Also when homogenising at 580°C the Mn content did not affect the maximum extrusion speed. When the homogenisation temperature was lowered, the Mn content lead to a significant decrease in extrusion speed. These results indicate that the extrudability of a Mn-bearing alloy is mainly dependent on the dispersoid density and not on the Mn-content itself.

Ørsund (1991) has investigated the effect of time before cooling after extrusion on recrystallization. This work shows that as time before cooling increases, the amount of stored energy decreases. The surface zone that often consists of large recrystallized grains will then extend deeper into the material. Also the recrystallized grain structure will be coarser.

Tundal et al. (1994) have pointed out some conclusions regarding the effect of the Mn content on a recrystallized microstructure. If an alloy containing Mn recrystallizes, the recrystallized grain structure will be coarser than in an alloy without Mn since the dispersoids only will lead few nuclei to grow.

The mechanical properties in a recrystallized alloy may thus not be better than in a recrystallized alloy without Mn-dispersoids.

Effect of dispersoids on the recrystallization behaviour of Al-Mg-Si alloys:
Increasing content of Mn and Cr prevents recrystallization in Al-Mg-Mn alloys. However, when increasing the deformation temperature and the strain rate, recrystallization is promoted. (Hulley and Lorimer 1992).

Investigations performed on the AA6060 deformed in torsion testing and plain strain compression shows that with increasing strain, the density of nucleation sites increases and hence the grain size decreases (Pettersen, Vatne, and Nes (1999).

Investigations performed by Ayres (1979), show that the warm ductility of aluminium (25-250°C) is increased by magnesium additions up to 6wt%. The ductility was characterised by tensile elongation at quasi-static strain rates. This result is in contrasts with other investigations that are performed at significant higher temperatures and strain rates. Also alloying Al with magnesium appears to increase the dynamic recovery occurring at strain rates 10^{-4} to 10^{-1} and deformation temperature up to 250°C.

2.5.2 Larger particles, precipitation series.

If the solubility of an alloying element increases with increasing temperature, the alloy might undergo a precipitation reaction. Annealing above the solvus line, which makes the alloying elements distribute into solid solution, is referred to as the homogenisation heat treatment. As temperature is reduced below the solvus line, one expects the ß-phase to precipitate out. However, rapid cooling to a sufficient low temperature might suppress precipitation, and alloying elements are present in supersaturated condition in the crystal structure. When annealing this alloy at a higher temperature, one often observes the formation of a so-called meta-stable phase, which leads to a strengthening of the material. The AA6082 is referred to as unstable at room temperature, which means that alloying elements form clusters at room temperature. Marioara (2001). This natural ageing in the AA6082 after solution treatment at 530°C for 10 minutes is shown in *Figure 2.5.3*.

URN:NBN:no-2108

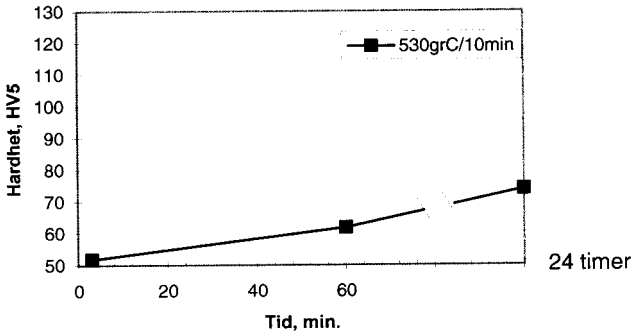

Figure 2.5.3 *AA6082, Natural ageing. Pedersen and Ulseth, (1997)*

Al-1.2% Mg_2Si ages noticeably at room temperature. After only a few hours at room temperature, an increase in strength greater than 10% has been observed. Jacobs, M.H. (1999).
Precipitate transformations that occur when increasing the annealing temperature of the super-saturated alloy from room temperature to the solvus temperature are referred to as the precipitation sequence. Marioara, Andersen and Høier (2001) found that below 85°C no metastable phase is present, but the alloying elements formed atomic clusters. Annealing above 125°C leads to the transformation of GP zones into ß''. ß'' is the metastable phase main responsible for the precipitating hardening effect in the AA6082. At temperatures above 200°, nucleation of the ß' phase is predominately taking place on the ß'' phase, as this phase dissolves. The density of the ß‘ phase is less than the density of the ß'' phase, and it coarsens quickly with annealing time. At temperatures above 300°C, the ß' phase dissolves quickly. The observed Mg-Si containing phases in the AA6082 by Marioara et al (2001) is shown in *Figure 2.5.4*.

Phase	Formula	Unit-cell	Morphology / Typical size
GP	Si/Mg >1	Unknown	Spherical / 1-2 nm
β''	Mg_5Si_6	Monoclinic C2/m [1] a = 1.516 nm, b = 0.405 nm, c = 0.684 nm, β ~ 105.3º	Needles / 4 x 4 x 35 nm^3
β'	$Mg_{1.7}Si$	Hexagonal [1,2,5,6] a = 0.705 nm, c = 0.405 nm	Ribbons / Several μm long
β	Mg_2Si	fcc (CaF_2-type) [1,2,7,8] a = 0.639 nm	Plates or cubes / Up to 10-20 μm diameter
B'	Mg/Si~1	Hexagonal [2,3,9] a = 1.03 nm, c = 0.405 nm	Ribbons / Probably up to 1 μm
Si		fcc (diamond type) a = 0.543 nm	Thin plates / Up to 10-20 μm diameter

Figure 2.5.4 *The observed Mg-Si containing phases in the AA6082.*
Marioara, C.D., Andersen, S.J. and Høier, R. (2001)

Lorimer (1976), points out that the pseudo-binary aluminium-Mg_2Si alloy system has a eutectic at 595°C and a maximum solubility of Mg_2Si of 1.85wt%. The precipitation sequence is denoted by Lorimer as:

Supersaturated → GP zones → ß' → ß (Mg_2Si)

The GP zones have the same crystal structure as the matrix (fcc). These are needle-shaped zones along the <110>ŭ. The ß' phase is a rod-shaped precipitate which lies along the <110> of the matrix. The ß phase is found to be formed as platelets on the matrix {100}-planes with the orientation relationship with the matrix of (110) Mg_2Si || (100)ŭ. This is in accordance with the investigations performed by Marioara et al. (2001), except for a more complex sequence of phases given by Marioara et al (2001):

URN:NBN:no-2108

Supersaturated → clusters/co clusters of Mn and Si→ GP zones→ ß''→ ß' → ß (stable)

The difference is partly explained by the fact that some authors use the term GP1 zones for the GP zones, and GP2 zones for the ß''.

Marioara, Andersen, Jansen and Zandbergen (2001) has investigated the influence of temperature and storage time at 20°C on nucleation of ß''-phase in a 6082 Al-Mg-Si-alloy. Fully coherent GP1 zones are formed from clusters created as a result of natural ageing. However, increasing holding time at room temperature reduces the number of nucleation sites for the ß'' particle significantly.

2.6 Strain hardening

This chapter summarises some basic theories of strain theories (Dieter, 1988). It gives the basis for evaluation of stress-strain relationships in the experiments performed in this thesis.

The simple power law relationship is:

$$\sigma = K\varepsilon^n \qquad \textbf{(Equation 2-9)}$$

Where n is the strain hardening exponent and K is the strength coefficient, describes the flow curve of many metals in the region of uniform plastic deformation. The strain-hardening exponent, n, is zero for perfectly plastic solids, and 1.0 for elastic solid. Most metals have n in the range of 0.1 to 0.5. The definition of n is given in equation 2-10:

$$n = \frac{d(\log\sigma)}{d(\log\varepsilon)} = \frac{d(\ln\sigma)}{d(\ln\varepsilon)} = \frac{\varepsilon}{\sigma}\frac{d\sigma}{d\varepsilon} \qquad \textbf{(Equation 2-10)}$$

This leads to the definition of the rate of strain hardening:

$$\frac{d\sigma}{d\varepsilon} = n\frac{\sigma}{\varepsilon} \qquad \textbf{(Equation 2-11)}$$

The definition of the true strain rate is given by equation 2-12:

$$\dot{\varepsilon} = \frac{d\varepsilon}{dt} = \frac{d\left[\ln(L/L_0)\right]}{dt} = \frac{1}{L}\frac{dL}{dt} = \frac{v}{L} \qquad \textbf{(Equation 2-12)}$$

2.7 Recrystallization

In the experimental work, the deformed material was exposed to subsequent annealing. This was performed in the attempt to investigate recrystallization processes in the material due to different modes of deformation. Theories and conclusions from today's knowledge about recrystallization of deformed material containing precipitates are summarised in this chapter.

2.7.1 Nucleation of recrystallization

Recrystallization nucleation is a critical factor in determining both the size and orientation of the resulting grains. There are today several well-known mechanisms that control what might be an origin for a new grain.

One mechanism is *Strain Induced Grain Boundary Migration* (SIBM), which was first reported, by Beck and Sperry in 1950. The driving force for SIBM is presumed to arise from a difference in dislocation density on opposite sides of a grain boundary, and as the grain boundary migrate it leaves a dislocation free structure behind.
The preformed nucleus model, is based on the theory that nucleation occurs by the growth and coalescence of subgrains.
Nucleation may origin at *shear bands*, *transition bands* or on *grain boundaries*. Origin for recrystallization probably occurs at grain boundaries as the grain boundaries give rise to inhomogeneity of slip, and this again leads to areas of high local misorientations.

The material may contain a second phase in the form of dispersed *particles*, which are present during deformation, or if the matrix is supersaturated, the particles may precipitate during the subsequent anneal. These particles have three important effects on recrystallization:

- The driving force (stored energy) for recrystallization may be increased.
- The large particles may act as nucleation sites for recrystallization
- Both high and low angle boundaries may be pinned by particles – particularly at small interparticle spacing. This particle effect is the only one from these three that prevent recrystallization. The first two promote recrystallization, Humphreys and Hatherly (1996).

During deformation, the particles have significant effect on the development of the deformed microstructure. From this, there are in particular three aspects of the deformation structure that influence on recrystallization during subsequent annealing:

- The effect on the overall dislocation density from the particles. Higher dislocation density provides force for recrystallization.
- How the particle affect the inhomogeneity of deformation in the matrix. This has effect on the number and kind of nucleation sites.
- The nature of the deformation structure in the vicinity of the particles. PSN (particle Stimulated Nucleation) might be possible.

PSN (particle Stimulated Nucleation)

As a result of deformation of the material with non-deformable particles, a zone built up with dislocations creating a gradual increase in misorientation as distance to the particle surface is decreased. Subgrains inside these zones are found to be able to act as nucleation sites for recrystallization, Humphreys and Hatherly (1996).

Ørsund and Nes (1988) reported for aluminium manganese alloys that for temperatures above 300°C, new grains were nucleated at the core of the deformed zone. At lower temperatures, it seems that matrix oriented subgrains grow into the deformation zone and consume this. These two mechanisms result in two distinct different recrystallized textures. As nucleation originate inside the deformed zone, it leads to a random texture, while matrix oriented subgrains will lead to a recrystallization texture closely linked to the rolling texture.

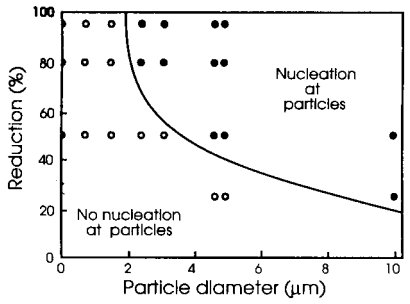

Figure 2.7.1 *The effect of rolling reduction and particle size on the occurrence of PSN. Humphreys (1977)*

Deformation at high temperatures will influence strongly on the formation of deformation zones around particles. Dynamic recovery will result in annihilation of dislocations, and deformation zones may not surround small particles.

2.7.2 Grain growth.

The driving force for growth of recrystallized grains is a reduction in the energy that is stored in the material in the form of grain boundaries. The main factors that influence on the grain growth are:

- *Annealing temperature*, -as grain growth involves high angle grain boundary migration. The mobility is strongly influenced of the temperature. Significant grain growth is often found only at very high annealing temperatures.
- *Solutes and particles*. Boundary migration will be strongly affected by the pinning effects of solutes and second phase particles. Nes, Ryum and Hunderi (1985) has pointed out that particle size and distribution might have significant effect on the recrystallized grain structure. A structure with particles distributed on the banded substructure from cold rolling has been observed to lead to pancake-shaped grains in an Al-Mn Alloy. This effect, known as the Zener-drag, is a result from the interaction forces between particles and grain boundaries.
- *Texture.* A strongly textured material has a reduced driving force for grain growth, as it contains many low angle boundaries.

2.8 Texture

In this chapter, the basis knowledge for texture evolution during deformation and during subsequent annealing will be explained briefly.

2.8.1 Deformation texture

The deformation textures of materials that are deformed by uniaxial forming processes, such as tension, wire, drawing and extrusion are invariably fibre textures.
Humphreys and Hatherly (1996)

2.8.2 Recrystallization texture

As the recrystallized grains inherit the orientation of their subgrain nuclei, the nucleation is the first stage in determining the new recrystallization texture. But there are two rivalling theories as also the growth of grains might influence on the final texture: Oriented nucleation and oriented growth.
Oriented nucleation:
The nucleus posses preferred orientations. As grain grows, these orientations will determine the texture.
Oriented growth:
Nuclei with a broad spectre of orientations are formed. The nuclei with the best growth conditions due to the surrounding matrix will dominate the recrystallization texture. Vatne and Hutchinson (1999).

2.9 Forge2D

The simulations of the extrusion process are performed by the licensed programme Forge2D. A simulation calculation of an industrial deformation process is in principle build up of the thermo-mechanical analysis of the deformation sequence. It is necessary to use real data in order to obtain results with a high degree of confidence The programme Forge2D requires the sampling of the finite elements of the work piece, the tooling description and the rheology of the material. It also requires the general material data for the desired process parameters.

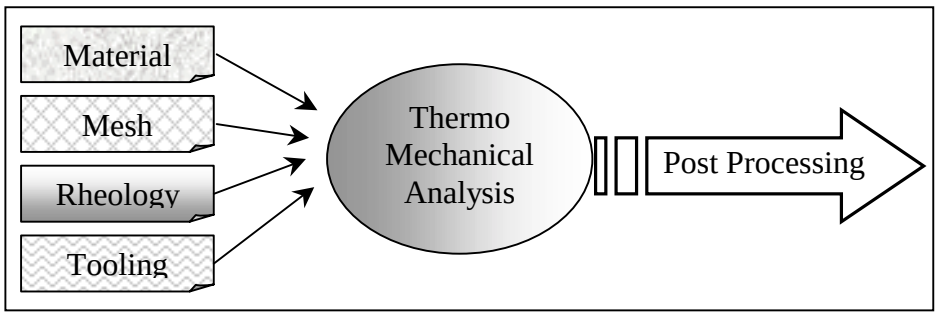

Figure 2.9.1 *Forge 2D Data file structure*

General data file modules

The data file provides nine different modules, which each represents a category of variables to define.

The “Fichier Module”: Specification of generated files and output files. Gathers all file names that will be used during a simulation calculation.

The “Rheology Module”: Gathers all data that defines the overall mechanical behaviour of the material (C, n, m, ß, Ů). This also includes the initial thermo-mechanical values and the interface contact conditions with the tooling (frictional data Ǔ, p). Also the work piece temperature is registered in this module.

URN:NBN:no-2108

The "Increment Module": During the simulation, this module gathers the characteristics of the increment calculation.

The "Execution Module": It gathers the characteristics of the calculation conditions and saves the results during the simulation. Visualisation.

The "Thermic Module": It performs a thermo mechanical calculation and gathers the data that describes it.

The "Mauto Module": It performs the automatic re-meshing calculation during the simulation, and gathers the defining variables for this process.

The "User Var Module": It gathers the data defining the variables that the user has programmed in the provided sub-routines.

The "Histoire Module": It gathers the history of the current simulation process.

The Rheology Module:

A more detailed description will be given of this module as it handles the material data due to specific material models. This creates the basis for all simulations.

In Forge2 the description of the rheology values of the material, is based on the following tensorial form of the Norton-Hoff law:

$$\mathbf{s} = 2 \bullet K(T, \bar{\varepsilon}, ...) \cdot (\sqrt{3} \cdot \bar{\dot{\varepsilon}})^{m-1} \cdot \dot{\varepsilon} \qquad \textbf{(Equation 2-13)}$$

In this equation, the deviatoric stress tensor ***s,*** is linked to the strain rate tensor $\dot{\varepsilon}$, through a function for consistency K(T, $\bar{\varepsilon}$ ...) and a function for the sensitivity to the strain rate m. The K-function depends on the thermo-mechanical conditions.

When this function is considered as a constant in the sphere of the expected thermo mechanical conditions, the consistency will be defined with a unique value.

When the consistence is ascertained through a function of the thermo-mechanical values, the strain-hardening power law combined with the Arhenius' law for the temperatures, T, gives the following formula:

$$K(T,\bar{\varepsilon}) = K_0 \cdot (\bar{\varepsilon} + \varepsilon_0)^n \cdot \exp\left(\frac{\beta}{T}\right) \qquad \textbf{(Equation 2-14)}$$

This law requires the input and definition of the following terms: K_0 (the constant term), Ů (the term of strain hardening regulation), n (the strain hardening power law) and ɓ (the temperature term).

The flow constraint depends on the temperature, strain rate and the total deformation. For a three dimensional configuration, the Norton and Hoff works conjugation, is written as follows:

$$\sigma_0 = (\sqrt{3})^{m+1} \cdot K \cdot \bar{\dot{\varepsilon}}^m \qquad \textbf{(Equation 2-15)}$$

Where: *n* is the strain-hardening exponent
m strain rate sensitivity
ß is temperature sensitivity

In order to determine the parameter input, compression test were carried out at different deformation temperatures and different strain rates. The stress-strain cures were plotted in Microsoft Excel, and by the use of iteration, the parameters that describe the experimental curves best were determined. Compromises had to be done for all parameters, in order to choose parameters that correlate with theoretical known values.

Post processing is done by the subprogram isofor2. Results can then be visualised as isoplots showing strain rates, stresses, strains, velocities and the applied force. Deformed grids and shape at chosen stages of deformation might be performed using Cremarq. Before printing of the results, the result file must be converted to a *.pos* file using a postscript preparation program.

All information in this chapter (chapter 2.9) is based on the Forge2® V2.4 User Manual.

URN:NBN:no-2108

3 Alloy Selection and Experimental techniques

Technical information about the equipment and the material that has been used is given in this chapter. Also, the procedures that were followed to perform the experiments or investigations are explained in detail.

3.1 The investigated alloys

The experimental work that is carried out through this project was mainly performed on two 6000-series aluminium alloys. The commercial Aluminium Alloy 6082 was chosen due to the project's connection to industrial processes and challenges. The grain structure in this material is columnar in the received condition as a result of the extrusion process. Also, compression tests were performed on the industrial aluminium alloy 6063 in order to observe effects from the Si-content and grain structure on yield strength. One alloy was specially designed for this project. It has the same chemical composition as the AA6082 except for the Mn-content. In this alloy, no Mn was added through the production process in order to get a fully recrystallized grain structure in the received material. The alloy is therefore denoted Alloy "R" in this thesis. The background for investigations performed on this alloy, was to determine the effects of Mn-addition on grain structure, recrystallization kinetics and forming properties.

Materials production
All alloys were produced at Raufoss ASA, Norway. The temperature during the casting process was approximately 710°C. No stirring were performed during the casting process, and billet length was approximately 2.0 meters. The AA6082 and the alloy "R" were homogenised for approximately 4 hours at 520°C and 580°C respectively. The AA6063 was only used in a limited number of compression tests, and the delivered material was not produced specifically for this project. The production was in accordance with specifications given for the AA6063 in Alloy Digest (1991). This reference also gives typical values for composition and mechanical properties.

The extrusion process was performed in a 2300 tons hydraulic press, with the following process parameters:
Container temperature: 410°C, Billet temperature: 500°C,
Billet diameter: Ø203mm, Extrusion speed: 12 m/min,
Die temperature: 480°C.
The temperature of the extruded bolt as it left the die, was measured/estimated to app. 530°.

3.1.1 Chemical composition and mechanical properties

The chemical analyses of the investigated alloys are shown in Table 3.1.1. All chemical analysis has been performed at Hydro Aluminium ASA, Sunndalsøra, Norway. Mechanical properties obtained from tensile testing at Raufoss ASA of the specially produced alloys AA6082 and Alloy "R", are given in Table 3.1.2.

Table 3.1.1 *Chemical composition of the investigated alloys*

Alloy	***Content (weight %)***								
	Si	**Mn**	**Mg**	**Fe**	**Ti**	**Zn**	**Ga**	**Ni**	**V**
AA6082.51	0.89	0.56	0.59	0.13	0.02	0.00	0.01	0.01	0.01
Alloy"R"	0.87	0.00	0.58	0.12	0.02	0.00	0.01	0.01	0.01
AA6063	0.45	0.02	0.57	0.20	0.01	0.01	0.01	0.00	0.00

Table 3.1.2 *Mechanical properties of the AA6082 and the Alloy "R".*

Alloy	***$Rp_{0.2}$ [MPa]***	***Rm [MPa]***
AA6082	327	345
Alloy "R"	285	307

3.2 The experimental work – A technical overview.

In Figure 3.2.1 an overall view over the experimental work in this project is illustrated. As can be seen from this figure, the materials studied are extruded bars with a diameter of Ø28.8 mm. From the exact centre of these bars, small compression test specimens with a diameter of 10 mm are produced. The specimen height is 15mm.

URN:NBN:no-2108

With this preparation, no surface effects from the 28.8mm bar are present in the test piece.
For the forward extrusion experiments, test pieces are cut out from the 28.8mm bar on the whole diameter. The length is 85 mm.

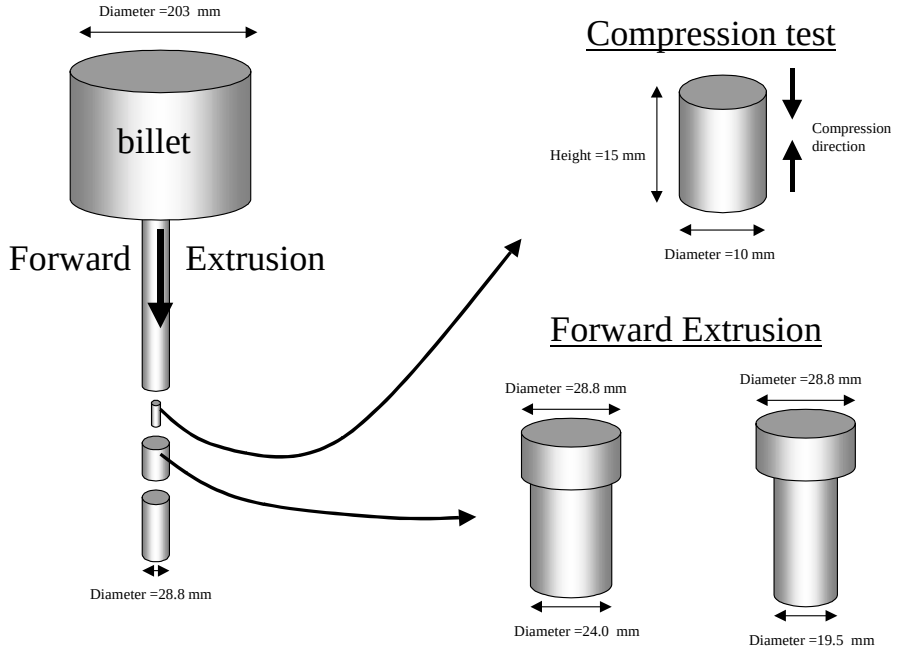

Figure 3.2.1 *Experimental work –from start material to test specimen.*

3.3 Compression testing

Two different deformation experiments are performed in this project, -compression and forward extrusion. In this chapter, the experimental procedure and technical specifications for the compression tests are explained in detail. The reason for choosing compression testing is based on the amount of information obtained about microstructure evolution and mechanical properties under

URN:NBN:no-2108

controlled conditions. Also, the industrial process that initiated this investigation is forging. Compression testing gives indications of the material behaviour under forging conditions.

3.3.1 Materials preparation and technical equipment

The compression testing was performed in a MTS 880servo-hydraulic testing machine at the department of Metallurgy, NTNU. A climate chamber was mounted so that compression could be performed in the range 20°C to 300°C. This chamber required an extension ram to be mounted on the moving ram. In order to control the movement of the moving ram, a guiding cylinder was produced. The force on the test specimen would then be normal to the end planes even under heavy loads. The test rig is illustrated in Figure 3.3.1.

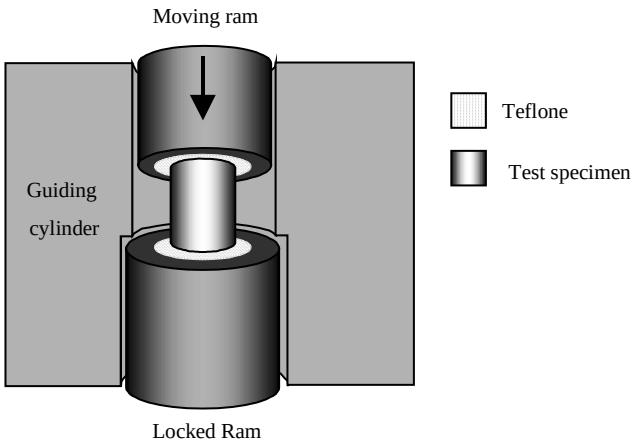

Figure 3.3.1 *Sketch of the compression testing equipment.*

Friction between the test piece and both rams is essential during the compression experiments. It is of great importance to control friction during the tests and keep it to a minimum. In order to achieve this, a piece of Teflon was placed on both ends of the test piece as shown in Figure 3.3.1. In addition, a layer of Molycote G-rapid plus with a

friction coefficient μ=0.04 between –35°C and 450°C was applied to both ends between the Teflon and the test piece. This was done to secure a minimum friction because the work piece cut through the Teflon at high degrees of deformation.

Dimensional information about the specimen is given in Chapter 3.2.

3.3.2 Experimental procedure

As shown in Table 3.3.1 the test parameters are the same for all investigated alloys, except the ram speed. The compression test has been performed at three different ram speeds for the AA6082 and the alloy "R".

Table 3.3.1 *Test parameters for compression experiments.*

Alloy	AA6082	AA6063	Alloy "R"
Ram speed [mm/s]	1, 100, 250	1	1, 100, 250
Deformation temperature [°C]	20, 200, 250, 300	20, 200, 250, 300	20, 200, 250, 300
Max. True Strain, ε	0.8	0.8	0.8

The material condition is mainly T4 – solution treated and aged at room temperature. A limited number of tests were performed in the W-condition (solution treated) in an attempt to get a better understanding of the effects of precipitates on strength evolution.

3.4 Forward Extrusion

From the compression testing, each test specimen has its unique history even if the test parameters are identical. Small variations in temperature, friction, equipment performance or mechanical treatment might give significant variations in microstructure and response to post heat treatment. Even in the forward extrusion experiments, every specimen has its unique temperature and deformation history. Complex mass flow during the first stage of the deformation creates non-uniform conditions in the lower part of the

bolt in Figure 3.4.1. The upper part is protected from the direct water-cooling because of the die. Thus the investigated areas are located in the hatched area in Figure 3.4.1. The assumption of similar deformation conditions for square 1 and square 2 in Figure 3.4.1 is an essential assumption in this project.

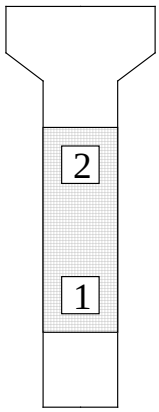

Figure 3.4.1 *Work piece*.

3.4.1 Materials preparation and technical equipment

The extrusion press

All forward extrusion experiments were performed in an 800kN vertical laboratory press at SINTEF in Trondheim. According to moderate high test temperatures and small reduction ratios which leads to relatively low ram force, an extern force-controller specially designed for low forces has been applied to the press. This press is equipped with a numerical control unit, so that the experiments can be performed according to a pre-programmed cycle. To collect the experimental data, a Labtech notebook data acquisition program is used. The following parameters have been saved from each test: ram speed, ram force, ram position. The operator may vary the ram speed from 2 mm/s to a maximum of 30 mm/s. The forward extrusion equipment that was used was originally designed to fit into the press. To perform my experiments, some modifications to this equipment were necessary. These modifications consist of a cooling unit that is active directly after the end of the deformation process.

URN:NBN:no-2108

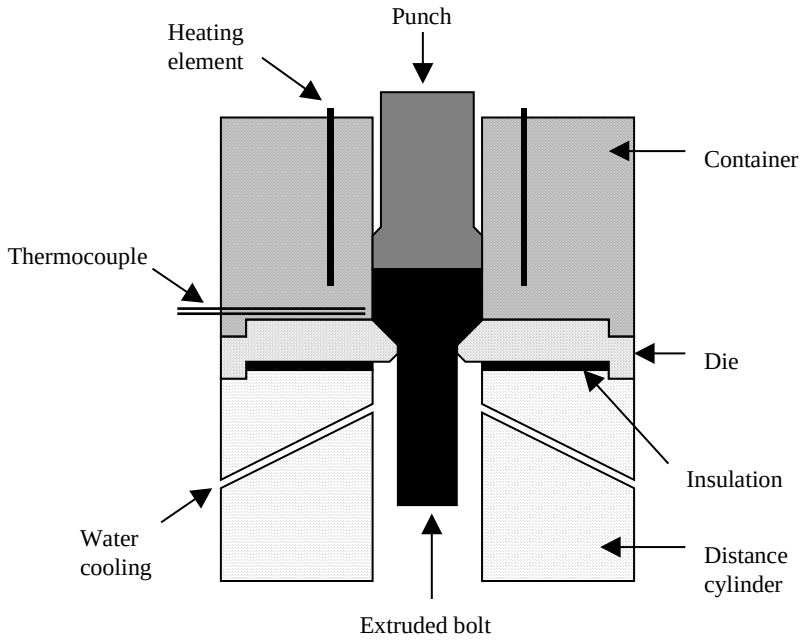

Figure 3.4.2 *The forward extrusion equipment.*

The dies used in these experiments were produced for similar applications in earlier projects at Raufoss ASA. Data related to the dies are given in Table 3.4.1.

Table 3.4.1 *The dies.*

Inner diameter (mm)	Reduction ration (R) (see equation 3-1)	True strain
19.5	2.1	0.4
24.0	1.4	0.2

$$R = \frac{A_0}{A_1} = \frac{r_0^{\,2}}{r_1^{\,2}} \qquad \textbf{(Equation 3-1)}$$

3.4.2 Experimental procedure

Preheating
The container was held at prefixed test temperature by heating elements. The location of these 3 elements is indicated in Figure 3.4.2. The die was also held at the same temperature due to heat conduction from the container. The die was formally insulated from the cold container by use of a mica sheet.
The ram unit was preheated to the test temperature by the use of an external gas flame.
The test specimen was preheated in an induction-heating coil that was situated close to the container.

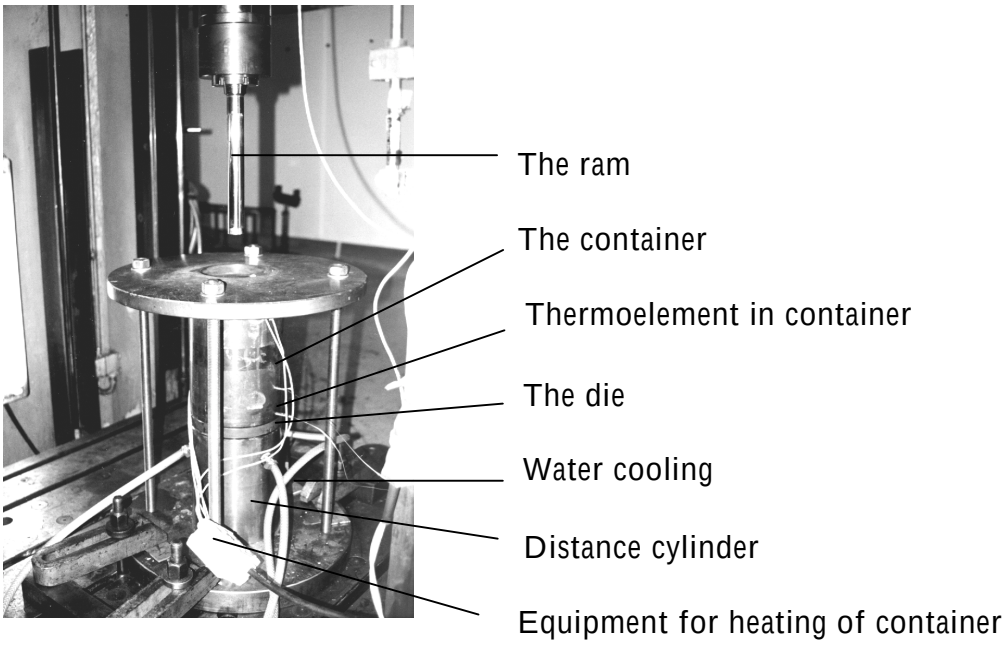

Figure 3.4.3 *The test site for the forward extrusion experiments.*

URN:NBN:no-2108

Temperature control:
The temperature in the container was measured through a small hole, which placed the thermo element to a point only a few millimetres from the inside and close to the bottom of the container. Thermo element specifications: 0.5mm, K-type, connected to an extern digital unit.

The ram temperature was measured on the surface of the lower end of the ram by use of a thermoelement connected to a digital controller.

In order to have the predetermined temperature in the test piece when the deformation process started, it was necessary to simulate the process route of the test piece from room temperature until the ram hit it. This was performed by use of a dummy specimen with a thermoelement that measured the temperature in the middle region of the material. Due to some air-cooling during the transfer of the specimen from the induction coil to the container, the temperature was set to a maximum a few degrees Celsius higher than the predetermined test temperature.

The pre-heating procedure of the specimen:

- Induction heating in coil.
- Time from room temperature to 250°C: 30 sec.
- Transfer time from coil to container: 5 sec.
- Holding time in container (at deform. temp) until press start: 20 sec.
- Press time: 5 sec at 10 mm/s.
- This resulted in a total time at the deformation temperature of approximately 30 seconds.

Cooling:
As the ram movement was reversed after the press, cold water was flushed directly on the deformed part of the test piece for 10 seconds. Immediately after the first water cooling, the extruded bolt was carefully pushed out of the container and water-cooled to room temperature in a bucket.

Surface treatment/lubricant
All bolts were coated in a license-protected process at Raufoss Technology. The process is a two-step process, which covers the material with a calcium aluminate inner layer and a sodium stearate topcoat. This coating process gives excellent coating with a minimum friction at room temperature deformation. It was observed that a degradation of the coating took place at the highest deformation temperature (300°C), but the lubrication was to prevent sticking between the die and the bolt even at this temperature.

3.5 Heat treatment

Isothermal flash annealing was performed in the experimental work in order to study recrystallization or to perform solution heat treatment.

3.5.1 Technical equipment and experimental procedure.

The heat treatment was carried out in salt baths calibrated in the temperature range from 275°C - 550°C.

The solution heat treatment was 15 minutes at 530°C for all alloys. This is above the solvus temperature for the strengthening precipitates dissolve. 15 minutes holding time at temperature was found to be sufficient for dissolutions to be completed within the entire specimen thickness.

For the recrystallization experiments, the holding time was increased from a few seconds to several hours in order to determine isothermal recrystallization kinetics.

After annealing, water quenching (20°C) was carried out.

URN:NBN:no-2108

3.6 Scanning electron microscope and EBSP

The scanning electron microscope has become a significant tool in characterising the microstructure in metallic materials. The EBSP signal is derived from diffraction of electrons on crystal planes, and bands of high intensity becomes visible on a phosphor screen inside the vacuum chamber. The unique orientation of each single crystal is determined due to a map of angular relationship between zone axis, Wahl and Dingley.

3.6.1 Materials preparation and technical equipment.

The electron backscattering diffraction (EBSD) examination was performed using a JEOL 840 Scanning electron microscope. This was equipped with an electron backscatter diffraction instrument in order to characterise the crystallographic orientation of the different grains. The equipment consisted of NORDIF hardware and CHANEL software. This made fully automatic recording and indexing of diffraction patterns possible.

The distribution of crystallographic orientations is represented by a colour-coded image. This is called an orientation map, where the colours represent the Euler angles that characterise the local orientations.

For the investigations performed in this project, subgrain boundaries are set to be limited by misorientations between 5° and 15°.
Grain boundaries (high angle boundaries) are defined to be bounded by misorientations larger than 15°.

The specimen were grounded and polished to a surface finish of 1µm, and polishing with OPS. Followed by an electrochemical etching in the A2 electrolyte for 4 sec. at 40V.

3.7 Optical microscope

Despite the investigations performed in the SEM, it was of great importance to carefully study each specimen in the optical microscope. This gave valuable information of material flow and grain size and grain shape as a result of the deformation processes.

3.7.1 Materials preparation and technical equipment.

The investigations were carried out in a Reichert MeF3A optical microscope using polarised light.

Grain size measurements were performed by the linear intercept method. As the investigated areas in some cases was only 1 mm wide, it was necessary to perform several countings from each area in order to minimise measuring uncertainty.

The specimen were grounded and polished to a surface finish of 1µm. After an electrochemical etching in the A2 electrolyte for 4 sec. at 40V, followed by anodising in a water solution of 5%HBF4 at 20V for 120 seconds, the grains appeared clearly in the optical microscope.

3.8 Hardness Measurements

When measuring the hardness, the applied load was 1 kg, and loading speed was 100µ/sec. All measurements are given in VHN. The specimen surface was ground to 1200µm before determining the hardness.

3.9 Forge 2D – numerical simulations.

All simulations performed in Forge 2D are carried out on computers connected to the SINTEF network in Trondheim.
The theory for the material model is given in Chapter 2.9.

URN:NBN:no-2108

4. Experimental results

Part I: Plastic deformation. Stress-strain relationships.

As described in earlier sections, two different deformation techniques have been used to perform controlled, plastic deformation of the selected materials. In this chapter, the results that describe relationships between stress and strain for various deformation modes are presented and commented.

4.1 Compression tests

True stress-true strain curves were obtained from axisymmetric compression testing as described in chapter 3.2. Three alloys were tested: The AA6063, the AA6082 and the Alloy ''R''.
All alloys are tested at four different deformation temperatures. These are 20°C, 200°C, 250°C and 300°C. The test specimens are all deformed to a true strain of approximately 0.8.
For the AA6082 and the Alloy ''R'', compression testing with variations in the ram speed is carried out. The ram speeds used were 1mm/s, 100mm/s and 250mm/s.
The material condition is mainly T4 (solution treated and aged at room temperature). A few tests were performed in the W-condition (solution treated, water cooled, kept in liquid nitrogen and no ageing at room temperature) in attempt to get a better understanding of the effects from precipitates. Details about the material condition are given in chapter 3.1.

4.1.1 AA6063: Stress-strain curves as a function of deformation temperature.

As can be observed from ***Figure 4.1.1***, variations in the deformation temperature results in different true stress - true strain relationships. In all true stress - true strain graphs shown in Chapter 4, the lowest deformation temperature demands the highest applied true stress. At a true strain of 0.8, the true stress for the 20°C-curve is approximately 270 MPa.

The three curves that describe the deformation temperatures from 200°C to 300°C show values from 130 MPa to 185 MPa for the same true strain value. True stress-true strain curves for all deformation temperature seem to follow a power law relationship. At true strain values higher than approximately 0.5, the four curves seem to be more or less parallel. There is also no sign of reaching a steady state condition for any of them.

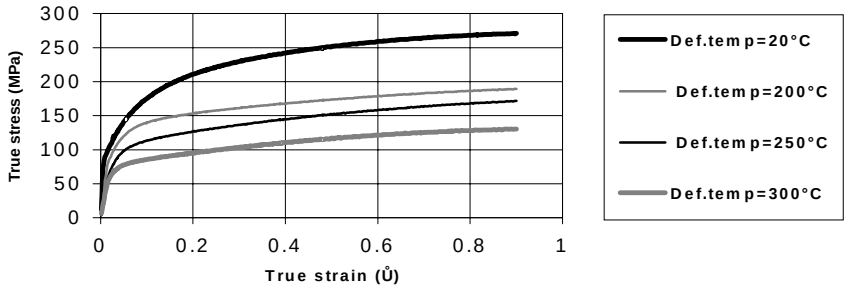

Figure 4.1.1 *True stress-true strain curve for AA6063. Ram speed=1mm/s, T4-condition.*

4.1.2 AA6082: Stress-strain curves as a function of deformation temperature and piston rate.

In ***Figure 4.1.2***, ***Figure 4.1.3*** and ***Figure 4.1.4***, the true stress-true strain curve for ram speed of respectively 1mm/s, 100mm/s and 250mm/s are shown. The test material is in a T-4 condition.

At ram speed equal to 1/s, the compression test performed at room temperature does not reach a steady state condition during deformation up to a true strain of 0.8. At this true strain it reaches a maximum stress of almost 350 MPa. On the other hand, the 200°C and the 250°C curves seem to reach steady state from a true strain of approximately 0.3. Steady state is found to stabilise at 230Mpa and 200 MPa respectively for these curves. When compression is performed at the highest temperature, it seems that for true strain values higher than 0.5, the applied stress is slightly reduced from the maximum value of 170 MPa.

URN:NBN:no-2108

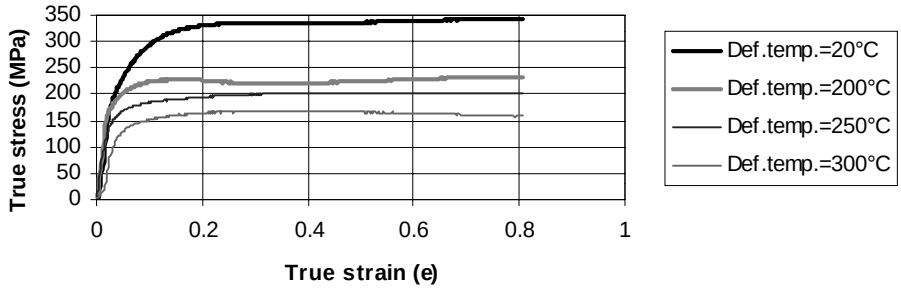

Figure 4.1.2 *True stress-true strain curve for AA6082. Ram speed=1mm/s, T4-condition.*

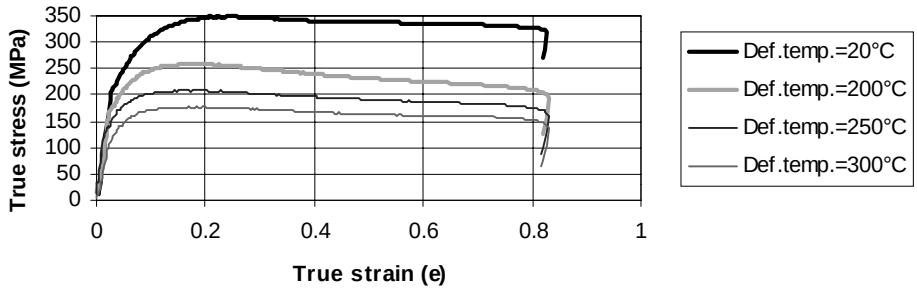

Figure 4.1.3 *True stress-true strain curve for AA6082. Ram speed=100mm/s, T4-condition.*

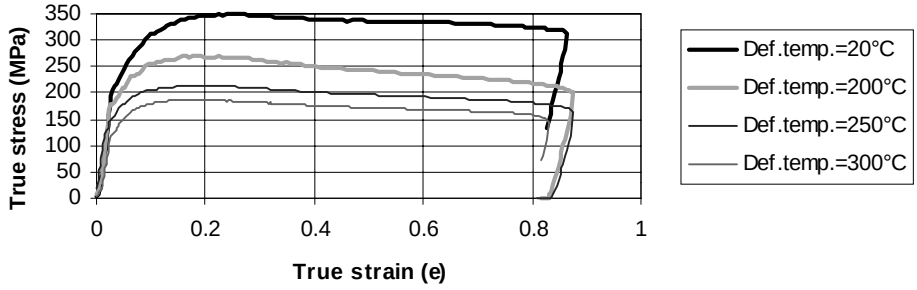

Figure 4.1.4 *True stress-true strain curve for AA6082. Ram speed=250mm/s, T4-condition.*

In ***Figure 4.1.4*** and ***Figure 4.1.5*** the ram speed is 100mm/s and 250mm/s respectively. True stress-true strain curves for all deformation temperatures

URN:NBN:no-2108

in these two figures show the same behaviour as true strain is increased from κ=0 to κ=0.8. It is observed that both curves for room temperature testing reaches a maximum at κ=0.25, while the curves for elevated temperatures all reaches a maximum at a true strain of 0.15. The maximum true stress is slightly higher for the highest ram speed than for the slower deformation speed. As the true strain increases, the true stress drops faster for deformation performed at the highest ram speed than for the slower ram speed.

In ***Figure 4.1.5*** the AA6082 is deformed in the W-condition. Details concerning testing parameters are given in Chapter 3.3.2. The curve for testing at room temperature does not reach a steady state in the true strain range that is investigated. When testing is performed at 200°C, true stress only slightly increases from a true strain of 0.4, while the curve for 250°C reaches steady state at a true strain of 0.4. Deformation performed at the highest temperature reaches a maximum true stress for true strain equal to 0.3, while further deformation above 0.5 leads to a small decrease in true stress.

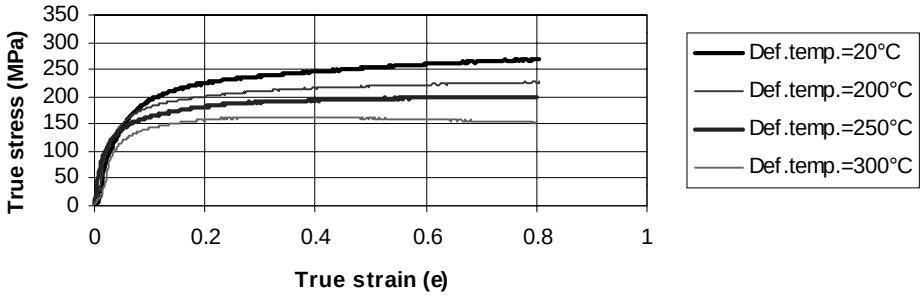

Figure 4.1.5 *True stress-true strain curve for AA6082. Ram speed=1mm/s, W-condition.*

4.1.3 Alloy ''R'': Stress-strain curves as a function of deformation temperature and piston rate.

In ***Figure 4.1.6***, ***Figure 4.1.7*** and ***Figure 4.1.8*** the results from compression testing of the Alloy ''R'' in the T4-temper is shown. The ram speed increases from 1mm/s to 100mm/s and finally to 250mm/s with respect to the figures referred to above.

URN:NBN:no-2108

For a ram speed equal to 1mm/s, all curves show an exponential relationship except the one that is deformed at the highest temperature. This one reaches a steady state at approximately a true stress of 160 MPa and a true strain of 0.5.

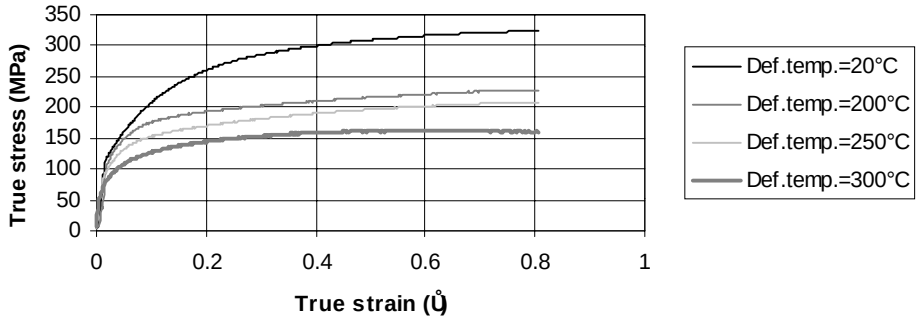

Figure 4.1.6 *True stress-true strain curve for Alloy "R". Ram speed=1mm/s, T4-condition.*

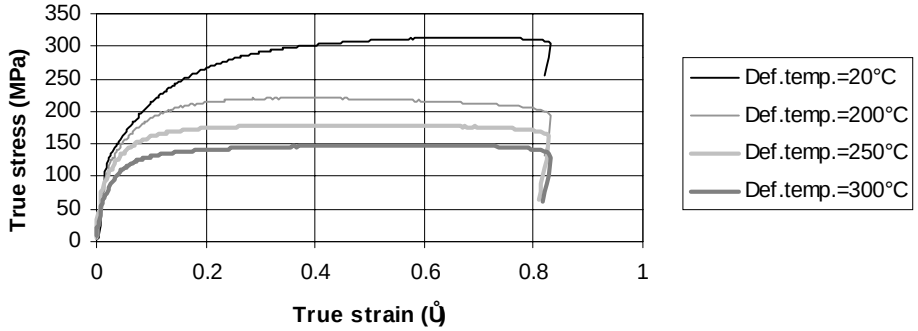

Figure 4.1.7 *True stress-true strain curve for Alloy "R". Ram speed=100mm/s, T4-condition.*

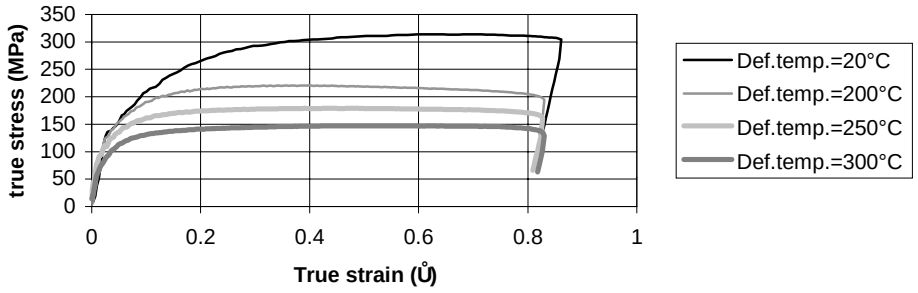

Figure 4.1.8 *True stress-true strain curve for Alloy "R". Ram speed=250mm/s, T4-condition.*

For ram speeds at 100mm/s, the curves for all deformation temperatures reach a maximum true stress value, and then slightly drop. The maximum true stress value for each deformation temperature is constant whether the Ram speed is 100mm/s or 250mm/s.
For the highest Ram speed of 250mm/s and the two highest deformation temperatures, 250°C and 300°C, it seems that a steady state condition is reached.

In ***Figure 4.1.9*** true strain-true stress relationships are shown for testing of the Alloy ''R'' in the W-temper. The ram speed is 1mm/s. The curves that describe deformation at room temperature, 200°C and 250°C only show a small reduction in true stress for fixed true strain values. They all have an exponential form, and have their maximum true stress values between 210 MPa and 240 MPa. The curve that describes deformation at 300°C, differs significantly from the three others described above. This one almost immediately reaches a steady state condition at about 140 MPa. Unfortunately, only one specimen was prepared for this test parameter. This unique shape of the graph should have been confirmed by additional tests.

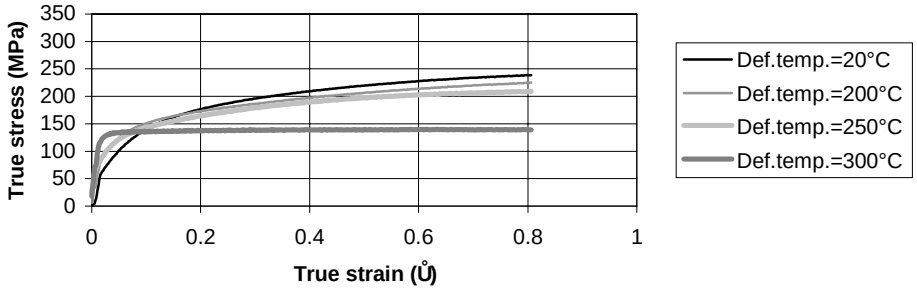

Figure 4.1.9 *True stress-true strain curve for Alloy ''R''. Ram speed=1mm/s, W-condition.*

URN:NBN:no-2108

4.2 Forward Extrusion

Forward extrusion experiments are performed as described in Chapter 3. The investigated alloys are the AA6082 and the Alloy ''R''. For each reduction ratio, deformation is performed at 3 different temperatures: 20°C, 200°C and 300°C. The start material has a diameter of 28.8mm, and by using dies with an inner diameter of 24.0mm and 19.5mm, the reduction ratios are 1.4 and 2.1 respectively. Corresponding true strain values are 0.2 and 0.4.
For further use of these results, one is requested to read chapter 3.4 and 5.3 due to technical problems with the force cell,

4.2.1 AA6082: Stress-strain curves as a function of deformation temperature and reduction ratio.

As can be seen from *Figure 4.2.1*, ram force decreases significantly as the deformation temperature is raised from room temperature to 200°C. Further increase in temperature reduces ram force even more. As the ram starts to push the bolt through the die, the ram force rapidly increases until a peak

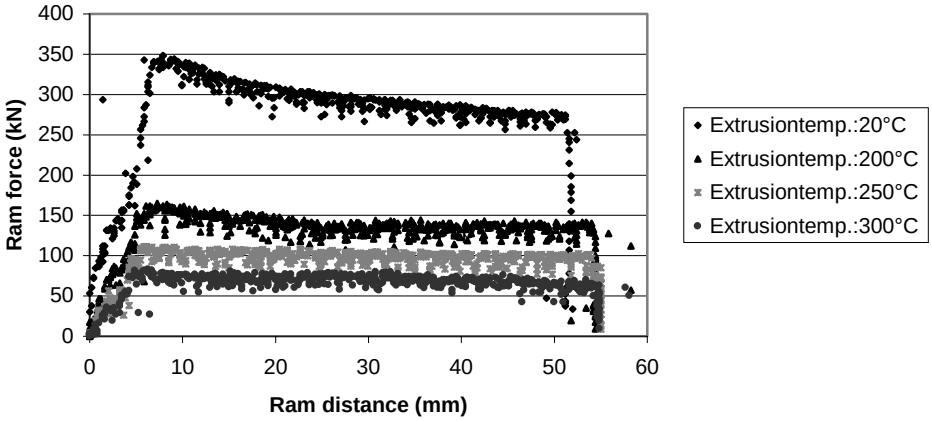

Figure 4.2.1 *Forward extrusion of AA6082.*
Ram force versus ram displacement.
All deformation temperatures, ram speed: 10mm/ s
Reduction ratio=2.1.

force is reached. The ram force then starts to decrease as ram displacement increases. In order to compare the curves for different dies and for different deformation temperatures, the peak load and the load after a ram displacement of 50mm are determined.
The peak load for deformation at room temperature is significant higher than the final load. This difference is reduced for higher deformation temperatures, and for extrusion at 300°C the ram force is almost constant during the deformation process. For extrusion performed at a lower reduction ration (R=1.4), the ram force was significantly lower at all deformation temperatures.

4.2.2 Alloy "R": Stress-strain curves as a function of deformation temperature and reduction ratio.

In *Figure 4.2.2* one observes the same relationships between peak load and final load for each deformation temperature as in *Figure 4.2.1.* The extrusion performed at the highest temperatures has almost constant ram force during the press. As for the AA6082, the ram force was significantly lower at all deformation temperatures for extrusion performed at a lower reduction ration (R=1.4).

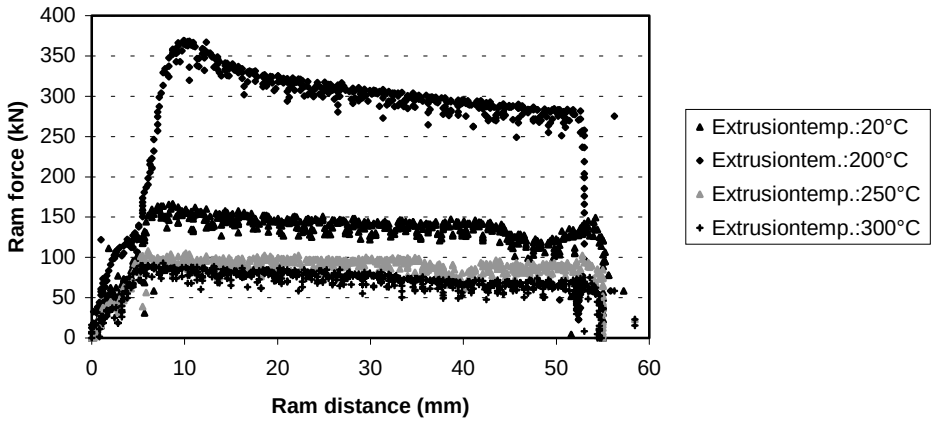

Figure 4.2.2 *Forward extrusion of Alloy "R".*
Ram force versus ram displacement.
All deformation temperatures.
Reduction ratio=2.1. Ram speed:10 mm/s.

URN:NBN:no-2108

Part II: Characterisation of the deformation microstructure.

In Part I, detailed information about how the investigated materials responded to different deformation processes was given. Obviously, variations in deformation temperatures and true strain made the material respond differently. In this part, the material that was deformed by forward extrusion is carefully investigated by using the SEM and the EBSP-technique that is described in Chapter 3.6.

4.3 Investigations performed in centre of the extruded bolt

The microstructure in the centre of the forward extruded AA6082 and the Alloy "R" bolts are shown in separate chapters (Chapter 4.3.1 and Chapter 4.3.2 respectively). All investigated areas are taken from the same location in the extruded bolts. These areas are assumed to have uniform deformation modes, since effects like strain gradients due to surface friction are negligible in the centre.

4.3.1 AA6082: Both reduction ratios.

The AA6082 has a columnar grain structure due to the presence of dispersoids that contain Mn. These have prevented recrystallization to occur during the previous extrusion of the Ø210mm billet. The material that is investigated in this chapter has been reduced from Ø28.8mm to diameters of 19.5mm or 24.0mm.

4.3.1.1 Microstructure (EBSP-investigations)

The AA6082 microstructure is shown in *Figure 4.3.1* and *Figure 4.3.2* for every reduction ratio and deformation temperature. Both figures also include the microstructure in the bolt before deformation. High angle boundaries are defined by misorientations higher than 15°. These boundaries are marked with a thin dark line. One observes that larger reduction ratio leads to shorter radial grain diameter. Measurements of the columnar width before and after deformation are given in *Figure 4.3.9*. Subgrain limited by misorientations between 5° and 15° are not marked on

the figures, due to the small subgrain size. Measurements performed with a step size of 0.5 µm indicate a subgrain size of 1-3 µm.
Deformation bands approximately 45° to extrusion direction are observed in the deformed structure. These bands (marked with "B", see *Figure 4.3.1*) can quite easily be seen in the dark grain on the lower area for extrusion temperature=20°C in the above referred figure. The orientation of the microstructure, when comparing the orientations of the crystals on both sides of a deformation band boundary (marked "BB" in *Figure 4.3.1*), shows very small rotations. Therefore these bands appear as lighter zones in the dark grain.
The rotation of the structure in *Figure 4.3.1* and *Figure 4.3.2* for deformation at 300°C is due to rotation of the specimen in the SEM probe chamber.

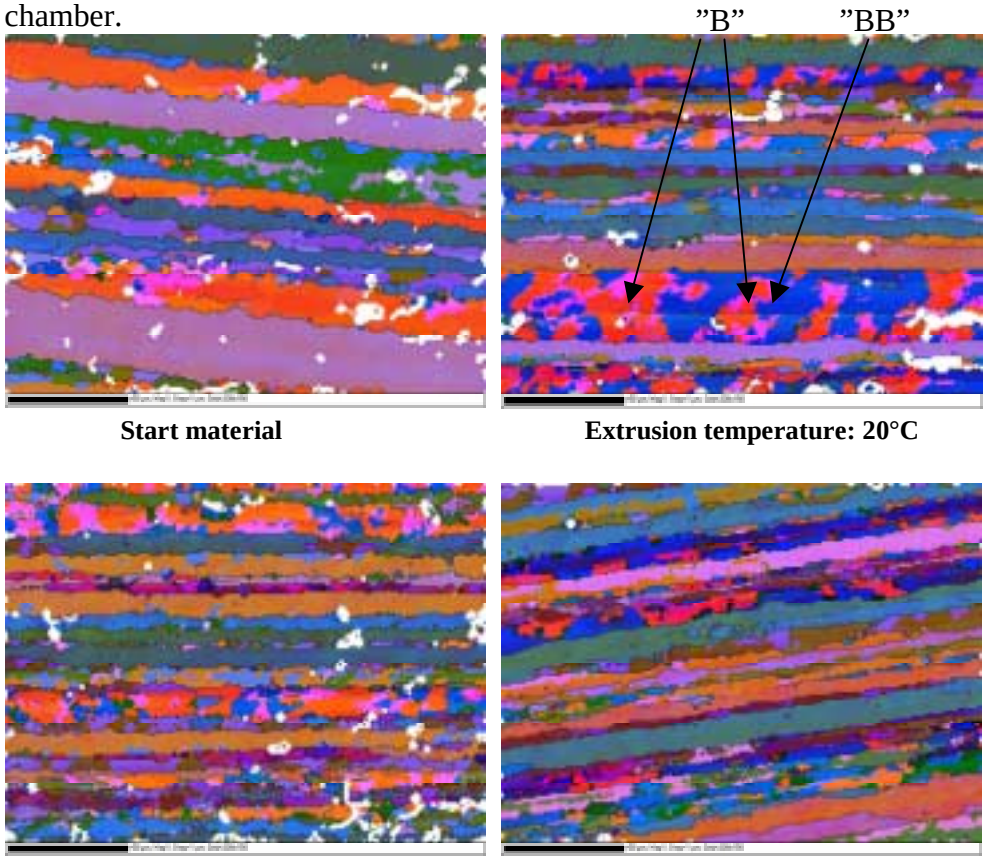

Figure 4.3.1 *Microstructure in centre of extruded bolt. Investigations performed in SEM/EBSP. Alloy AA6082. All deformation temperatures. Reduction ratio=2.1.*

URN:NBN:no-2108

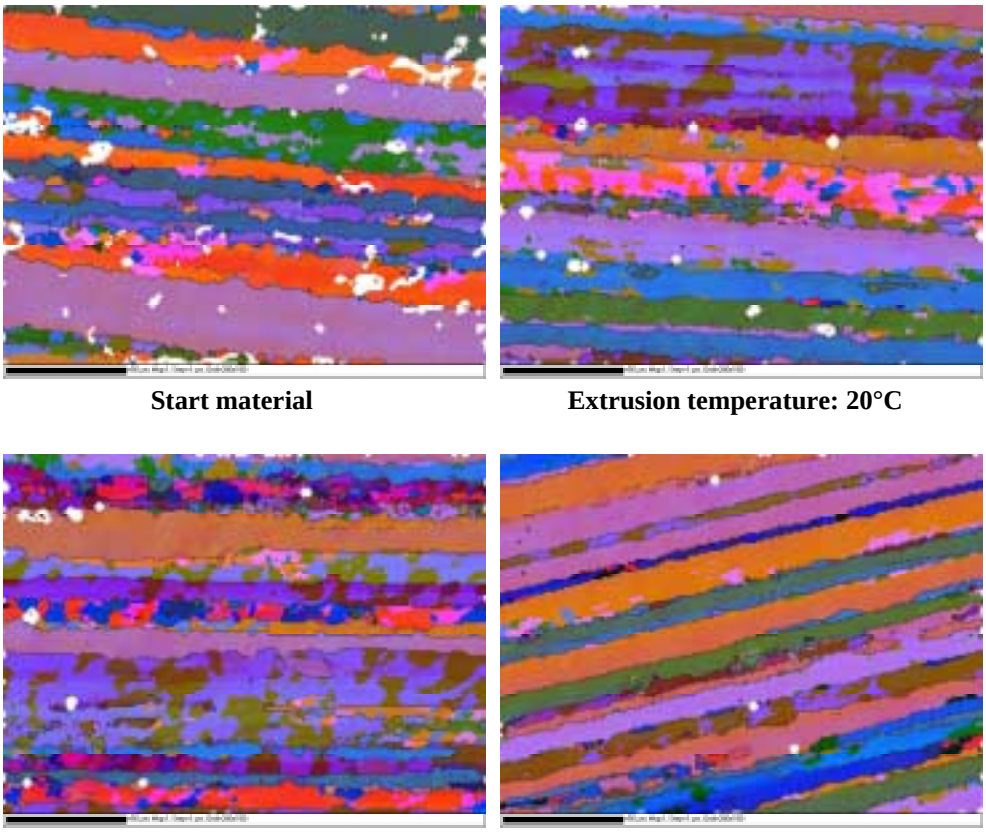

Start material **Extrusion temperature: 20°C**

Extrusion temperature: 200°C **Extrusion temperature: 300°C**

Figure 4.3.2 *Microstructure in centre of extruded bolt. Investigations performed in SEM/EBSP. Alloy AA6082. All deformation temperatures. Reduction ratio=1.4.*

4.3.1.2 ODF's from the EBSP-measurements.

EBSP measurements from the areas in the centre of the extruded bolts also consists data from which Orientation Distribution Functions can be constructed. ODF's for each deformation temperature and reduction ratio are shown in *Figure 4.3.3* and Figure 4.3.4.

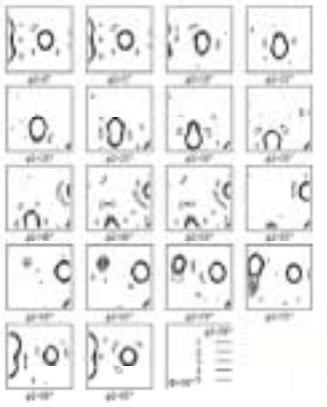

Start material

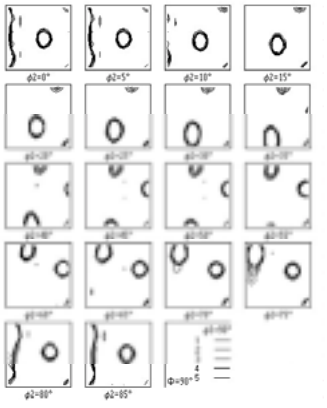

Extrusion temperature: 20°C

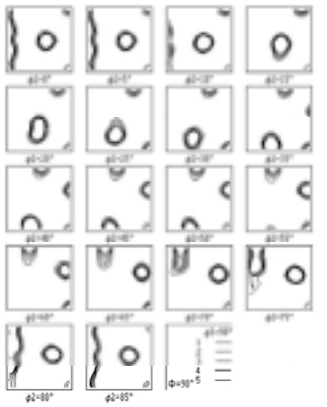

Extrusion temperature: 200°C

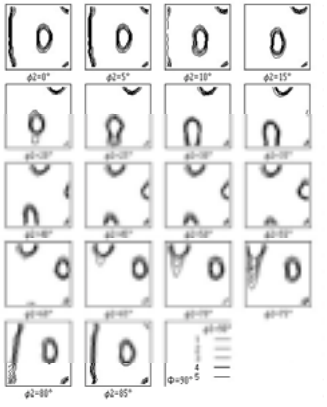

Extrusion temperature: 300°C

Figure 4.3.3 *ODFs from the areas shown in Figure 4.3.1. Investigations performed in SEM/EBSP. Alloy AA6082. Reduction ratio=2.1.*

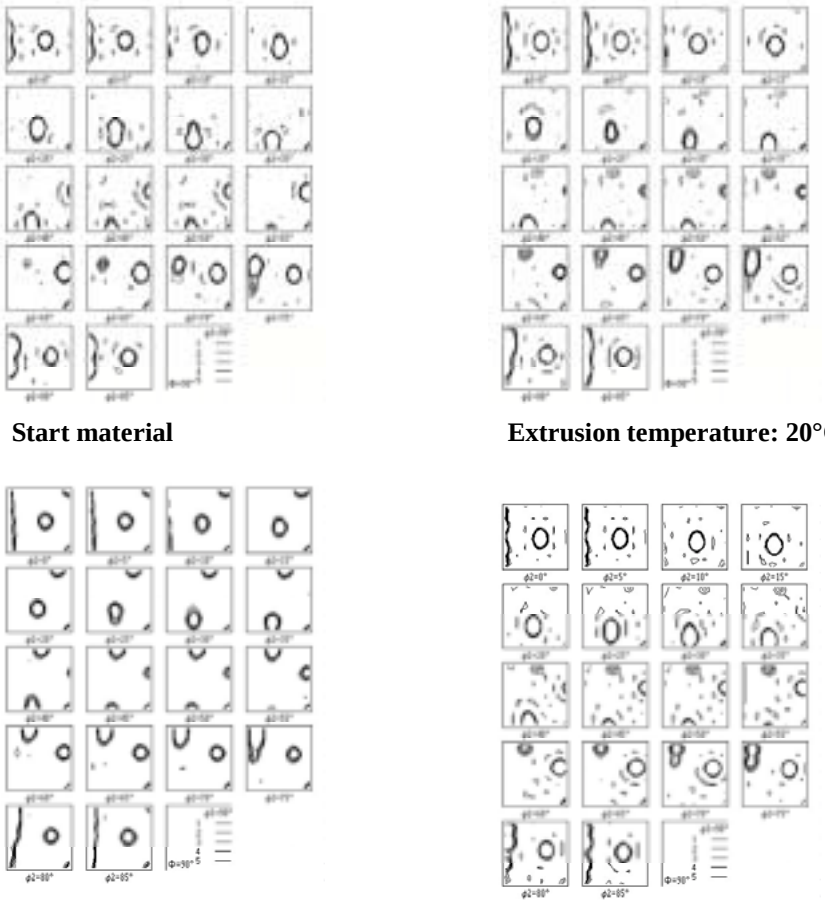

Start material **Extrusion temperature: 20°C**

Extrusion temperature: 200°C **Extrusion temperature: 300°C**

Figure 4.3.4 *ODFs from the areas shown in Figure 4.3.2. Investigations performed in SEM/EBSP. Alloy AA6082. Reduction ratio=1.4.*

To evaluate the evolution of texture, the materials history must be taken into consideration. First the billet with a diameter of 203mm was forward extruded to bolts with diameter equal to 28.8 mm. This represents a reduction ratio, R=50. A bolt with this dimension is the “start material” for

the experiments in this thesis. A following forward extrusion to diameters of 24.0 mm and 19.5 mm does not represent a considerable change in the materials reduction ratio compared to the original size of 210 mm. The respective reduction ratios for these extruded bolts from 28.8 mm to 24 mm and 19.5 mm are 1.4 and 2.1 respectively.
As both figures show, the start material has a texture that mainly consists of cube-oriented grains that are rotated around the <100> direction and the <111> direction.

There is not observed any effect on the deformation texture as the material diameter is reduced from 28.8 mm to 24 mm or 19.5 mm. All data collections show the same texture. Also there are not observed any significant effect of changing the deformation temperature from 20°C to 300°C on the texture evolution.

4.3.2 Alloy "R". Both reduction ratios.

The Alloy "R" has a recrystallized microstructure in the Ø28.8 mm due to the absence of Mn. There are no Mn-containing dispersoids that prevents recrystallization in the extruded bolts from the original billet. The microstructure in the start material with a diameter of Ø28.8 mm is shown in both *Figure 4.3.5* and *Figure 4.3.6*. Unfortunately, there are no data for the deformation at 300°C at the lowest reduction ratio, but this does not considered to be critical in the effort of discussing trends in the results.

4.3.2.1 Microstructure (EBSP-investigations).

In *Figure 4.3.5* and *Figure 4.3.6* thin black lines describes a misorientations between neighbouring grains of at least 15° (high angle boundaries). Subgrain boundaries (5°-15°) are not marked due the high density of these boundaries as a result of the heavily deformed structure. However, careful investigations of the start material revealed an almost dislocation free microstructure.
As for the AA6082, areas with deformation are observed for all deformation temperatures and both degrees of deformation grades. These can easily be detected in the upper left corner for deformation at 20°C in *Figure 4.3.6*. As different colours result from different orientations, one can easily see that

the deformation bands are small, parallel bands with small misorientations in between.
The extrusion direction is horizontal in the figures, and the grains are elongated in this direction during extrusion. The deformation bands are located approximately 45°C to the extrusion direction.

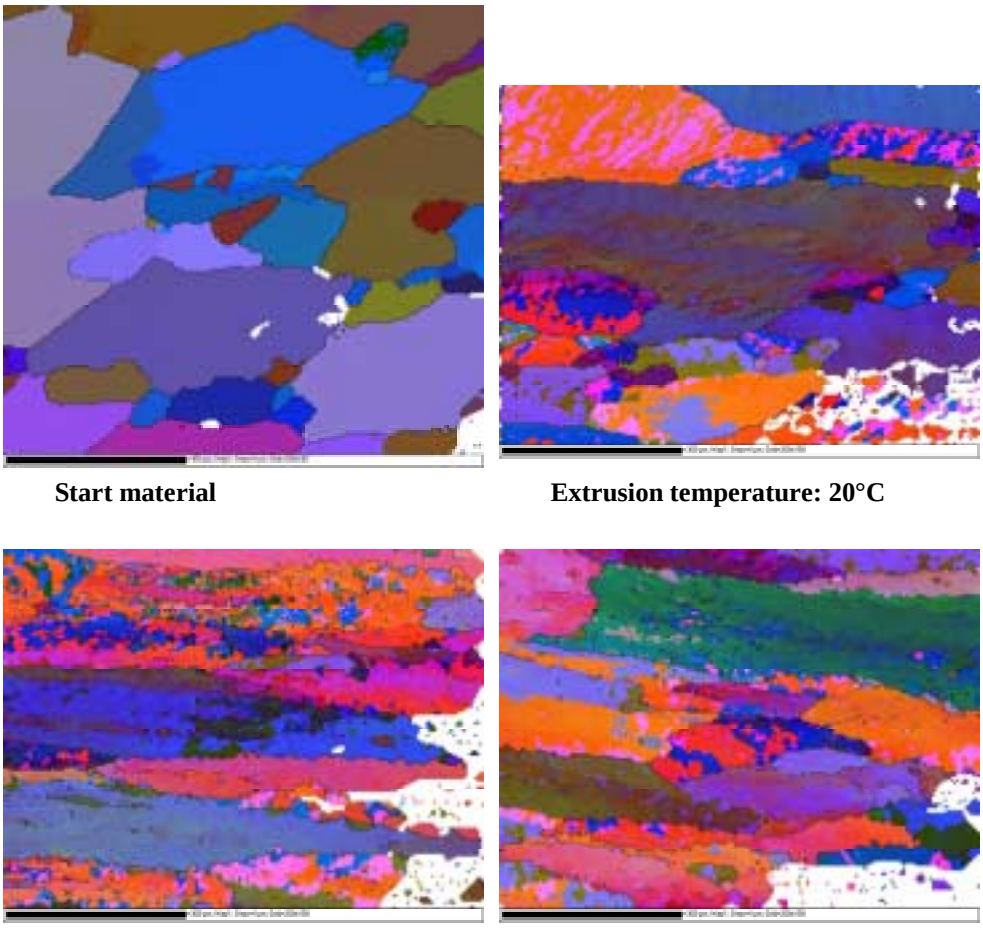

Figure 4.3.5 *Microstructure in centre of extruded bolt. Investigations performed in SEM/EBSP. Alloy "R". All deformation temperatures. Reduction ratio=2.1.*

Start material

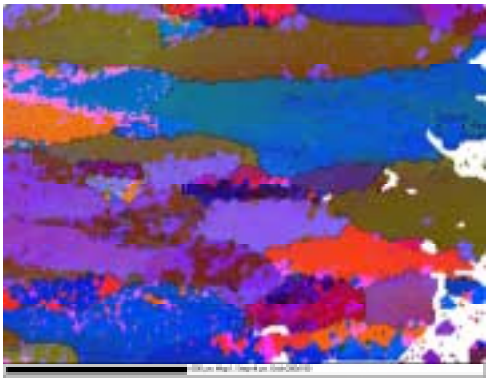

Extrusion temperature: 20°C

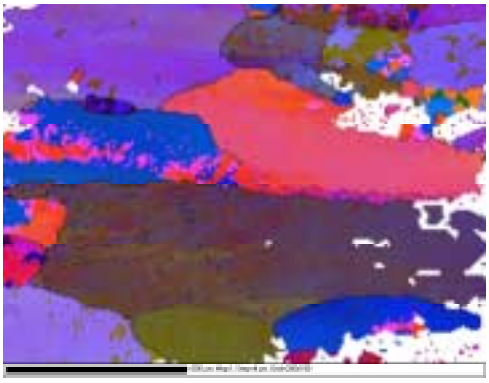

Extrusion temperature: 200°C

Figure 4.3.6 *Microstructure in centre of extruded bolt.*
Investigations performed in SEM/EBSP. Alloy "R".
Start material, def. temp:=20°C and 200°C. Red. ratio=1.4.

4.3.2.2 ODF's from the EBSP-measurements.

The collected EBSP data from the areas that are shown in *Figure 4.3.5* and *Figure 4.3.6* are used to create ODF's for the same areas. This means that the ODF's represents areas of 800µm*600µm, and hence a small number of

URN:NBN:no-2108

grains. Additional investigations are performed to support the observations from the figures shown here.
The texture components that are found to dominate in the start material, is a rotated cube component around the <100> direction. The cube texture component rotated around the <111> axis is not observed in this alloy.

Start material

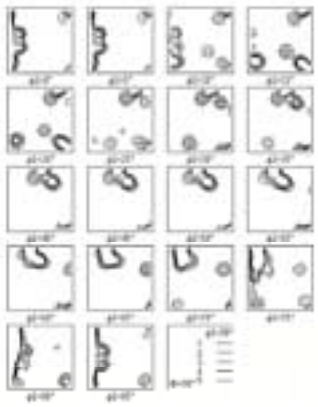

Extrusion temperature: 20°C

Extrusion temperature: 200°C

Extrusion temperature: 300°C

Figure 4.3.7 *ODFs from the areas shown in Figure 4.3.5. Investigations performed in SEM/EBSP. Alloy "R". Reduction ratio=2.1.*

The investigations indicate that the texture does not change during the forward extrusion deformation with reduction ratio of R=2.1 and R=1.4. There is also no effect from changing the deformation temperature.

Start material

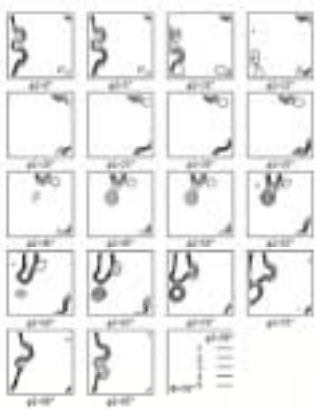

Extrusion temperature: 20°C

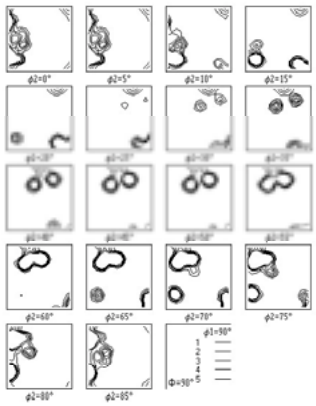

Extrusion temperature: 200°C

Figure 4.3.8 *ODFs from the areas shown in Figure 4.3.6. Investigations performed in SEM/EBSP. Alloy "R". Reduction ratio=1.4.*

URN:NBN:no-2108

4.3.3 Grain measurements performed in SEM (EBSP).

The Channel software and the EBSP measurements are very well suited for measuring grain size. As *Figure 4.3.9* shows, the grain size in the radial direction in the AA6082 start material was 10µm. When it was deformed in the Ø24mm die, the grain size was reduced to approximately 8µm. Deformation in the Ø19.5mm die resulted in a radial grain diameter of approximately 5µm.
For the Alloy "R", the start material's grain size in the radial direction was app. 85µm. A reduction ratio of 1,4 resulted in a grain size of approximately 70µm, and the 19.5mm bolt had a grain size of approximately 40µm. This is shown in *Figure 4.3.9.*

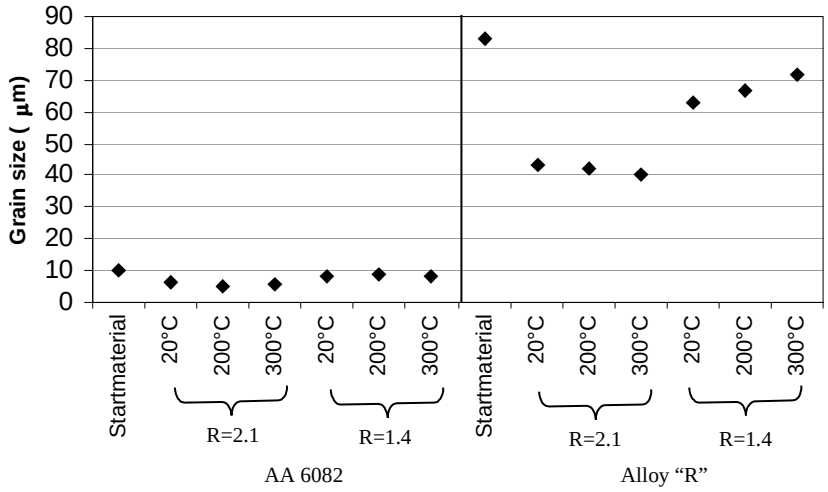

Figure 4.3.9 *Grain size measurements performed in SEM/EBSP. Grain size is defined as high angle boundaries in the radial direction.*

4.4 Investigations performed on a cross-section of the AA6082.

Due to friction between the material and the die, the material flow through the press is quite complex. As a result from the extrusion process, one therefore observes that the deformed microstructure is a result of the distance from the bolt surface. In this chapter, two bolts of the AA6082 are studied at specific distances from the surface at a cross section. All micro structural data are collected from small areas with centres located 1, 3, 6 and 9 mm from the surface of the bolt. The investigations are performed in the SEM with the EBSP mapping technique. These investigations are limited to bolts with reduction ratio equal R= 2.1 and deformation temperatures 200°C and 300°C. Several attempts were made to analyse the deformed microstructure at room temperature, but due to the heavily deformed material and limitations in the EBSP technique, this was not possible. However, in the heat treatment experiments, this bolt is also analysed.

4.4.1 Microstructure (EBSP-investigations).

In *Figure 4.4.1* and *Figure 4.4.2*, the deformed microstructure is shown for bolts with extrusion temperature at 200°C and 300°C respectively. A common observation is that radial grain size is smaller as one move from the centre to the surface. It is obvious that friction between the die and the bolt has caused a tougher deformation in the outer part of the bolt. In the referred figures, subgrain boundaries are not visualised with black lines. This is due to the high density of misorientations that meet the requirements to low angle boundaries (5°-15°).
Measurements are performed on the grain size defined with high angle boundaries (>15°) and on the subgrain size (5°<d<15°). These results are shown in *Figure 4.4.3*. All measurements are in the radial direction. One observes that both the grain size and the subgrain size are very similar in the two investigated bolts. This means that changing the deformation temperature from 200°C to 300°C does not clearly affect the radial grain size. At areas 1-3 mm from the surface, the subgrain size is found to be approximately 1.5 µm. Areas located 6 mm and 9 mm from the surface, has grain radius equal to 2.2µm and 3.2 µm respectively.

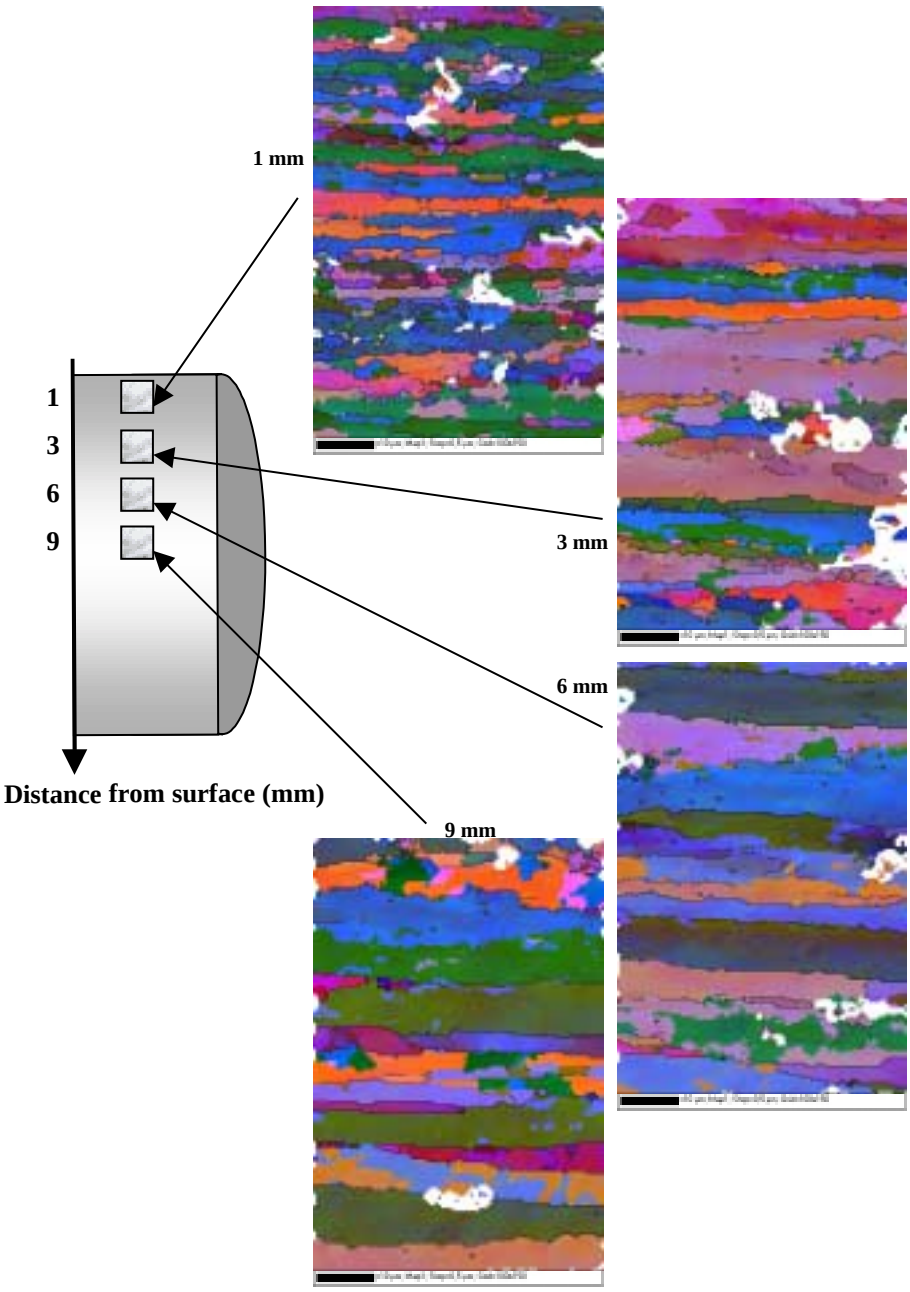

Figure 4.4.1 *Microstructure after forward extrusion. Investigations performed in SEM/EBSP. Alloy AA6082. Deformation temp.: 200°C. Reduction ratio=2.1.*

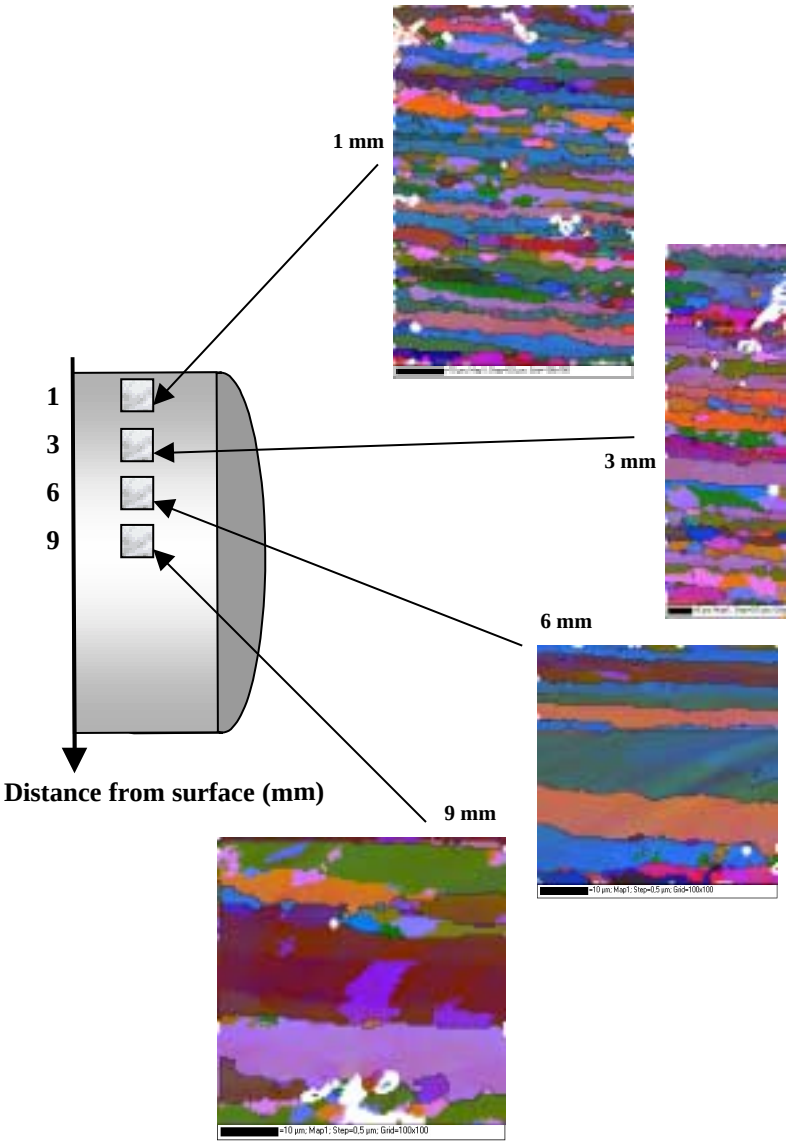

Figure 4.4.2 *Microstructure after forward extrusion.*
Investigations performed in SEM/EBSP. Alloy AA6082.
Deformation temp.: 300°C. Reduction ratio=2.1.

URN:NBN:no-2108

The grain size is also very small close to the surface. Measurements show that 1 mm from the surface it is only 2µm wide. 2 mm closer to the centre, the grain size has increased to approximately 3µm. 6 mm from the surface and in the centre, the grain size is 5µm and 5.8µ respectively.

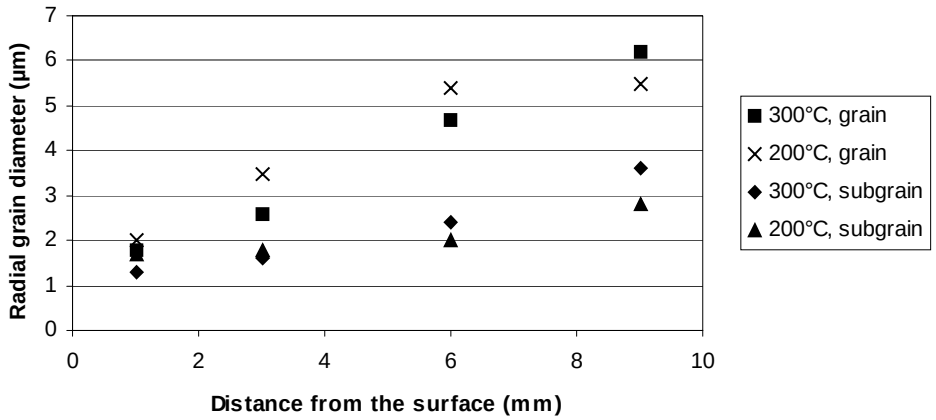

Figure 4.4.3 *Investigations performed on a cross section. Grain size (misorientation>15°), and subgrain size (5°<misorientation<15°)*

4.4.2 ODF's from the EBSP measurements.

From the areas that were investigated in chapter 4.4.1, the EBSP data has been used to create Orientation Distribution Functions. These are shown in *Figure 4.4.4* and *Figure 4.4.5*. The crystal orientation is compared as one moves from the surface to the centre. Also comparisons are made between the same locations, but in bolts that are deformed at different temperatures.

URN:NBN:no-2108

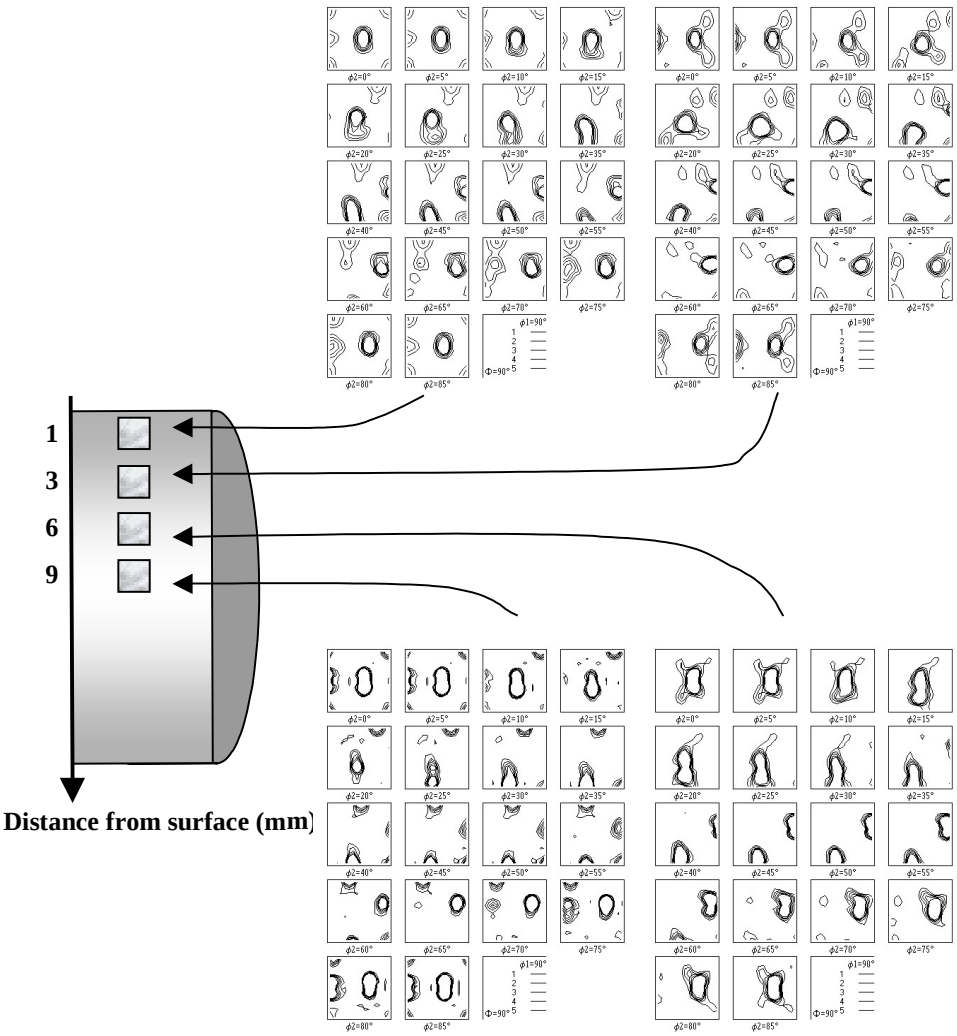

Figure 4.4.4 *ODF's from the areas shown in Figure 4.4.1. Investigations performed in SEM/EBSP. Alloy AA6082. Deformation temp.: 200°C. Reduction ratio=2.1.*

URN:NBN:no-2108

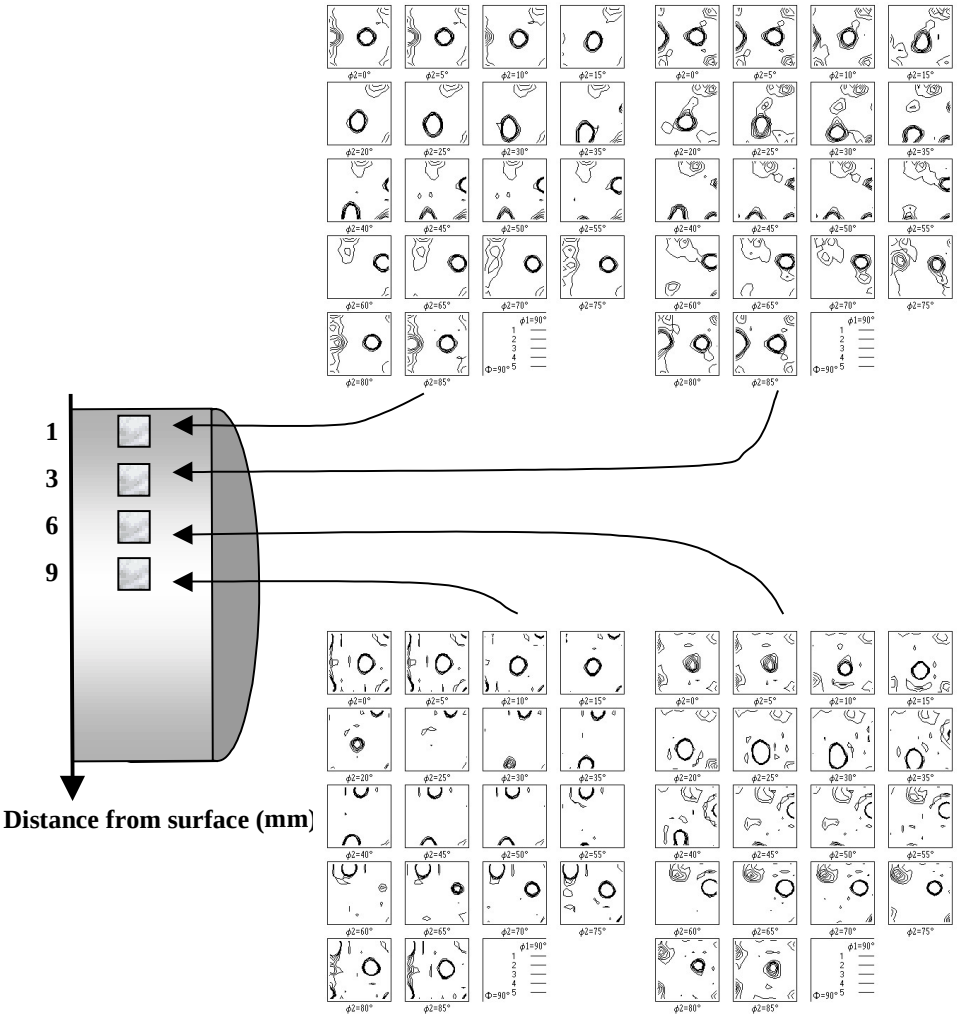

Figure 4.4.5 *ODF's from the areas shown in Figure 4.4.2. Investigations performed in SEM/EBSP. Alloy AA6082. Deformation temp.: 300°C. Reduction ratio=2.1.*

4.5 Numeric simulations performed in Forge2D.

All forward extrusion experiments are simulated in the numeric simulation programme Forge2©. Details concerning input data, material models and general information about the programme is given in Chapter 2.9.

The results from these simulations give valuable information about strain evolution, strain rates during the forming process, temperature evolution and forge load during the forming process.

The material model implies an exponential relationship between true stress and true strain. In compression, AA6082 reaches a steady state, while the alloy ''R'' shows an exponential curve. Therefore these simulations will give most reliable results when compared to the investigations performed on the alloy ''R''. The simulations are only part of the experimental work in this thesis, and the goal was to get results that would give reasonable indications on the material behaviour during the forward extrusion process. In agreement with these limitations, the simulation results are used in part III that concern recrystallization behaviour in the AA6082. The simulation results are discussed in greater detail in chapter 5.4.

4.5.1 Evolution of strain

In *Figure 4.5.2* and Figure 4.5.3 it is visualised how true strain varies over a cross section of the extruded bolt. Enlarged areas from these two figures are shown in Figure 4.5.4 and Figure 4.5.5. In the first stage of the press, the material flow is quite complex. This can be seen in the lower area in the end of the bolt on the figures. Therefore approximately 2 cm of the bolt were cut off from the end before cutting out specimen for investigations.
All figures show that the true strain in the centre reflects the total true strain for the bolt when reducing the diameter from 28.8mm to 19.5mm or to 24mm.
At the surface of the bolt the true strain is significant higher for all deformation temperatures and deformation grades. For the deformation to 19.5mm, the maximum true strain at the surface was calculated to be approximately 2.8 for the elevated temperatures, and 2.9 for deformation at room temperature. For deformation to a bolt diameter of 24mm, the

maximum, true strain at the surface was approximately 4.5 for all deformation temperatures.

When comparing corresponding values for radial distance from surface versus true strain, the increase in true strain is quite similar for all deformation temperatures as one moves from centre to surface. This observation is the same for both reduction ratios.

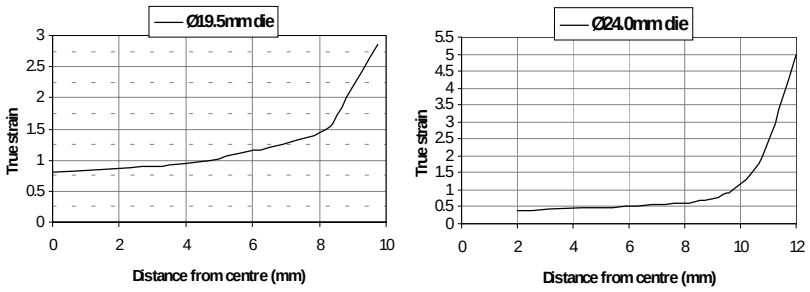

Figure 4.5.1 *True strain versus distance from centre. Both reduction ratios. Results are similar for all deformation temperatures.*

In *Figure 4.5.1* one observes how true strain increases as one move from the centre of the extruded bolt to the surface.
The centre zone where the true strain is quite similar to 0.8 for the 19.5mm bolt is limited to a radius of approximately 2 mm. As one observes, the true strain at 5 mm is 1.0 and at 8 mm it is almost 1.5. The true strain value increases rapidly in the 2 mm wide zone closest to the surface.
For the bolt with a diameter of 24.0 mm, a radius of approximately 3 mm limits the zone that reflects the true strain of 0.4. It then slowly increases as one moves closer to the surface, and from a point 8 mm from the centre with a value of 0.5, it increases rapidly in the 2mm wide zone closest to the surface.

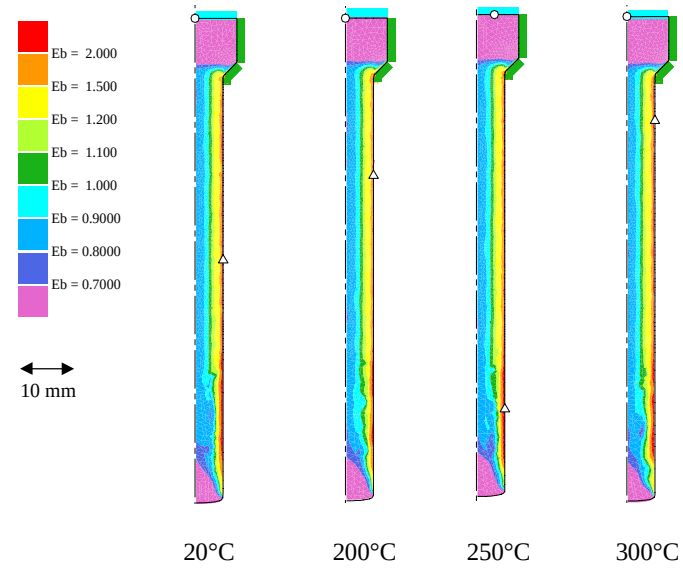

Figure 4.5.2 ***True strain.*** *Die diameter: Ø19.5 mm. Reduction ratio=2.1. Simulations for all deformation temperatures. Diagram to the left shows the simulated true strain value.*

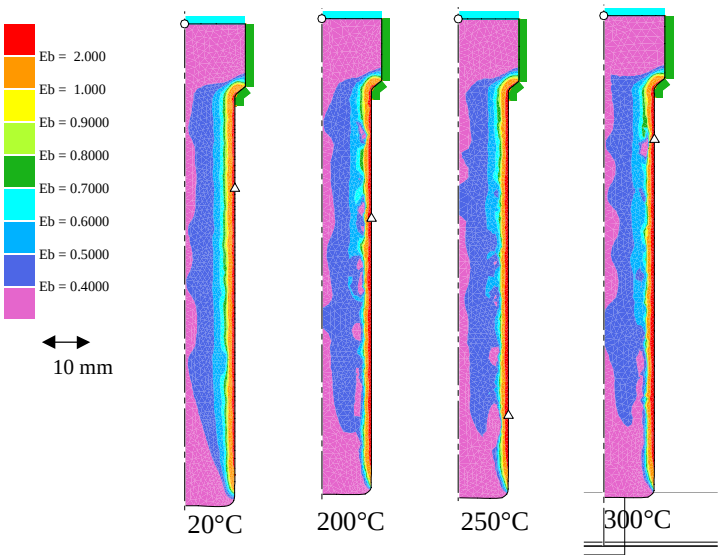

Figure 4.5.3 *True strain. Die diameter: Ø24.0 mm. Reduction ratio=1.4. Simulations for all deformation temperatures.*

URN:NBN:no-2108

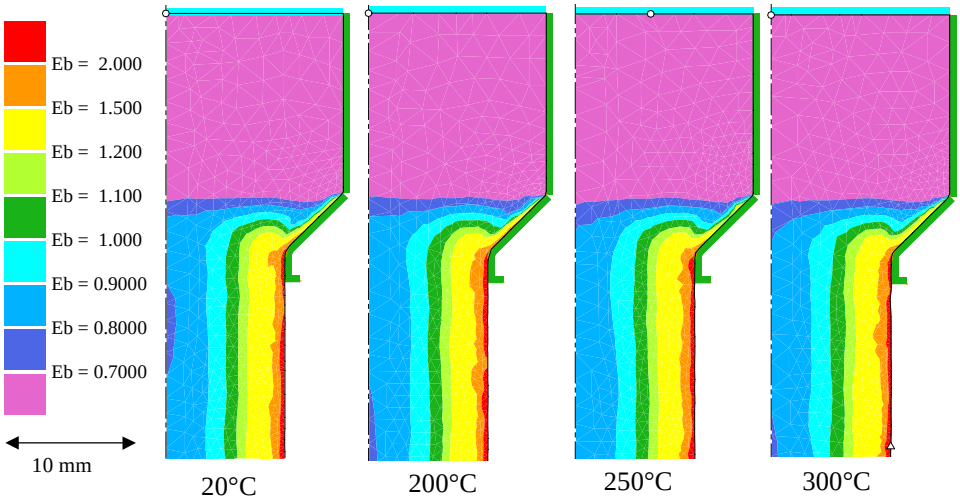

Figure 4.5.4 ***True strain.*** *Die diameter: Ø19.5 mm. Reduction ratio=2.1. Simulations for all deformation temperatures. Diagram to the left shows the simulated true strain value.*

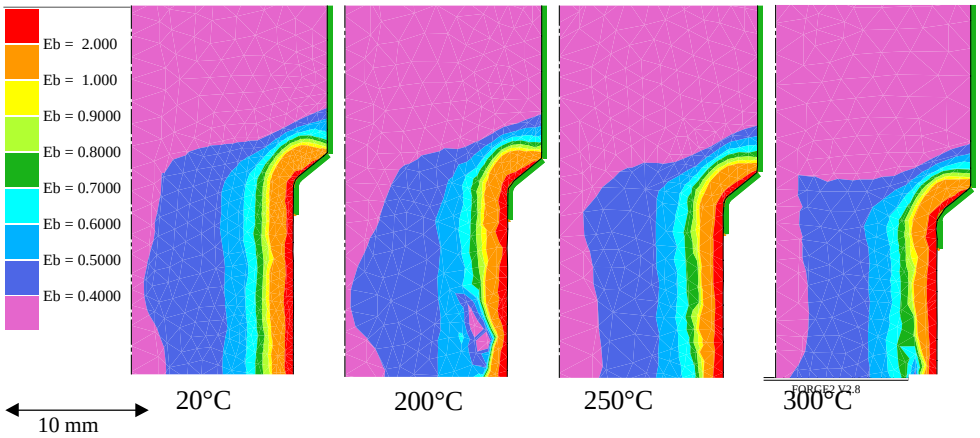

Figure 4.5.5 *True strain. Die diameter: Ø24.0 mm. Reduction ratio=1.4. Simulations for all deformation temperatures. Diagram to the left shows the simulated true strain value.*

URN:NBN:no-2108

4.5.2 Strain rate during forward extrusion

Each material element will follow a specific trace during the forward extrusion process. This trace is dependent on where the element was located in the start material bolt with a diameter of 28.8mm. As the extrusion process proceeds and each material element goes through the die, it will be given a strain rate according to what trace it follows through the die. As can be seen from *Figure 4.5.6* and *Figure 4.5.7*, the material that passes closest to the surface reaches the highest strain rate. For the bolt with an outer diameter of 19.5mm, it seems like the material in the centre part reaches a strain rate of 2.0 – 3.0/s during the forming process. Closer to the surface, the strain rate is quickly rising to maximum above 6.0/s. This is shown in *Figure 4.5.6*. In the next figure, -*Figure 4.5.7*, the strain rates in the 24.0m bolt is shown. For a wide centre region which covers almost 2/3 of the bolt diameter, the strain rate is found to be 0.5 – 1.0/s. Then, in the outer part of the bolt, it raises to over 6.0/s.

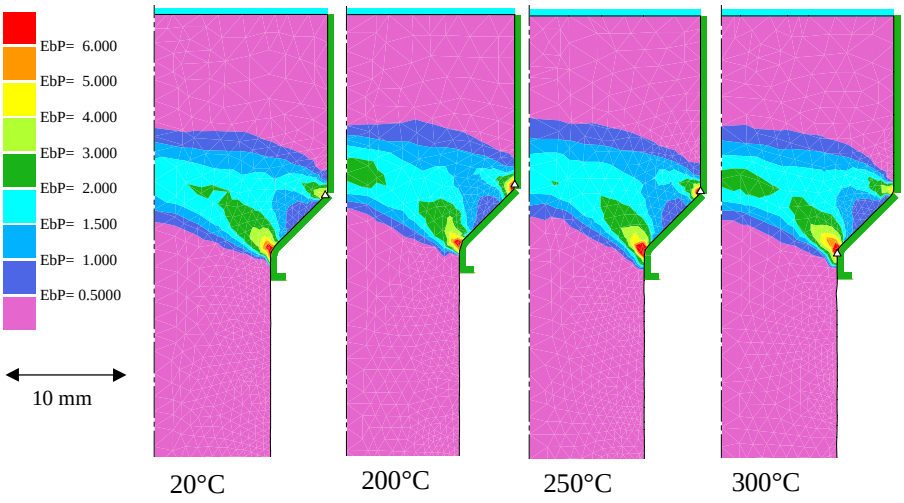

Figure 4.5.6 ***Strain rate.*** *Die diameter: Ø19.5 mm. Reduction ratio=2.1. Simulations for all deformation temperatures. Diagram to the left shows the simulated strain rates.*

URN:NBN:no-2108

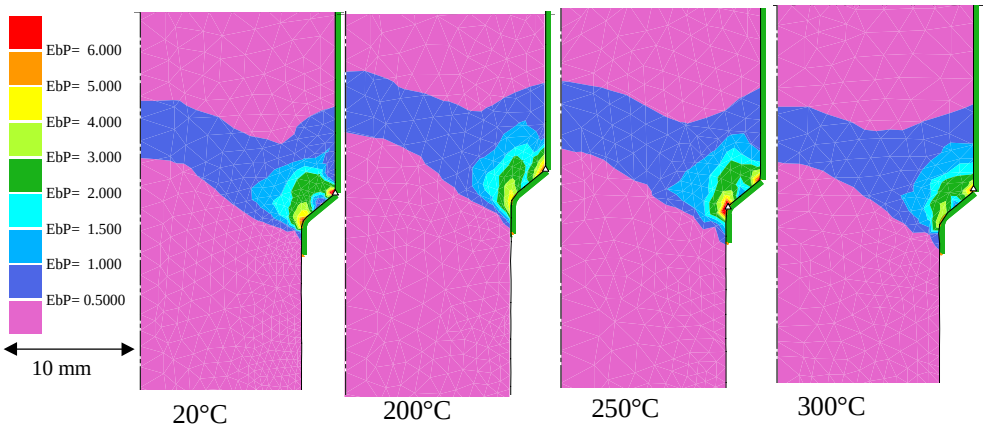

Figure 4.5.7 ***Strain rate.*** *Die diameter: Ø24.0 mm. Reduction ratio=1.4. Simulations for all deformation temperatures. Diagram to the left shows the simulated strain rates.*

4.5.3 Temperature evolution

Due to the reduction of the bolt radii and the friction between the die and the bolt, the temperature will raise as the deformation process goes on. In *Figure 4.5.8* and *Figure 4.5.9* this is shown for both reduction ratios. One observes that the temperature raise is significant for all deformation temperatures. The maximum temperature is reached at a corner of the die. The first part of the bolt that was pressed through the die did not get the same raise in temperature as the last part. For the highest reduction ratio, the temperature difference between the top and the bottom of the extruded material is between 20- 25°C. The bolt with the lowest reduction ratio had an corresponding temperature difference of the deformed material at 10-20 °C. The highest temperature difference reflects the lowest deformation temperature. In *Figure 4.5.10* The maximum and minimum temperature in the deformed bolt is shown for all deformation parameters. *Figure 4.5.11* illustrates the temperature evolution as a function of deformation temperature and reduction ration ratio. The Heat evolution is highest for the highest reduction ratio, and within the same die diameter the raise in temperature is highest the lower the deformation temperature is.

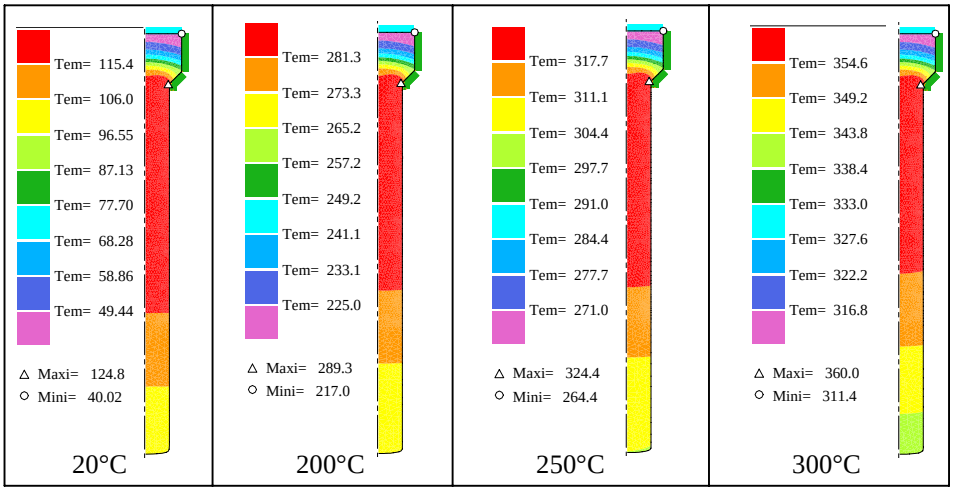

Figure 4.5.8 *Die diameter: Ø19.5 mm. Reduction ratio=2.1. Simulations for all deformation temperatures. Diagram to the left shows the temperature evolution.*

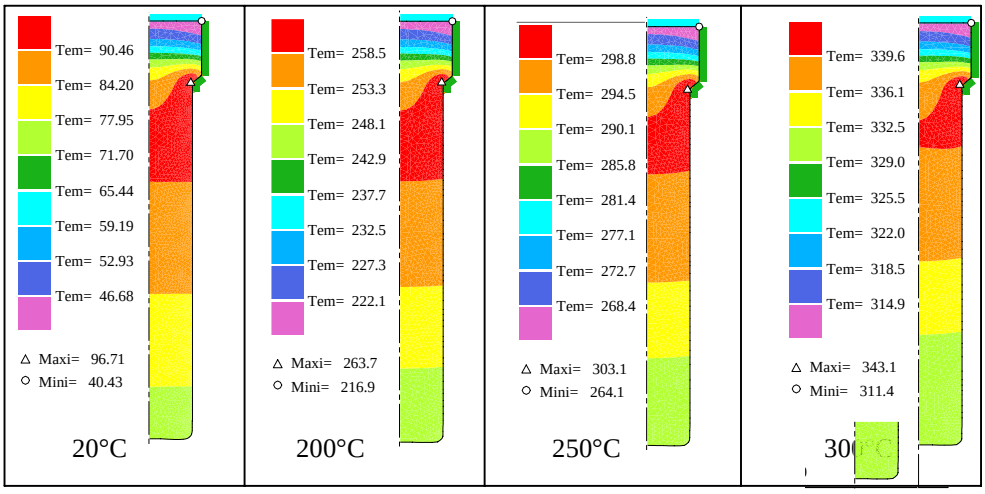

Figure 4.5.9 *Die diameter: Ø24.0 mm. Reduction ratio=1.4. Simulations for all deformation temperatures.*

URN:NBN:no-2108

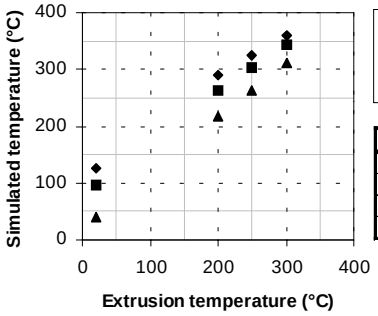

	R=2.1,max. °C	R=2.1,min.°C	R=1.4,max.°C	R=1.4,min.°C
20°C	125	40	97	40
200°C	289	217	264	217
250°C	324	264	303	264
300°C	360	311	343	311

Figure 4.5.10 *Simulated maximum and minimum temperatures for both reduction ratios. Data from Figure 4.5.8 and Figure 4.5.9.*

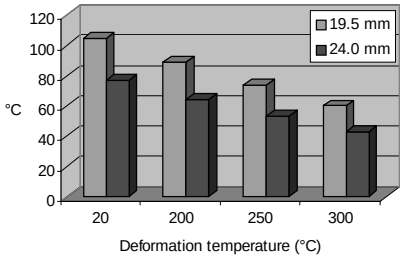

	19.5 mm	24.0 mm
20°C	105	77
200°C	89	64
250°C	74	53
300°C	60	43

Figure 4.5.11 *The maximum raise in temperature for both dies and all deformation temperatures during the forward extrusion process.*

4.5.4 Estimations of stress-strain relationships

The Forge2 programme has been used in an attempt to predict the required ram force for the forward extrusion experiments. The results are shown in *Figure 4.5.12* and *Figure 4.5.13*. The curves show that at the same deformation temperature, the highest reduction ratio demands the highest ram force. When performing the extrusion at different temperatures but with the same die, the higher the deformation temperature is the lower ram force is needed. Also all curves have the same shape. During the first stage of the

URN:NBN:no-2108

press, the ram force increases rapidly until a peak is reached. It then slowly decreases as the ram continues to press the material through the die.

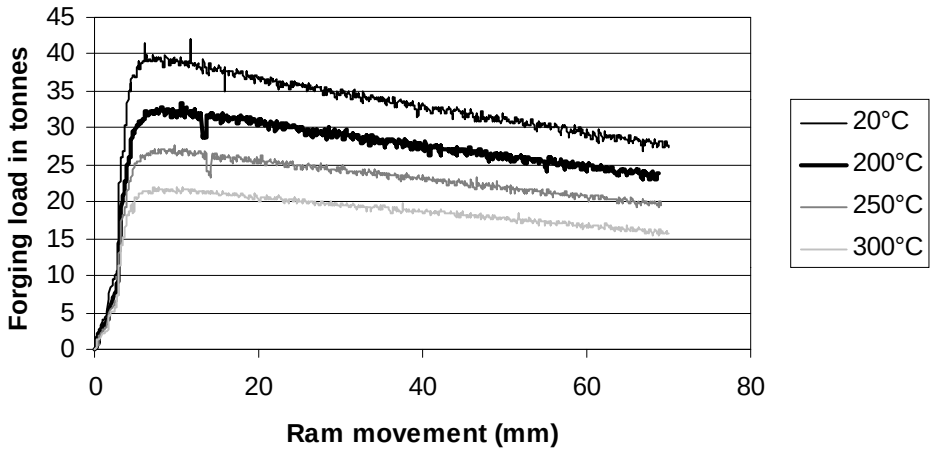

Figure 4.5.12 *Forging load as a function of ram position. Die diameter Ø19.5mm. Reduction ratio = 2.1. Simulations for all deformation temperatures.*

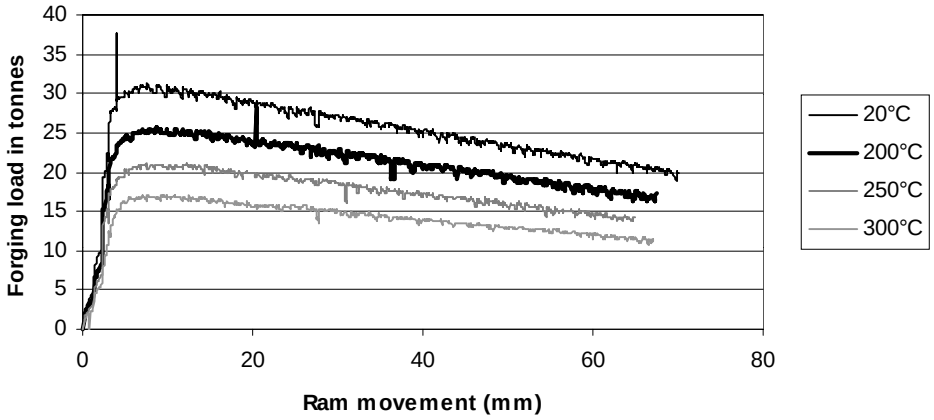

Figure 4.5.13 *Forging load as a function of ram position. Die diameter Ø24.0mm. Reduction ratio = 1.4. Simulations for all deformation temperatures.*

URN:NBN:no-2108

Part III: Recrystallization of deformed material

Heat treatment of the deformed material was performed at specific temperatures and holding times. This gave valuable information of the amount of stored energy in the extruded material as a result of different deformation parameters.

4.6 Recrystallization in centre and near surface of extruded bolt.

In this chapter, recrystallization of both AA6082 and Alloy "R" are investigated. The investigations are limited to grain measurements in the centre of the extruded bolts and to measurements in a heavily deformed zone approximately 1.5 mm from the surface. In all figures in Chapter 4.6, grain size means grain diameter in the radial direction.

4.6.1 Grain growth, basic observations.

In *Figure 4.6.1* bolts with extrusion temperature=250°C are batch annealed for increasing holding times. The microstructure is checked for recrystallization after 5, 15, 30, 60 and 900 seconds. The recrystallized grain size is measured in the centre and close to the surface.
The effect of Mn-containing dispersoids is evident as no grain growth is observed for all investigated specimens. The largest grains (app. 50µm) are found in the centre of the bolt with the smallest reduction ratio. Recrystallization in this specimen occurs after annealing in the range 15 to 30 seconds. The bolt with the highest deformation ratio has more stored energy available for nucleation of recrystallization. The microstructure in the centre of this bolt consist of grains with radial diameter, d=30µm. The smallest recrystallized grains are found close to the surface in bolts with both reduction ratios. One observes that the grain size is equal for R=0.2 and R=0.4.

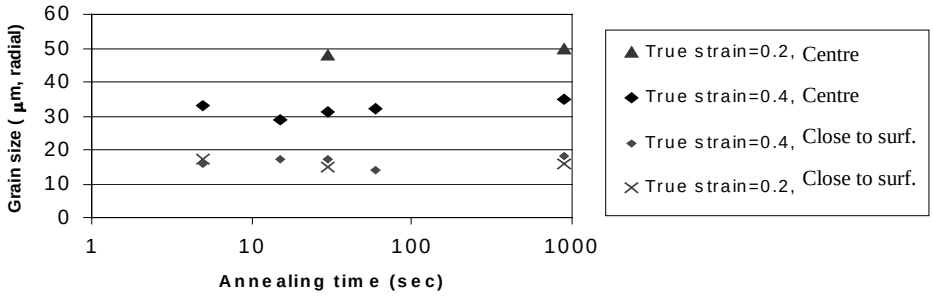

Figure 4.6.1 *Recrystallized grain size as a function of increasing holding times at 530°C. AA6082. Extrusion temp.: 250°C. Measurements performed at centre of extruded bolt and app. 1.5 mm from the surface.*

In *Figure 4.6.2*, the results from batch annealing of the Alloy "R" after deformation at 250°C is shown. Grain growth is observed in all specimen. Except from this observation, all conclusions are the same as for *Figure 4.6.1*. The largest deformation leads to the smallest recrystallized grains. One also observes that close to the surface, the grain size is independent of degree of reduction in the range 0.2 to 0.4.

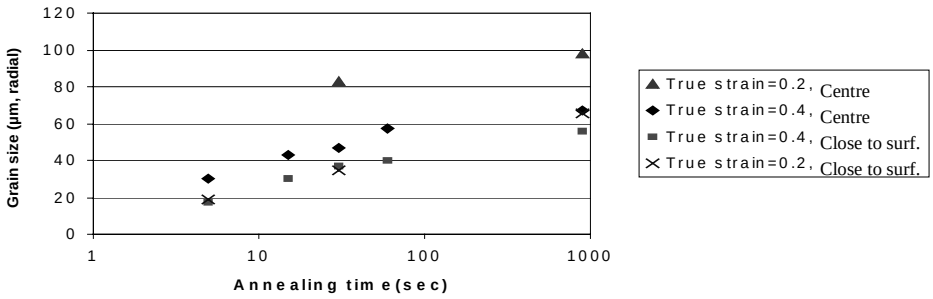

Figure 4.6.2 *Recrystallized grain size as a function of increasing holding times at 530°C. Alloy "R". Extrusion temp.: 250°C. Measurements performed at centre of extruded bolt and appr. 1.5 mm from the surface.*

URN:NBN:no-2108

4.6.2 Recrystallized grain size in AA6082 and Alloy "R".

In this chapter, the annealing temperature and the holding time are both constant ($T_{annealing}$= 530°C, $time_{annealing}$= 15 minute). Measurements are as in the previous chapter performed in the centre of the bolts and in an area close to the surface. The results are plotted versus the deformation temperature.

AA6082:
From *Figure 4.6.3* and *Figure 4.6.4* one observes that the recrystallized grain size increases as deformation temperature increases. Regarding the grain size closest to the surface, there is a slight tendency for grain size to increase with decreasing reduction ratio at the highest deformation temperatures. For the measurements performed in the centre, increased degree of reduction leads to a significant decrease in grain size at all deformation temperatures. For both reduction ratios, it is observed that a small increase in grain size is observed for deformation at 200°C and 250°C compared to extrusion at 20°C. As extrusion temperature reaches 300°C, grain size increase significantly.

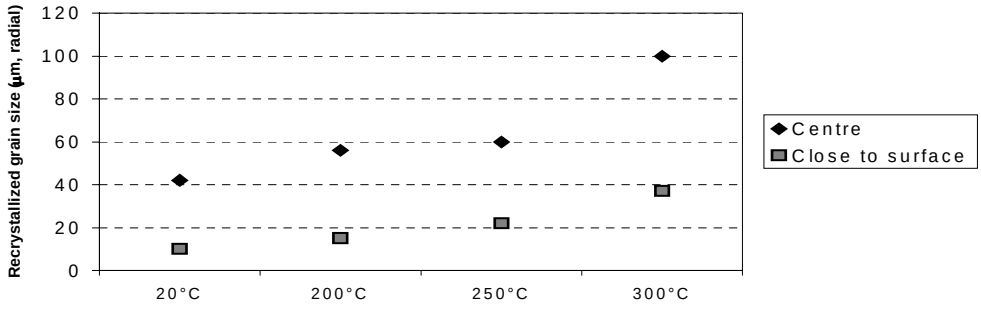

Figure 4.6.3 *Radial recrystallized grain size after annealing at 530°C for 15 minutes versus extrusion temperature. AA6082. Reduction ratio=1.4.*

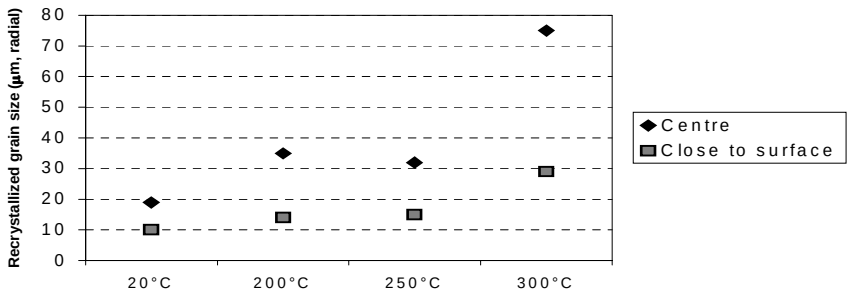

Figure 4.6.4 *Radial recrystallized grain size versus extrusion temperature. Annealed at 530°C for 15 minutes. AA6082. Reduction ratio=2.1.*

Alloy "R":

In *Figure 4.6.5* and *Figure 4.6.6*, the recrystallized grain size in the Alloy "R" is plotted as a function of annealing temperature. For measurements in the area close to the surface, approximately same grain size is found. This is typical 60µm in the radial direction, independent of deformation temperature or reduction ratio. However, in the centre the grain size increases as the deformation temperature increases for both reduction ratios. Also it is a common trend, that a small increase in grain size is observed for deformation at 200°C and 250°C compared to extrusion at 20°C. As extrusion temperature reaches 300°C, grain size increase significantly.

URN:NBN:no-2108

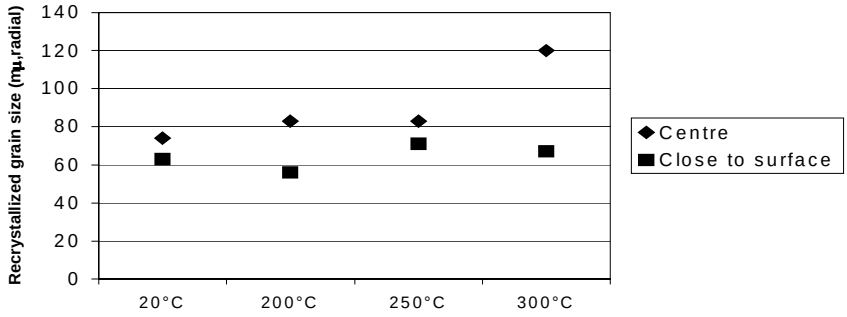

Figure 4.6.5 *Radial recrystallized grain size versus extrusion temperature. After annealing at 530°C for 15 minutes. Alloy "R". Reduction ratio=1.4.*

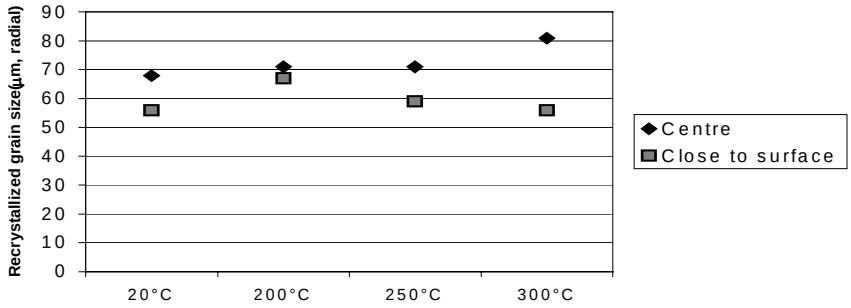

Figure 4.6.6 *Radial recrystallized grain size after annealing at 530°C for 15 minutes versus extrusion temperature. Alloy "R". Reduction ratio=2.1.*

4.7 Investigations performed on a cross section of the AA6082.

The results in this chapter are directly connected to Chapter 4.4. The same material and locations are investigated in both chapters. In Chapter 4.4, the deformed microstructure was carefully studied, but in these sections the same material has been heat treated at 530°C for 15 minutes. The material is the AA6082 that was extruded to a final diameter of 19.5 mm (R=2.1). In chapter 4.4, only results from the material that was deformed at 200°C and 300°C was given due to technical limitations with the equipment. As it is the recrystallized structure that is investigated in this chapter, it was possible to make accurate measurements on the bolt that was extruded at 20°C.

4.7.1 Characterising the recrystallized microstructure.

Grain size measurements:
Grain size measurements were performed from the EBSP data. In these results, there is a difference between the diameter in the radial/extrusion direction, and the grain diameter. The grain diameter is calculated from the formula for circle equivalent diameter, while the grain diameter in the radial direction, is the average length of the grain size in this direction.

From *Figure 4.7.1* and *Figure 4.7.2* one observes that the ratio obtained from dividing the grain diameter in the extrusion direction on the grain diameter in the radial direction is approximate 1.5 on the entire cross section of the bolt that was extruded at 20°C.
When increasing the extrusion temperature, the same ratio also increases. For the bolt extruded at 200°C, R=1.6 for measurements performed 1 and 3 mm from the surface, while it increases to 1.8 for the two measurements closest to the centre.
The recrystallized grains in the bolt that was extruded at 300°C are even more elongated in the extrusion direction on the entire cross-section. The ratio is approximate 2.0 close to the surface and 4.5 in the centre of the bolt.

URN:NBN:no-2108

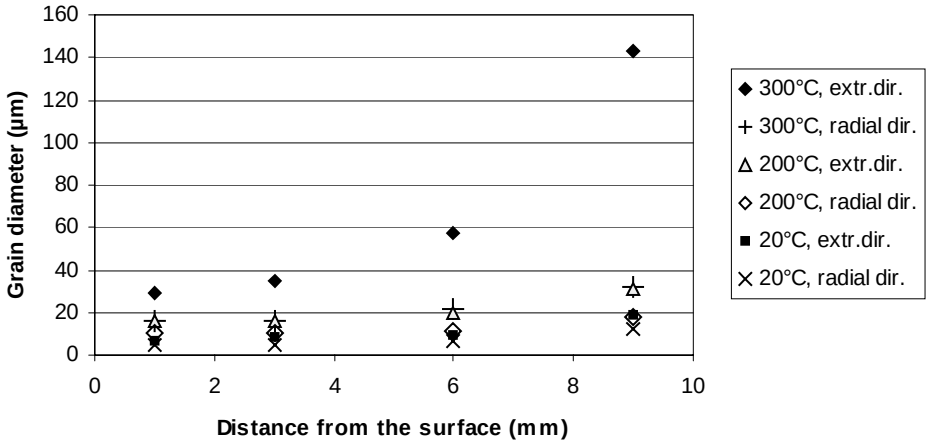

Figure 4.7.1 *Recrystallized grain size in the AA6082. Grain diameter in the radial- and extrusion direction is shown as a function of the distance from the bolt surface. Deformation temp. is given in [°C].*

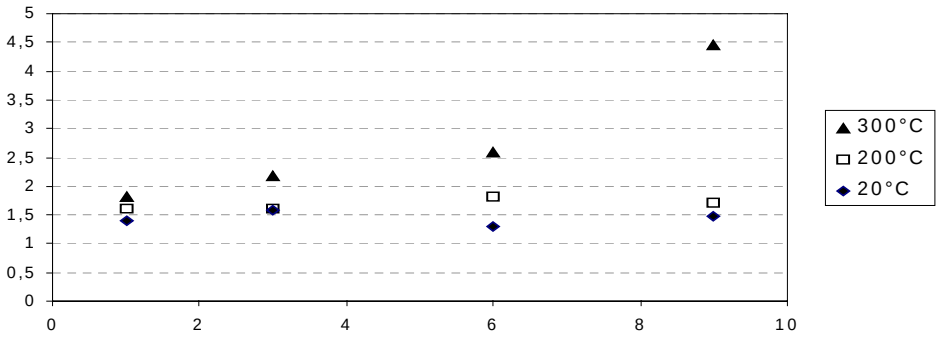

Figure 4.7.2 *The figure illustrates the ratio R=(grain diameter in the extrusion direction) / (grain diameter in the radial direction). The ratio is shown as a function of the distance from the bolt surface. Deformation temp. is given in [°C].*

URN:NBN:no-2108

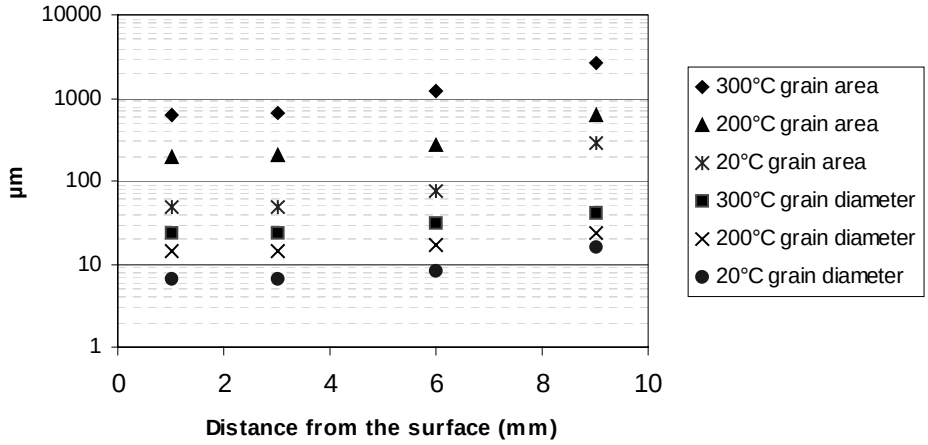

Figure 4.7.3 *Grain area and grain diameter plotted as a function of the distance from the bolt surface. The reduction ratio for the bolt is 2.1. Data are given in* Table 4.7.1

Table 4.7.1 Grain size data used in ***Figure 4.7.3***

	Grain area			Grain diameter		
	20°C	200°C	300°C	20°C	200°C	300°C
1 mm	48	195	615	6,7	14	24
3 mm	48	202	660	6,7	14,5	24
6 mm	77	278	1192	8,1	17	32
9 mm	280	640	2612	16	24	41

The recrystallized grain area increases significantly for all investigated specimen as on moves from the surface to the centre of the bolt. This is shown in *Figure 4.7.3*. The grain area in the bolts deformed at 20° is approximately identical for measurements performed 1 mm and 3 mm from the surface. Then, the grain area increases significantly closer to the centre. The same results are found for the bolt with extrusion temperature 200°C. The grain area in the bolt that was deformed at 300°C increases in an exponential way from the surface to the centre of the bolt.

Texture measurements:
From the EBSP investigations, the texture distribution was analysed. All investigated areas from all deformation temperatures gave the same result. The texture components were randomly distributed in all specimens.

URN:NBN:no-2108

4.7.2 Microstructure – Illustrations from the EBSP work.

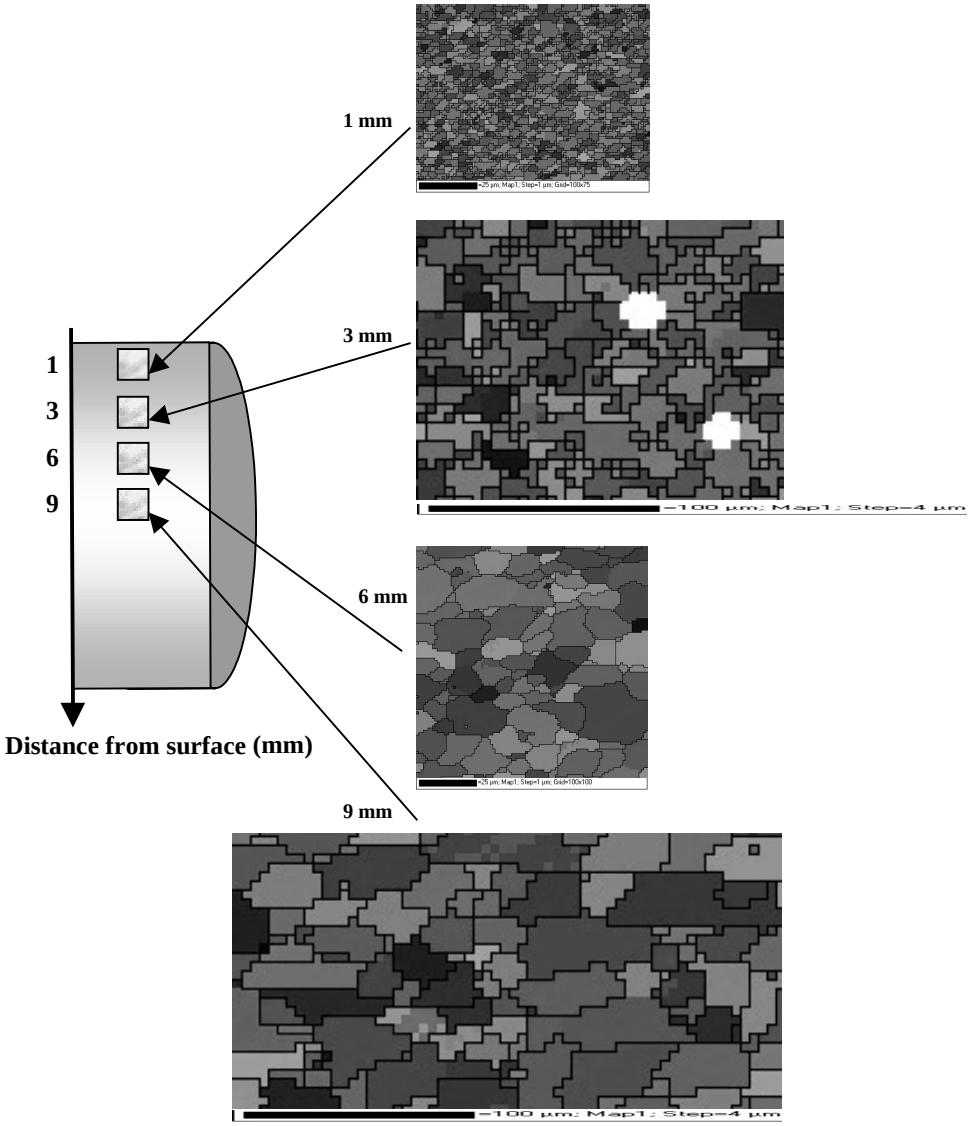

Figure 4.7.4 *Microstructure after annealing at 530°C for 15 minutes. Investigations performed in SEM/EBSP. Alloy AA6082. Deformation temp., T_{def}=20°C. Reduction ratio=2.1.*

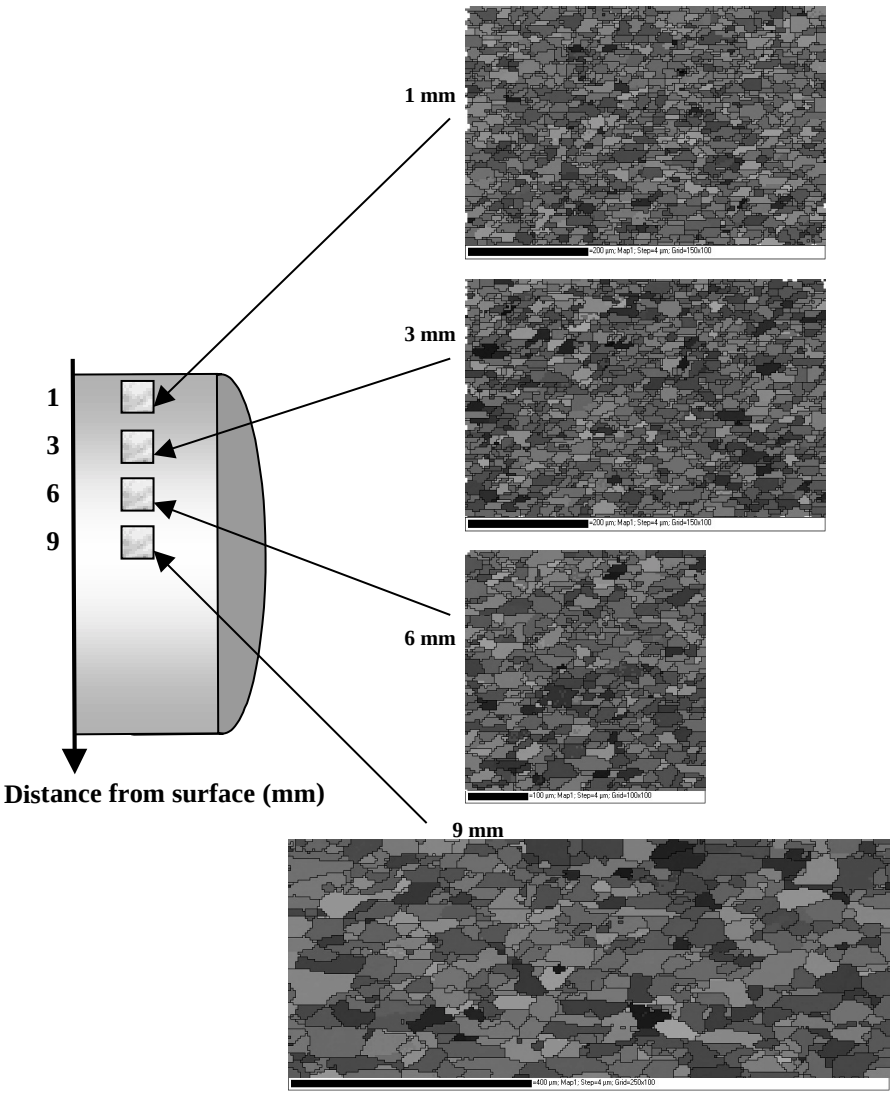

Figure 4.7.5 *Microstructure after annealing at 530°C for 15 minutes. Investigations performed in SEM/EBSP. Alloy AA6082. Deformation temp., T_{def}=200°C. Reduction ratio=2.1.*

URN:NBN:no-2108

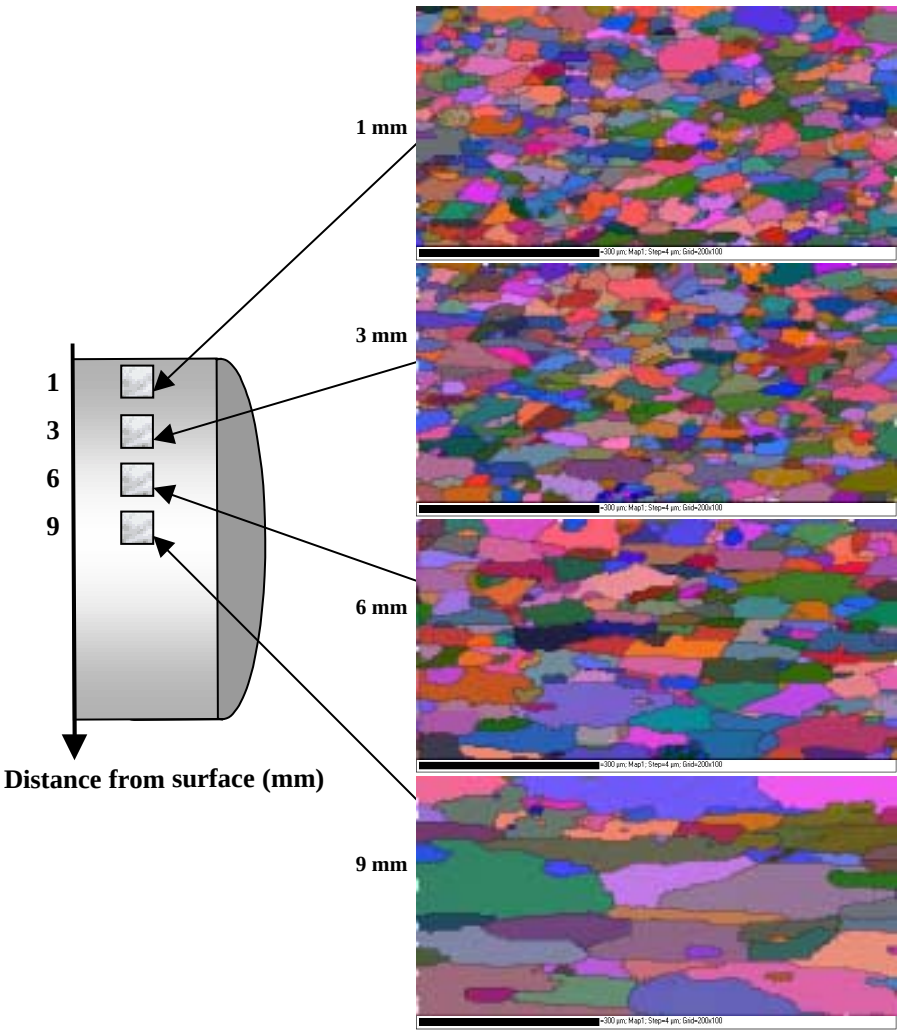

Figure 4.7.6 *Microstructure after annealing at 530°C for 15 minutes. Investigations performed in SEM/EBSP. Alloy AA6082. Deformation temp., T_{def}=300°C. Reduction ratio=2.1.*

4.8 Limits for recrystallization.

In this chapter, recrystallization in the AA6082 is investigated. The aim for these investigations is to measure the radial length of the recrystallized area on a cross section of the bolt.

4.8.1 Recrystallization as a result of varying annealing temperature.

The material is exposed to three different annealing temperatures in the range 400°C to 530C. The latter is the temperature for solution treatment. Holding temperature is 15 minutes for every heat treatment. As shown earlier there is no grain growth in this alloy. In these investigations the recrystallization in the bolt that was extruded at 250°C to a reduction ratio R=2.1 and R=1.4 is studied. Since 250°C is a typical "moderate temperature" for the experiments in this project, this deformation temperature is chosen.

Reduction ratio, R=2.1:
As can be seen from Figure 4.8.1 even the lowest annealing temperature at 400°C transformed the bolt into a fully recrystallized material.

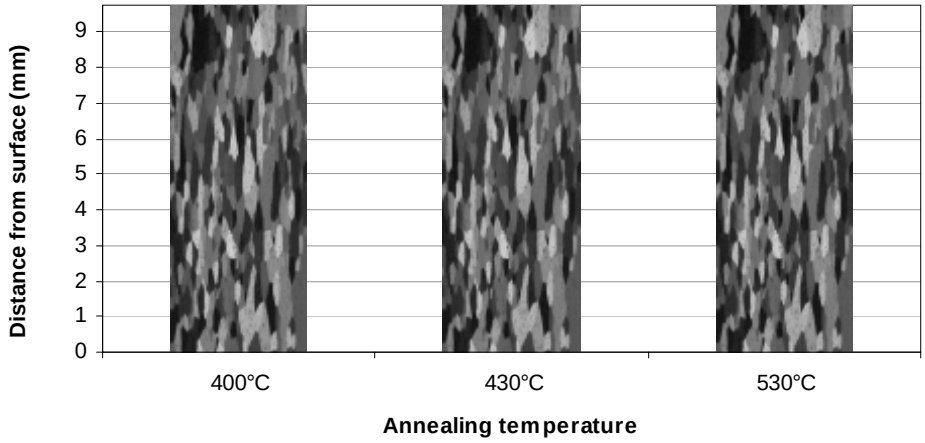

Figure 4.8.1 *Radial length of recrystallized area.*
Holding time at annealing temperature: 15 min.
Deformation temperature: 250°C, Die diameter: 19.5 mm

URN:NBN:no-2108

Reduction ratio, R=1.4:
From Figure 4.8.2 one observes that the material is fully recrystallized only for the bolt that was annealed at the highest deformation temperature.

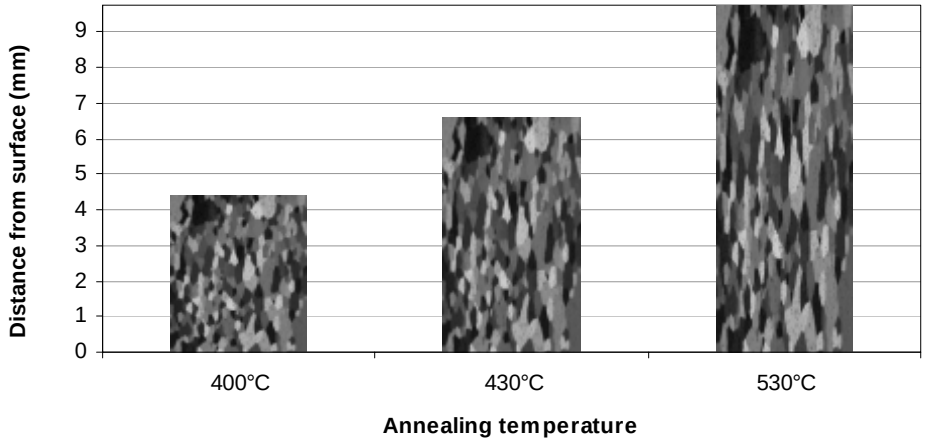

Figure 4.8.2 *Radial length of recrystallized area.*
Holding time at annealing temperature: 15 min.
Deformation temperature: 250°C,
Die diameter: 24.0 mm

4.8.2 Recrystallization as a result of different deformation parameters.

The annealing temperature of 430°C was chosen for these tests due to recrystallization behaviour observed in the previous chapter. Test specimens from all extrusion temperatures are investigated carefully, and they are held at annealing temperature for 15 minutes.

Bolts with reduction ratio, R=2.1:
As can be seen from Figure 4.8.3, only the bolt that was deformed at the highest temperature (T=300°C) did not recrystallize through the entire material thickness. A tendency of coarser grains due to higher extrusion temperature was observed.

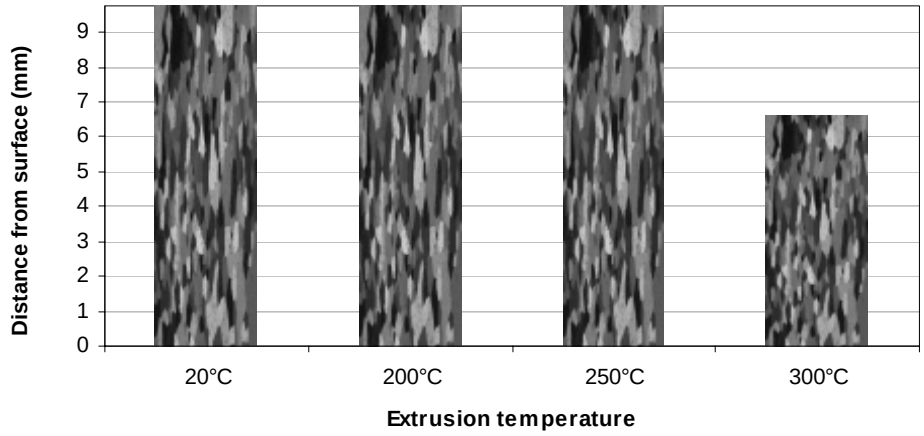

Figure 4.8.3 *Radial length of recrystallized area.*
Holding time at annealing temperature: 15 min.
Annealing temperature: 430°C, Die diameter: 19.5 mm.

Bolts with reduction ratio, R=1.4:

From Figure 4.8.4 one observes that only the bolt deformed at 20°C recrystallized completely as a result of annealing at 430°C for 15 minutes. The bolt that was deformed at 200°C was fully recrystallized in 7.2 mm of the material closet to the surface. This can also be seen in the figure. However, what the figure doesn't show is that on the remaining length from 7.2 mm to the centre, the material was partly recrystallized. In all other investigated specimens, a clear circular line could be drawn in order to see how deep into the material the structure was recrystallized. This indicates that the centre part of this bolt has extrusion parameters, which leaves it in the limit zone for recrystallization at 430°C. Coarser grains were also observed as deformation temperature was increased for annealing at 430°C for 15 minutes.

URN:NBN:no-2108

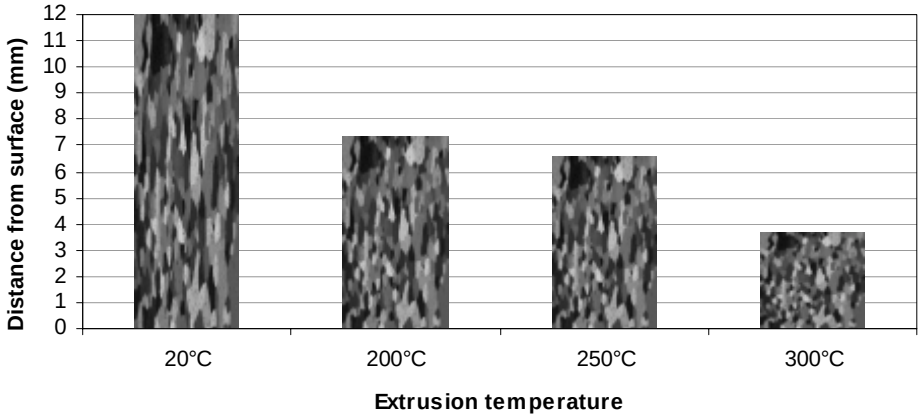

Figure 4.8.4 *Radial length of recrystallized area.*
Holding time at annealing temperature: 15 min.
Annealing temperature: 430°C, Die diameter: 24.0 mm.

5. DISCUSSION

In this chapter, the results presented in chapter 4 are discussed in detail. Comparisons of microstructure and testing conditions are done in order to determine the effect from variations in the chemical composition and from different deformation parameters on the resulting deformation microstructure. Concerning the recrystallization mechanisms of the investigated alloys, relationships between deformed microstructure, chemical composition, and annealing parameters are discussed. The numeric simulations performed in Forge 2D are compared to experimental results.

5.1 Evaluation of the lubrication efficiency in the temperature range 20°C–300°C:

A critical parameter in the forming operations performed in this work, is the friction between the materiel and the forming tools. Increased friction will influence on the material flow in the test piece. Sticking between the material and the tool may increase true strain close to the surface in the material. Also, increased friction may lead to increased temperature during the forming process. The raise in temperature may affect the material properties and also the material flow characteristics.

A lubrication process developed by Raufoss Technology ASA was used to minimize friction during the forming operations. This is described in Chapter 3.4.2.

For material that was deformed at 300°C, one observed that the coating had turned brown during the deformation. Valle (1999) pointed out that sodium stearate may be used as lubricant up to about 250°C, where chemical reactions destroy its lubrication capacity. Despite this conclusion, there was no sign of significant sticking in the forward extrusion experiments performed at 300°C. This observation may be due to the combined effect of the two layer lubricant coating. Valle also points out that the calcium aluminate layer has excellent lubrication performance, and it is possible that

URN:NBN:no-2108

this keeps up the total lubrication effect from the coating. Therefore, the effect from increased
friction at higher deformation temperatures is neglected as the results from the forming operations are investigated.

As indicated from the numeric simulations in Forge 2D, there is a significant temperature raise during the forward extrusion process. This is observed despite the fact that friction is held as a constant in the simulations. In the forming experiments, the expected small amount of raise in friction at high temperatures gives a small raise in the ram force. The increase in temperature will lead to reduced mechanical properties and hence a softer material. Therefore, as the true strain – true stress curves are discussed, the effect from higher friction at higher deformation temperatures are not taken into consideration.

5.2 Stress-Strain relationship.

Investigating the stress-strain relationships from both the compression testing and the forward extrusion experiments gives important information about the alloys. In this chapter, the results shown in chapter 4.1 and 4.2 are discussed in detail. It is shown how microstructural differences influence on the mechanical properties of the material.

5.2.1 Effect of Si-content on the stress-strain relationship.

To study the effect of Si-content, a comparison of the two alloys without manganese is performed. These alloys have a recrystallized microstructure before the compression testing experiments. The AA6063 has a Si-content of 0.45wt% and the “Alloy R” has a Si-content that is almost 2 times higher (0.87wt% Si). The grain size before compression testing was not measured. However, because the process parameters for both alloys are similar, the grain size is not considered to be significant different in the two alloys. Because there is no microscopy investigation to confirm this, an assumption of slightly smaller grains in the alloy with the highest Si-content (“Alloy R”) is made. Large Si-rich particle may have acted as nucleation sites of

recrystallization and hence raised the concentration of potential sites for nucleation of recrystallization. Also, Si may have

reduced the grain mobility and reduced the grain size. Anyway, as the main difference in the composition of the two alloys is the Si-content, the effect from increased content of Si can be seen out of the true stress - true strain curves for the alloys ”R” and 6063 in Figure 5.1.

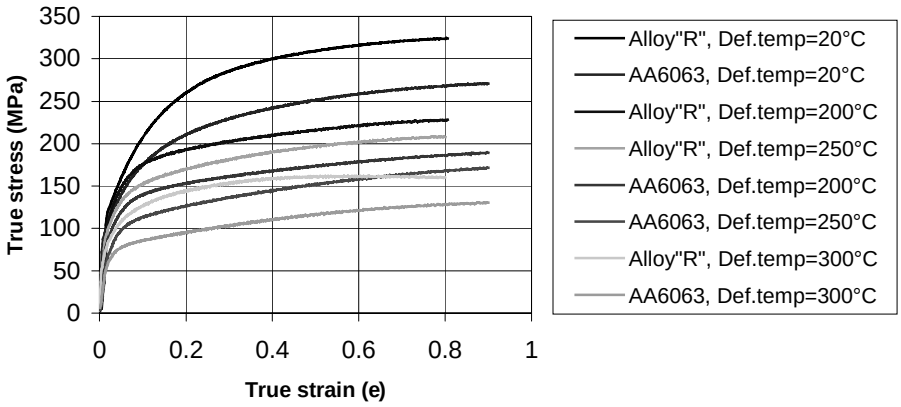

Figure 5.1 *The stress-strain curve for AA6063 and alloy ”R”. Piston rate=1/s, T4-condition. The figure shows variations in true stress versus true strain for both alloys as the deformation temperature varies.*

As can be seen from Figure 5.1, the alloy “R” with the highest Si-content requires the highest true stress for a given true strain value and deformation temperature. For this alloy a true strain of 0.8 corresponds to a true stress of 325 MPa at room temperature testing. As the deformation temperature is increased with 180 degrees Celsius, a significant drop in true stress of approximately 100 MPa is observed. Further raise in temperature to 300°C reduces the true stress with additional 70 MPa. From this it is obvious that deformation at higher temperature reduces the true stress needed to deform the material. This is well known as the needed activation energy for dislocation mobility is reduced as the material temperature is increased. D.Altenpohl (1965, pp223-232). Higher temperature alters the rate of recovery (R) through its effect on dislocation climb as shown in equation 5-1.

URN:NBN:no-2108

$$R = K\exp(\frac{-Q}{kT}) \qquad \text{Equation 5-1}$$

Q is typically equal to the activation energy for self-diffusion in Al (140kJ). Humphreys J. (1999).

The compression of the alloy "R" at a deformation temperature of 300°C is the only curve that shows a tendency of reaching a "steady state" stress level. This indicates that dislocations are formed at the same rate as they are eliminated.

The true stress-true strain curve for the alloy AA6063 shows the same curves as for alloy "R" with respect to variations in deformation temperature. For the same deformation temperature and same true strain, the true stress for the deformation of the "R"-alloy is significantly higher than for the AA6063-alloy. The reason for this is supposed to be related to the difference in the Si-content. It is well known that Si has an effect on the strength of aluminium alloys due to solid solution strengthening. The silicon atom has a significant larger atomic radius compared to the atomic radius of the Al atom. The relatively large Si-atoms introduce stress forces in the atomic structure and reduce the possibility of dislocation movements. E. Nes showed that for particle-strengthened alloys (AA1xxx, AA8xxx), both n (strain hardening exponent) and K (from Hollomon: $\sigma=K\varepsilon^n$) varies strongly with alloy content (Fe+Si). As wt%Si increases, n decreases and K increases. Nes E. (1987).

5.2.2 Effect of Mn-content on the stress-strain relationship.

In this chapter, alloys that can only be distinguished by a different Mn-content are compared. Discussions are made for comparisons of the AA6082 and the "Alloy R" for different deformation temperatures, different piston rate and different heat treatment condition:

In Figure 5.2. the two alloys AA6082 and the modified alloy "R" are compared from experiments where the piston rate was the same (1mm/s). For the same deformation temperature, one observes that as true strain increases, the true stress for the two different alloys reaches the same value after a certain amount of deformation. This point where the curves for the

two alloys crosses at the same deformation temperature, is not given by a constant true strain value. This true strain value increases as deformation temperature decreases. For the highest deformation temperature, the true stress-true train curve for both materials meet at approximately $\dot{\varepsilon}$=0.4. For deformation at room temperature, the curves have not reached a common true stress value at true strain value of 0.8.
This variation is explained by the fact that the "Alloy R" reaches the steady state condition at a higher true strain value than for the Mn-containing alloy for all deformation temperatures. The AA6082 reaches steady state condition between app. $\dot{\varepsilon}$= 0.18 (deformation at 300°C) and $\dot{\varepsilon}$= 0.2 (room temperature deformation). The "Alloy R" reaches steady state condition between app. $\dot{\varepsilon}$= 0.4 (deformation at 300°C) and $\dot{\varepsilon}$> 0.8 (room temperature deformation).

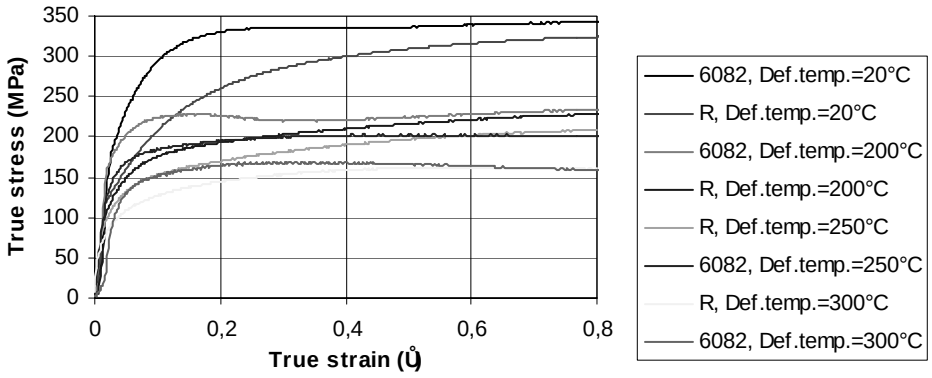

Figure 5.2 *True stress-true strain curves for the AA6082 and the modified alloy "R". T4 condition, Piston rate=1mm/s. The effect of manganese on the true stress curve.*

The phenomena "steady state" is related to the formation of dislocations and annihilation mechanisms as dislocation interact with each other in the microstructure. This is shown in equation 5-2. Equation 5-3 gives the relationship between dislocation density (ρ) and the flow stress. From this

URN:NBN:no-2108

equation, the effect of constant dislocation density and constant subgrain size on the flow stress can easily be seen, Nes and Martinsen (1999)

Stress saturation:

$$\frac{d\rho^{-}}{d\gamma} + \frac{d\rho^{+}}{d\gamma} = 0 \qquad \text{Equation 5-2}$$

The first part of equation 5-2 represents the annihilation of dislocations, and the second part represents the formation of dislocations.

Flow stress:

$$\tau = \tau_i + \alpha_1 Gb\sqrt{\rho_i} + \frac{\alpha_2 Gb}{\delta} \qquad \text{Equation 5-3}$$

In order to investigate the effect from Mn at very small strains, the left corner of Figure 5.2 is shown in Figure 5.3. It shows that at very small strains (Ů<0.04) there is no effect of the Mn-content on the stress-strain curve. For this observation, one must take into consideration that at this detailed level, the resolution of the equipment might not be good enough to give exact values of the true stress-true strain.

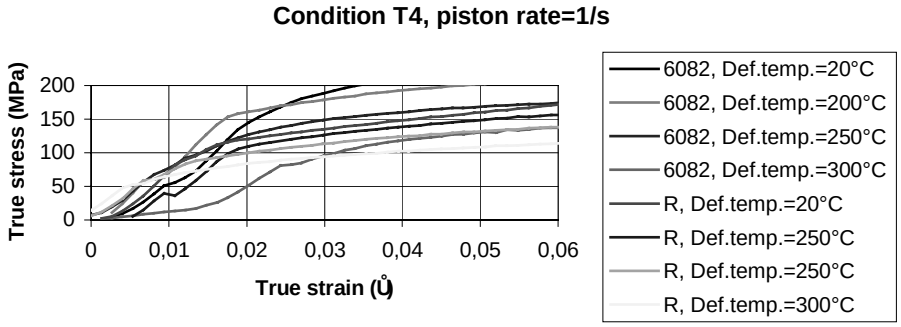

Figure 5.3 *Magnified area of Figure 5.2. High resolution of the area at small strains.*

5.2.3 Effect of changing the strain rate on the mechanical properties.

Compression tests of both alloys were performed at three different strain rates. As can be seen on Figure 5.4, there was no significant effect of change in strain rate during compression testing at room temperature or at 300°C. However, a common observation was made: For the lowest strain rate, the highest true stress value was found for a given value of true strain. An explanation for this might be the heat evolution at high temperatures. The higher the deformation rate is, the more heat evolution takes place during the deformation process. This elevation of the material temperature causes a softer material where dislocations can move easier. Form this follows the observation that the true stress is lowered as the deformation rate is elevated.

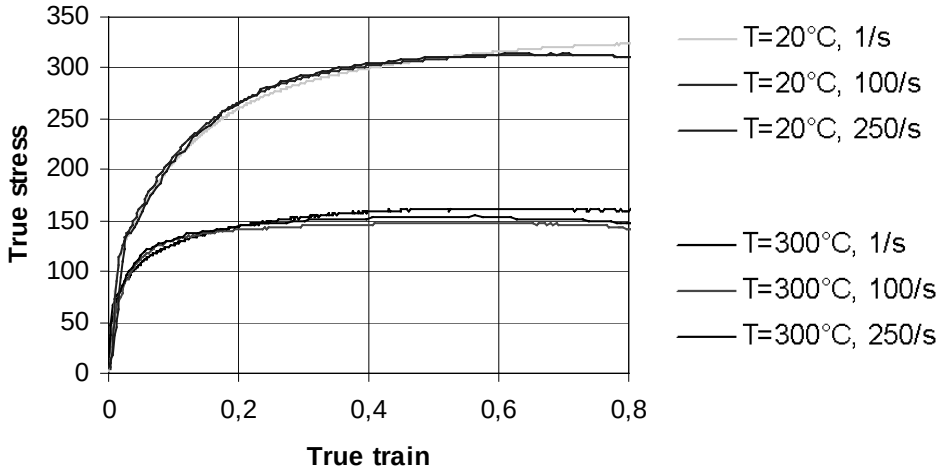

Figure 5.4 *Alloy "R", Compression temperature=20°C and 300°C. All piston rates. Heat treatment condition: T4.*

URN:NBN:no-2108

5.2.4 Effect from heat treatment condition on the mechanical properties.

The AA6082 and the "Alloy R" was formed by compression in two different conditions. In the rest of this work, only material in the T4-condition has been discussed. The additional condition that will be discussed here is the W-condition. Unfortunately, only one test specimen could be prepared for each alloy, and the uncertainty due to this fact has to be taken into consideration as these results are discussed.

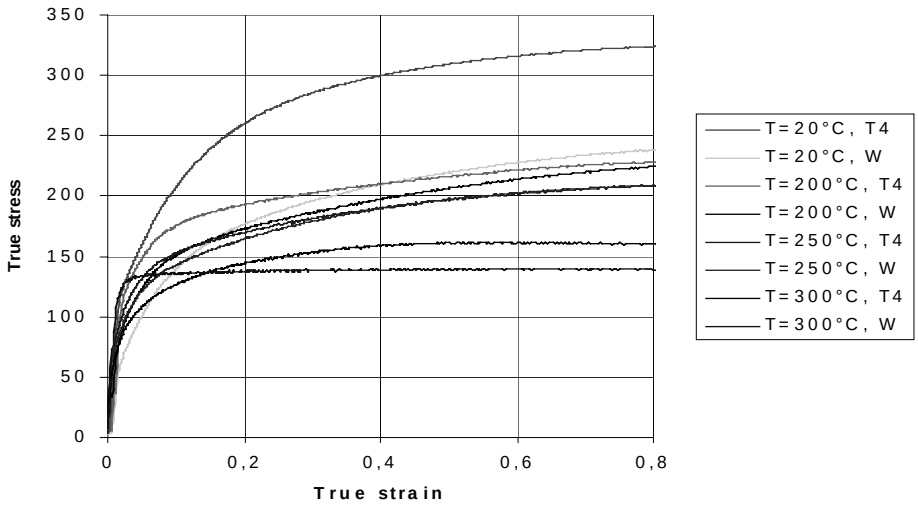

Figure 5.5 *Alloy R. The effect from different heat treatment conditions on the mechanical properties. Piston rate= 1/s.*

As can be seen from Figure 5.5, for a true strain value of 0.8, the two lines that corresponds to the highest true stress is for the test that was performed at 20°C. The two next lines with decreasing values of true stress is for the test performed at 200°, and then every next two lines is connected to increasing deformation temperature. This decrease in true stress for higher deformation temperatures is in correlation with observations that are discussed earlier. What is also observed in Figure 5.5, is that for every deformation temperature, the highest true stress is connected to the T4 temper, and the lowest true stress value is connected to the W-temper. For the test that was performed at room temperature, the difference is significant (almost 100 MPa), but for the higher deformation temperatures, there is only

a small difference in the true stress value. The difference in the strength for the alloy in the T4 condition and the alloy in the W-condition is due to micro structural changes that take place during the different heat treatment operations. Both alloys were solution annealed at 530°C for sufficient length of time to dissolve particles containing alloying elements. The alloying elements are distributed in the matrix. For the T4 temper, the material has been held at room temperature for sufficient length of time for the alloying elements to cluster and form new strengthening zones. The W condition is not a completely correct definition as a result of the heat treatment in connection to the forming operations. After the test specimen had been solution annealed, they were kept in liquid Nitrogen until they were placed in the specimen chamber for compression testing. This chamber was preheated to the desired test temperature. The ram, which also was preheated, moved until it touched the test specimen. It was then held in contact with the test piece for 1 minute in order to secure that the test temperature was constant and uniform through the entire thickness of the specimen. During this holding time, the raise in temperature may affect the distribution of the alloying elements in the material. A strengthening effect is supposed to take place, and this is the reason for the similarity of the true stress –true strain curves for each deformation temperature.

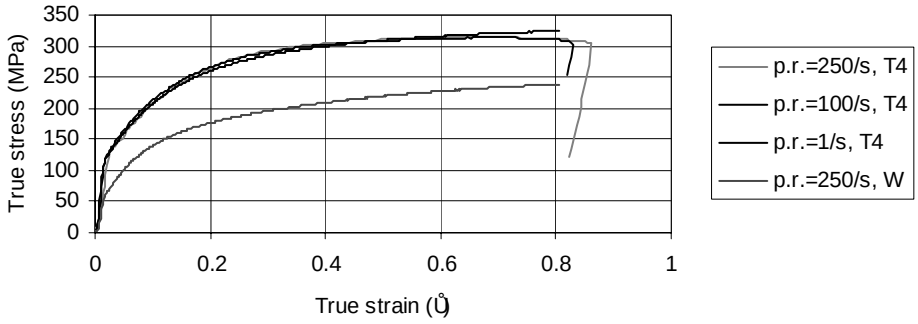

Figure 5.6 Alloy ”R”, Def.temp.=20°C

As can be seen in Figure 5.6, no effect on the true stress-true strain relationship was observe in the Alloy “R” due to variations in the ram speed. It hence illustrates that the W-condition has significant lower true stress for given values of true train compared to all test in the T4 condition.

URN:NBN:no-2108

5.3 Forward Extrusion experiments.

The forward extrusion experiments gave valuable results for microscope investigations on the cross section of an extruded test specimen. Also the stress-strain curve that was found was useful in order to see how temperature influenced on the mechanical. In addition the effect from reducing the die diameter could be investigated.
In order to investigate the stress-strain curves, two pairs of true tress – true strain data were chosen from every test. These values are referred to as "peak force" and "final force" in the following figures. The "peak force" is the "break through" force, which means the maximum external force that is needed in order to make the material start flowing through the die. Often this is seen as a "needle shape" on the true stress true strain curve at the lowest values for true strain. The "final force" is the true stress value at the end of the forward extrusion experiment. The ram moved exactly the same distance in all experiments, thus these values are comparable for all tests.

In Figure 5.7 and Figure 5.8, the "peak force" and the "final force" for all experiments are shown. The data from the forward extrusion performed at the smallest true strain value and the highest deformation temperature, are missing. Unfortunately, the equipment used for registration of the ram force was damaged during these tests.

Several conclusions can be drawn from Figure 5.7 and Figure 5.8:

- Both "the peak force" and the "final force" increase with decreasing deformation temperature. The difference in ram force is significant as temperature is reduced from room temperature to 200°C. The results from testing performed at 200°C and 250°C are slightly lowered at the highest temperature, and the ram force for testing at 250° and 300°C are almost identical.

- It is interesting to observe the relationship between the "peak force" and the "final force" as deformation temperature is lowered. At room

temperature, it is a difference of almost 100kN between these ram force values. This means that the breakthrough force that is needed is significant, compared to the force needed to push the test piece through the die as the deformation process has started. As deformation temperature is raised, the difference between the "peak force" and the "final force is" smaller, and it is almost negligible as extrusion at 250°C and 300°C are compared. These observations are believed to be strongly connected to the well-known relationship between temperature and dislocation movement. The activation energy for dislocation movement is reduced as the temperature is increased.

- When comparing the two alloys, one observes that for the same deformation temperature and identical die diameters, the ram force is the same. The "alloy R" and the AA6082 did not show this relationship in the compression testing at low values of true strain (<0.8). As shown in Figure 5.2, the curves for the two different alloys have the same true stress values at true strain values of 0.8 and higher. As shown in chapter 4.5.1, the simulated values for true strain shows that in the centre it is approximately the true strain value that corresponds to the reduction ratio of the extruded specimen. Closer to the surface, the true strain value increases significantly. This means that the extruded test specimen has high true strain values (>0.8) on the entire cross section. Seen in connection to Figure 5.2, this explains why there is no difference between the two alloys in Figure 5.7 and Figure 5.8. On a microscopic scale, one concludes that Mn has no significant effect on the strength of the alloy in the investigated temper and at these deformation parameters.

URN:NBN:no-2108

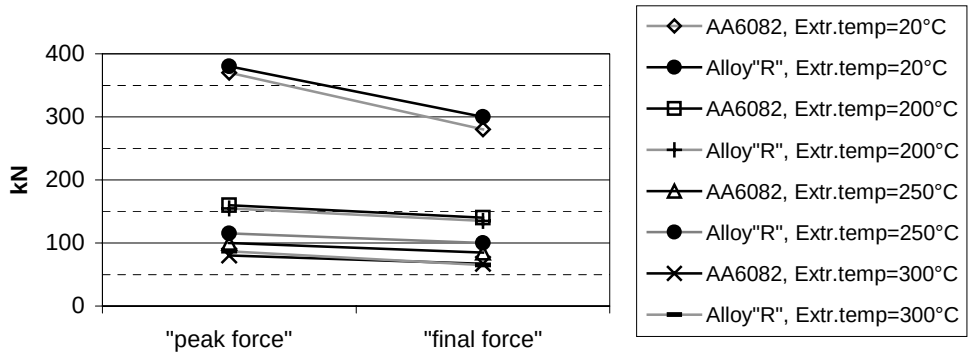

Figure 5.7 *Ram force as a function of Mn-content and extrusion temperature.*
Extrusion ratio R=2.1 (true strain= 0.8)

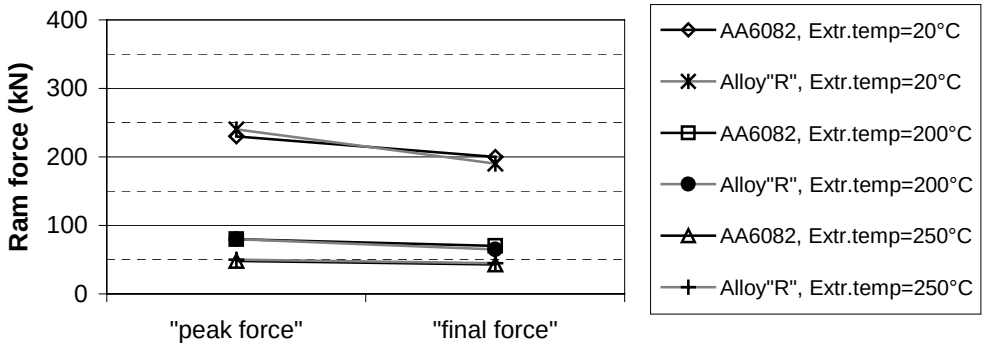

Figure 5.8 *Ram force as a function of Mn-content and extrusion temperature.*
Extrusion ratio R=1.4 (true strain= 0.4)

URN:NBN:no-2108

The force needed to perform the forward extrusion experiments was simulated in Forge2. The result is shown in Figure 4.5.12 and Fig. 4.5.13. The drop in ram force as deformation temperature increases is easily observed. Also, the same relationship between the "peak force" and the "final force" is found. The simulated values do not correspond very well to the experimental values. It is obvious that some parameters in the model are not related to the real experiments in a proper way. Also, it is difficult to cover friction effect during the press. Also the temperature in the test piece may differ from the assumed test temperature.

Another way of discussing the results is to convert true strain values and deformation parameters to the Zener-Hollomon parameter. The results obtained here may then be more easily compared to other published results. In Table 5.1, the Zener –Hollomon values for these experiments are calculated due to Equation 2-5 in Chapter 2.4.3. Data for room temperature testing is not included because the Zener-Hollomon parameter should not be used below approximately 200°C, as a rule of thumb.

Table 5.1 Estimating Zener-Hollom value -Z.

Die diameter (mm)	Extruding temperature (°C)	Z	Ln (Z)
19.5	200	$1.8 * 10^{19}$	44.3
19.5	250	$2.8 * 10^{17}$	40.2
19.5	300	$9.3 * 10^{15}$	36.8
24.0	200	$1.3 * 10^{19}$	44
24.0	250	$2.1 * 10^{17}$	39.9
24.0	300	$7.0 * 10^{15}$	36.5

The data from Figure 5.7 is shown in Figure 5.9, and the data from Figure 5.8 is given in Figure 5.10. The figures show an almost linear relationship between the Zener-Hollomon value and the true stress value in both figures. Despite of only a few Z-values, this assumption is made.

URN:NBN:no-2108

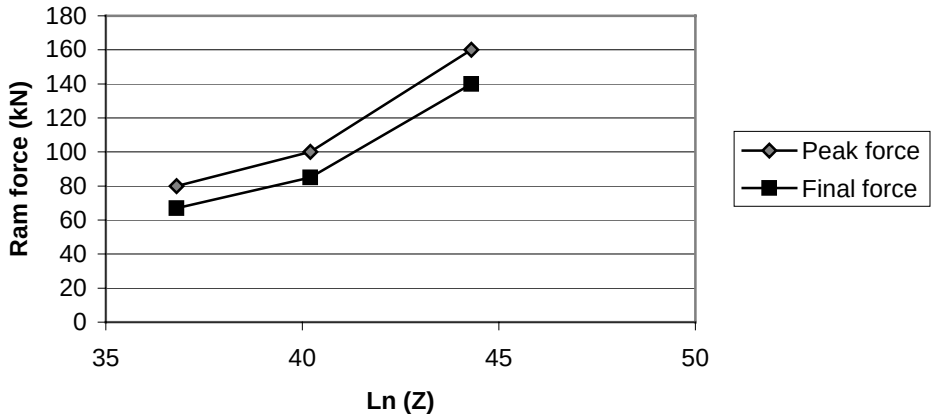

Figure 5.9 *Ram force as a function of ln (Z).*
Extruding temp.: 200°C, 250°C and 300°C.
AA6082, reduction ratio=2.1,
see Table 5.1 for Z-values.

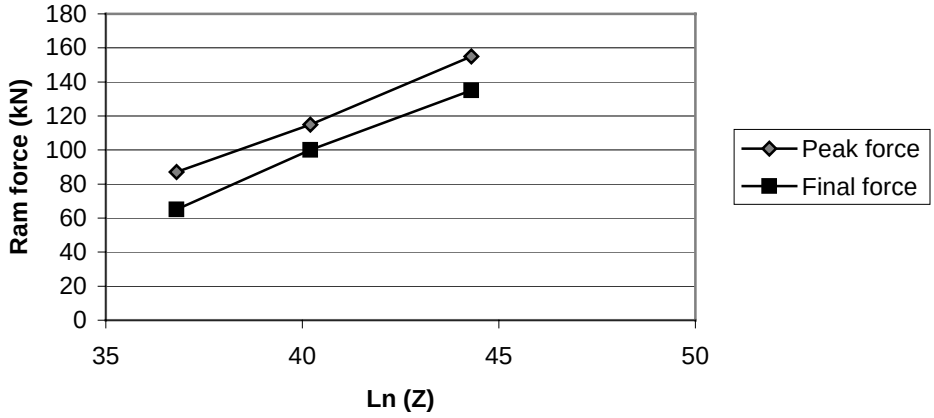

Figure 5.10 *Ram force as a function of ln (Z).*
Extruding temp.: 200°C, 250°C and 300°C.
Alloy "R", reduction ratio=2.1,
see Table 5.1 for Z-values.

In Figure 5.11, the data from Figure 5.7 and Figure 5.8 are compared. Also the experimental data from the smallest reduction ratio can be seen in this figure. The latter data with R=1.4, has a gradient that seems to be approximately the same as for the results from the die with R=2.1.

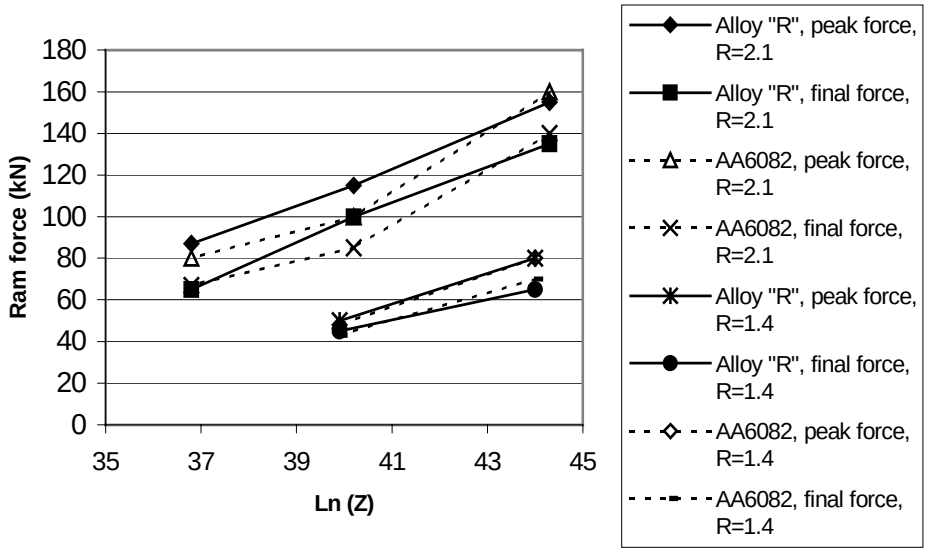

Figure 5.11 *Ram force as a function of ln (Z). Alloy "R" and AA6082, reduction ratio, R=2.1, and R=1.4. See Table 5.1 for Z-values.*

URN:NBN:no-2108

5.4 Forge2D – Numeric Simulations

5.4.1 General:

Forge2D might be a powerful tool to describe changes that take place in the microstructure during forming operations. But a lot of decisions have to be made by the user in order to perform simulations that describe the given deformation process as correct as possible.

The values of all the parameters in the material model have to be correct according to different process parameters, material type, material condition and lubrication conditions. Equation 2.1 gives the formula that describes the balancing of forces on every single element. The effect from "β", deformation temperature and strain hardening is given in equation 2.2. "K_0" is indicating the force level, "β" is connected to material softening as the temperature is raised. "n" is the strain-hardening coefficient. The material law used in the calculations is based on von Mice's criteria for material flow.

5.4.2 The "mesh size":

In the centre of the test piece the deformation mode is quite simple. As a single material element that is located in this position is analysed, one can see that it is deformed by pure compression. Closer to the surface, one observes that shear forces from friction creates a complex deformation mode as shown in Figure 5.12.

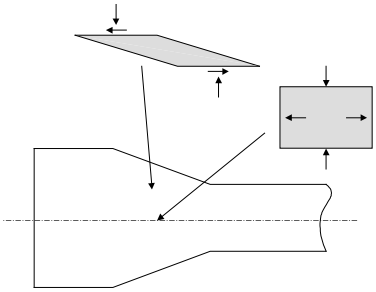

Figure 5.12 *Sketch of the forward extrusion process. Forces acting on a single material element due to the location of the element.*

One of the parameters one has to select when performing simulations in the Forge2 programme is the mesh size. The finer mesh, the more accurate calculations are given. This also implies a significant raise in the calculation time needed. One has to find a compromise where the result is detailed enough for the desired purpose. For the numeric simulations performed in this work, it would have been desirable to have an even finer mesh than the one that was applied. This is mainly based on the need to study deformation effects close to the surface of the extruded test piece. As a compromise between the computer possibilities and the accuracy of the simulations, the geometry and the accuracy of the mesh was as shown in Figure 5.13. In the area close to the surface and close to the part of the die where the diameter is reduced, the mesh size was relatively fine. This was done in order to capture most of the changes that takes place in this area of the extruded test piece. Close to the centre of the bolt, the mesh is relatively coarse as the material flow is not that complex in this area.

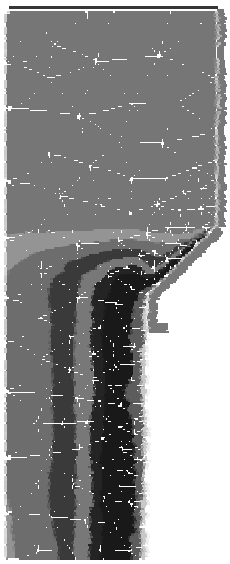

Figure 5.13 *Illustration of the mesh used for the numeric simulation.*

In the present work, some undesirable effects from areas with “too coarse mesh size” can bee seen in figure 4.5.3, 4.5.5, and 4.5.6. In the latter figure, the colour that describes strain rates between 2.0 and 3.0 indicates that for two deformation temperatures, the strain rate decreases from the surface to the centre of the extruded test piece. In the centre it seems to increase again. One has to conclude that because there are few notch points in the mesh in this region, the calculation in each notch point are influenced by the neighbouring notch points. There are in fact no reasons to assume that the material to flow slowly in a zone between the middle and the centre of the bolt.
For the extruded test piece that was deformed at 200°C (see figure 4.5.5), the pattern that illustrates the true strain distribution might seem a little irregular. This is only an effect from the computer calculation process and is related to the applied mesh size. As there are no reasons for this pattern to occur, average values are chosen in order to illustrate the true strain distribution. This kind of irregularity in the computer calculated pattern can also be seen in figure 4.5.3.

As an overall conclusion after evaluating the effect of the mesh size, it appears that the chosen notch point dispersion has given numeric simulation results that give an acceptable resolution and information of the size and distribution of the strain in the present this work.

5.4.3 Simulated true strain over a cross section:

Figure 4.5.1 shows how true strain varies on the cross section of the deformed test piece. It is not found any effect of variation in deformation temperature on the results obtained by the numeric simulations. No significant change in values of the true strain is observed as spots located at the same distance from the surface is compared for different deformation temperatures in the interval 20°C to 300°C. This observation is made for extruded test pieces deformed to the same reduction ratio. This result should be compared to Figure 4.4.3. Here investigations on a cross section of the AA6082 are shown. The radial grain size and the radial subgrain size are plotted as a function of the distance from the surface for two different

deformation temperatures (200°C and 300°C). One observes that both the grain diameter and the subgrain diameter are only marginally affected by the deformation temperature when measured at the same distance from the surface of the test specimen. A slight tendency for coarser grains for the higher deformation temperature can be seen. These results are, however, in accordance with results obtained at different deformation temperatures in Forge2D. As true train describes the amount of stored energy due to deformation alone, this is an expected observation.

As shown in figure 4.4.3, the variation in grain size increases initially and levels out when approaching the centre. The variation in subgrain size has an exponentially shaped curve.

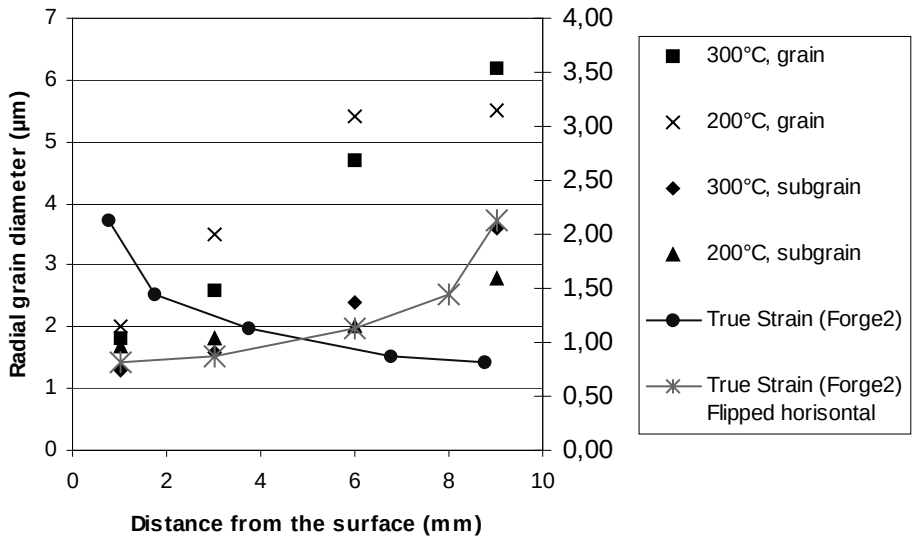

Figure 5.14 *True strain values from the numeric simulation performed in Forge2D as shown in Figure 4.5.1. These data are compared to the subgrain size and the grain size from figure 4.4.3 Also the true strain data from the numeric simulations are flipped horizontally.*

URN:NBN:no-2108

In Figure 5.14 the true strain as a function of the distance from the surface as obtained by Forge2 simulations is plotted. These data are also plotted as they are flipped horizontally at a distance from the surface equal to 4,875 (half the distance from the surface to the centre of the bolt). In addition, the data from figure 4.4.3 is plotted in this figure. The exponential shape of the curve that describes the flipped simulated true strain values matches very well with the slope that describes the evolution of the subgrain size as a function of the distance from the surface. The correlation between grain size and true strain does not match equally well. Also the results from the recrystallized material in figure 4.7.1 have the same exponential shape. From these observations, we can conclude that the subgrain size more than the grain size describes the amount of stored energy in the material after deformation. This can be seen by comparing the deformed and the recrystallized grain/subgrain data. By taking also the Forge2 simulations into account, the tendency is intensified.

In Figure 4.7.1, the recrystallized grain size in the AA6082 is shown. The grain diameter in the radial direction and the extrusion direction is shown as a function of the distance from the bolt surface. In Figure 5.15 these data are compared to the results from the numeric simulations that are shown in Figure 4.5.1. The true strain data from the numeric simulations are in this figure also plotted as they are flipped horizontally at a distance from the surface equal to 4,875 (half the distance from the surface to the centre of the bolt). In the diagram to the left in Figure 5.15, the scale for each of the y-axis are adjusted to show how the horizontally flipped simulated true strain data from Forge2D compares to the recrystallized grain size in the extrusion direction. This is shown for the extruded test piece deformed at 300°C. As can be seen from Figure 5.15, the slope of the curves matches almost perfect. In the diagram to the right, the y-axis is adjusted to show how the horizontally flipped simulated true strain values matches the grain diameter in the radial direction in the test piece that was deformed at 20°C. The slope of the curves matches very well also in this case.

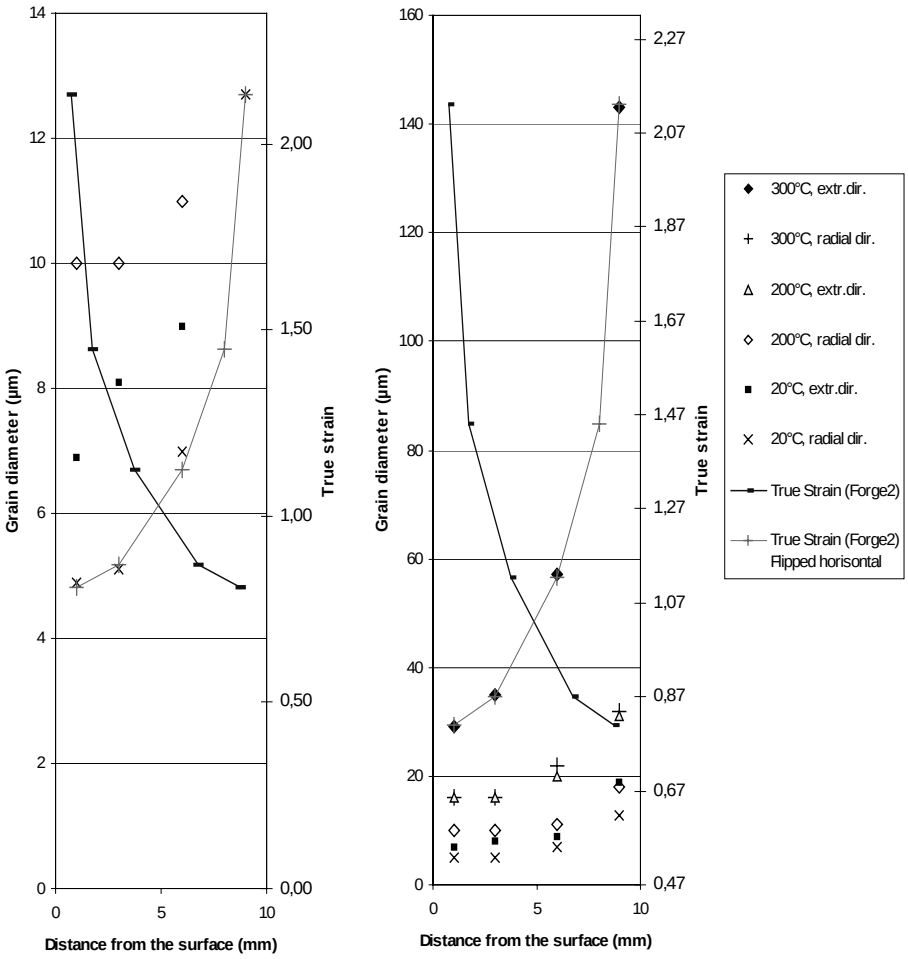

Figure 5.15 *True strain values from the numeric simulations versus recrystallized grain diameter in the extrusion direction and in the radial direction for the AA6082, R=2.1.*
Data from Figure 4.7.1 and Figure 4.5.1 are compared. The simulated data for true strain are also shown as they are flipped horizontally
The two diagrams contains the same data, but the scaling is different. From this, the results from the numeric simulations are compared to recrystallized grain size in the material deformed at high temperature and at room temperature separately.

URN:NBN:no-2108

These observations gives valuable information about the numeric simulation performed in Forge2 as well as the true material behaviour during deformation. Also, since recrystallization data are used in the comparison, the diagram connects true strain data in deformed material to recrystallization mechanisms. As Figure 5.15 shows, there is a strong connection between the true strain values and the recrystallized grain size both in the radial and the extrusion direction. The driving force for recrystallization of the billet is the stored energy in the material. The amount of stored energy decreases as one moves from the surface to the middle of the extruded test piece. This is based on the investigation of the recrystallized structure that is coarser in the middle and finer close to the surface. The probability for a dislocation free grain to nucleate and grow is much higher close to the surface because of the amount of stored energy in this region compared to the central part. During the annealing process, nucleation of recrystallized grains takes place on a huge number of heterogeneities. Thus true strain increases significantly close to the surface, and this indicates that also the amount of stored energy increases in this region. The slope of the recrystallized grain size curve (experimental values) and the slope that is based on simulated values for true strain have almost identical shape. The following conclusions can thus be drawn:

- The material behaviour during the forward extrusion process has been successfully simulated by the Forge2 program.
- In the simulation, the true strain values increases from the centre of the extruded test piece to the surface. This is a most likely variation. It is, however, impossible to find the correct value of the level of the true strain data. Anyway, the numeric simulated true train value is approximately 0.8 in the middle of the extruded material, and this is close to the correct value.
- The recrystallized grain size is related to the amount of stored energy in the material in a very convincing way.
- The recrystallized grain diameter is related to the amount stored energy in both the radial and the extrusion direction. This means that the grain growth in both directions is limited by the amount of stored energy.

Formula:

As described in chapter 2.9, the rheology module describes the behaviour of the material during deformation. This is based on the following tensorial form of the Norton-Hoff behaviour law:

$$\sigma_0 = (\sqrt{3})^{m+1} \cdot K \cdot \dot{\bar{\varepsilon}}^m \cdot \bar{\varepsilon}^n \cdot \exp\left(\frac{\beta}{T}\right) \qquad \textbf{(Equation 5-4)}$$

For every deformation temperature, the materials parameters have to be determined. In order to do this, compression tests were carried out in the MTS-machine. The test temperature and ram speed variation is given in Table 5.2. The number of parallels was limited to three due to limitations in test material at this point of the work.

Table 5.2 Compression test.

Deformation temperature	Ram speed (mm/s)		
20°C	1	100	250
200°C	1	100	250
250°C	1	100	250
300°C	1	100	250

Effect of friction:

Higher friction leads to higher maximum strain and the strain drops as the distance from the surface increases. The centre part of the extruded bolt with a true strain value of approximately 0.8 is broader at higher friction.
Also, the maximum temperature increases with increasing friction.

URN:NBN:no-2108

5.5 Hardness measurements

Hardness measurements were performed on the profile after 1 month storage at room temperature. During this time the material had reached maximum hardness as a result of aging. Also one undeformed extruded test specimen with the same heat treatment was measured.

As can be seen from the following figures, the hardness in the centre of the undeformed test specimen were approximately the same as for the test specimen that was deformed at the highest temperature. Deformation at lower temperatures resulted in increasing hardness. These results indicate that the age hardening potential in the extruded test specimen decreases as the deformation temperatures increases.
The hardness data is similar for both the AA6082 and the Alloy R, and this indicates that the Mn content has no significant effect on the strength of the material.

Hardness measurements are performed close to the surface and in the central part of the extruded test piece of both alloys and for all deformation temperatures. The hardness values in the centre versus close to the surface are very similar for deformation at elevated temperatures for both alloys. For extrusion at room temperature, the hardness close to the surface is somewhat higher. From this, it is obvious that the temperature in the material due to friction at forming at room temperature has not been high enough to lead to an efficient recovery reaction in the material.

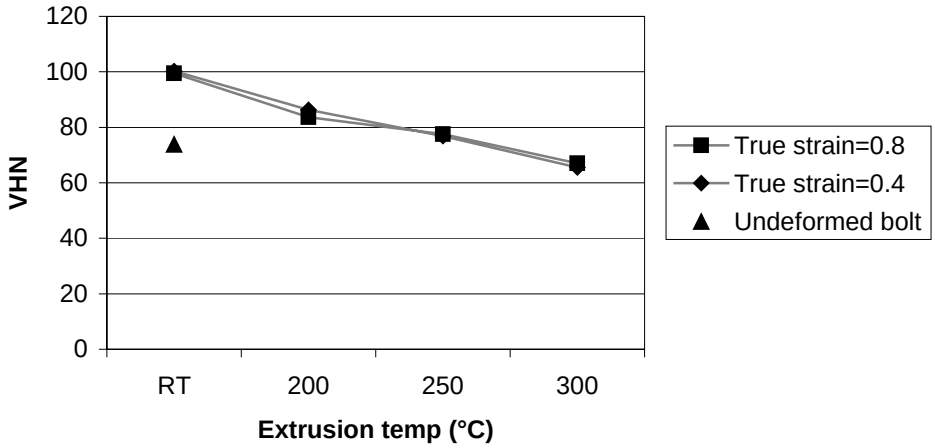

Figure 5.16 *AA6082.*
VHN measured in centre of extruded bolt.
Both deformation ratios.
All deformation temperatures.

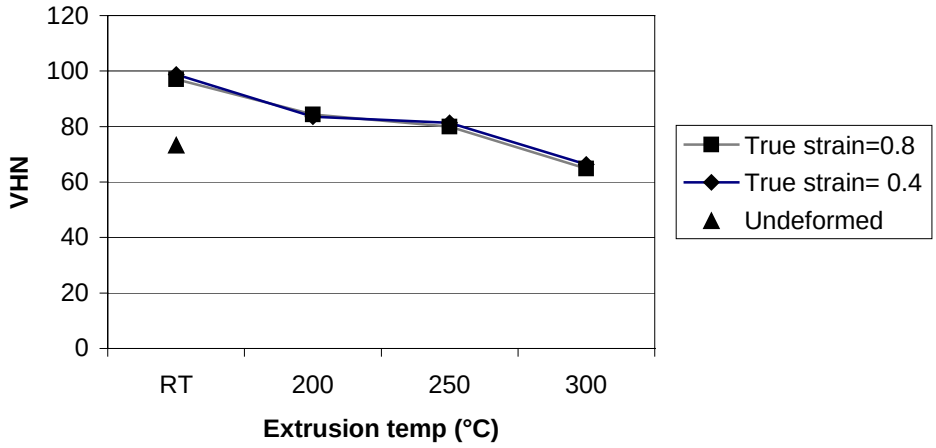

Figure 5.17 *Alloy "R".*
VHN measured in centre of extruded bolt.
Both deformation ratios.
All deformation temperatures.

URN:NBN:no-2108

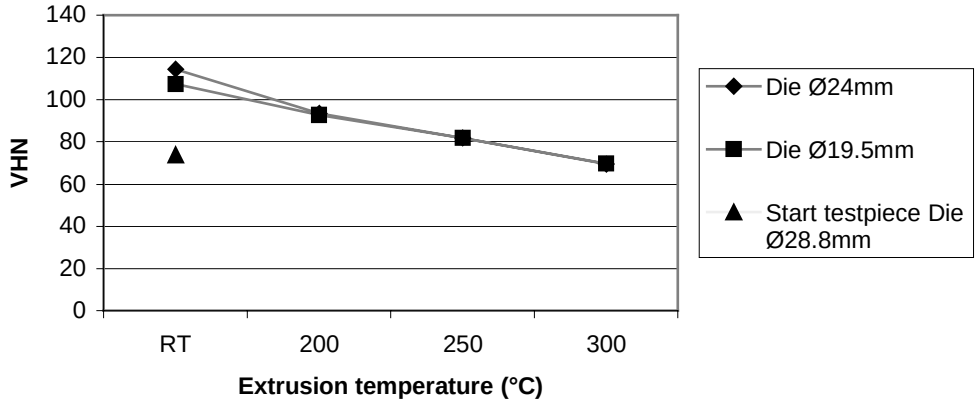

Figure 5.18 *AA6082.*
VHN measured 1 mm from surface of extruded bolt.
Both deformation ratios.
All deformation temperatures.

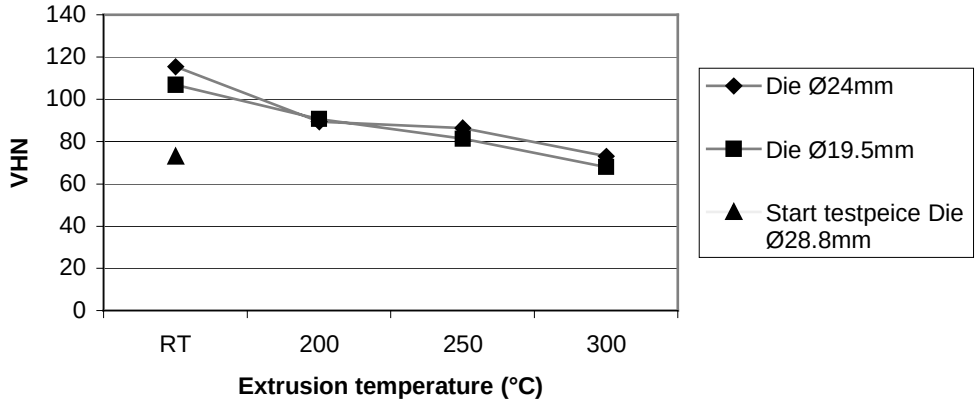

Figure 5.19 *Alloy "R".*
VHN measured 1 mm from surface of extruded bolt.
Both deformation ratios.
All deformation temperatures.

5.6 Recrystallization

In Figure 5.20 and Figure 5.21, the recrystallization data for the centre areas from Figure 4.6.3, 4.6.4, 4.6.5 and 4.6.6 are compared. As can be seen, the coarsest recrystallized grains are found in the "Alloy R, which does not have Mn-containing dispersoids. The effect from the Mn-addition on the recrystallized grain size is hence determined.

The smallest recrystallized grains in both alloys are found for the highest reduction ratio, and for the lowest deformation temperature. These observations clearly indicate the relationship between the stored energy in the material after deformation and the critical energy needed for a dislocation free grain to nucleate and grow. The more the material is deformed, the more energy is stored in the microstructure due to formation and pinning of dislocations. This effect is intensified as the deformation temperature is lowered. It then reduces the mobility of the dislocations in the crystal structure.

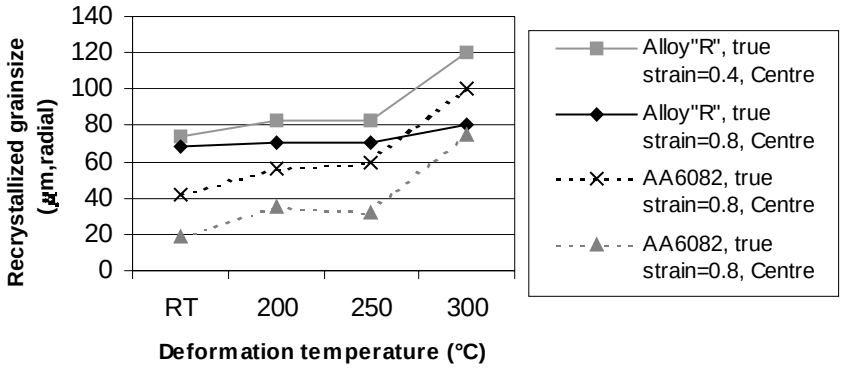

Figure 5.20 *Recrystallized grain size versus deformation temperature in centre of bolt.*
AA6082 and Alloy "R" at both reduction ratios.

URN:NBN:no-2108

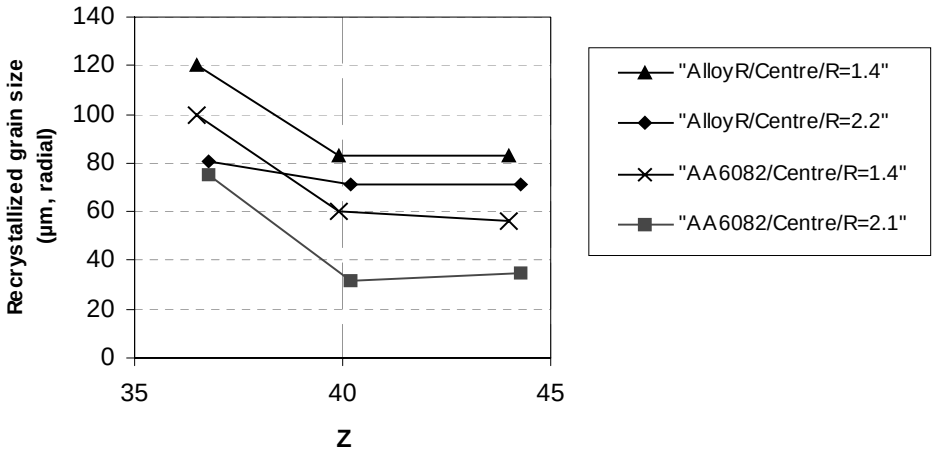

Figure 5.21 *The same data as shown in Figure 5.20. Shows the relation between the recrystallized grain size and the Zener-Hollomon parameter, Z.*

In Figure 5.22 the recrystallization data for the areas close to the surface from Figure 4.6.3, 4.6.4, 4.6.5 and 4.6.6 are compared. Three conclusions are based on the observations in Figure 5.22:

- Within each separate alloy, the test specimen with the smallest reduction ratio has slightly larger grains than the one with the highest reduction ratio. This result is due to the increased amount stored energy in the material that has been given the largest degree of deformation.
- The recrystallized grain size in the Alloy “R” is significant larger than in the AA6082 at comparable deformation parameters. This result is due to the effect of Mn-containing dispersoids in the AA6082.
- The recrystallized grain size in the Alloy “R” seems to be unaffected by the deformation temperature after annealing for 15 minutes. The observation of the AA6082 is quite different. A small increase in grain size is observed for both reduction ratios as the deformation temperature is elevated from 20°C to 200°C and further to 250°C. At extrusion temperatures of 300°C the recrystallized grains are

significant larger. This observation has been related to the reduction in stored energy in the material as deformation temperature increases.

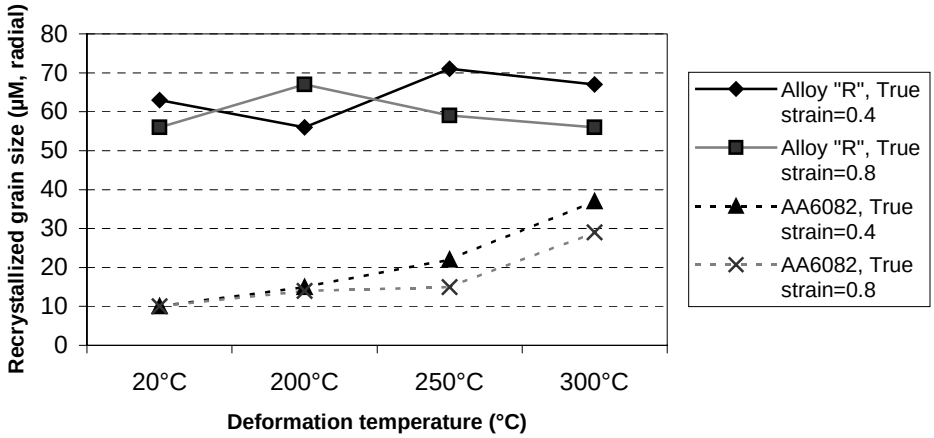

Figure 5.22 *Recrystallized grain size versus deformation temperature close to the surface (approximately 1-2 mm from the surface). AA6082 and Alloy "R" at both reduction ratios.*

The shape of recrystallized grains as a function of the deformation temperature: As shown in Figure 4.7.2, the recrystallized grains in the AA6082 are slightly elongated close to the surface. The effect from variations in the deformation temperature is insignificant at this location. For the test pieces that were extruded at 200°C and lower temperatures, the shape of the recrystallized grains were almost identical though the entire material thickness. For the material that was deformed at 300°C, a noticeable change took place. The grains became gradually more elongated the closer to the centre of the bolt the measurements were performed. It is believed that this is due to the amount of stored energy from the forward extrusion process. As deformation at 300°C probably implies significant lower stored energy in the material than at deformation at 200°C, the critical energy for nucleation of new dislocation free grains is higher. Also, the critical radius for a heterogeneity to act as a potential nucleation site is

URN:NBN:no-2108

larger. The conclusion to these considerations is that after deformation at 300°C the number of potential nucleation sites is reduced. As can be seen from Figure 4.7.1 the grain size in the radial direction is quite similar for all deformation temperatures. This observation indicates that the traces of coarse heterogeneities in the radial direction act as sites for nucleation at all temperatures. It also indicates that several heterogeneities in these traces are smaller than the critical size to act as potential sites for nucleation at the highest deformation temperature.

The recrystallized grain size as a function of the distance from centre of the extruded material: For all investigated specimen, the recrystallized grain size increases from the surface to the centre. These observations describe a decreasing amount of stored energy in the middle of the test piece. Even though attempts have been made to minimize friction, the die will introduce shear forces in the closest part of the extruded material.

Limits for recrystallization:
It is shown in Figure 4.8.1 that the AA6082 with a reduction ratio R=2.1/ deformed at 250°C, recrystallizes through the entire material thickness for all annealing temperatures above 430°C. As the reduction ratio,R=1.4, this is no longer valid. Figure 4.8.2 illustrates that in order to achieve a fully recrystallized test piece, the temperature is between 430°C and 530°C. The material has a recrystallized structure approximately 6.5 mm from the surface. Taken into consideration the fact that the numeric simulations in Forge2 indicates a uniform value of true strain for approximately half the material thickness, it is suggested that the annealing temperature that leads to a fully recrystallized extruded test piece is close to 430°C.

Figure 4.8.3 and Figure 4.8.4 show recrystallization in extruded test specimen as they are annealed at 430°C for 15 minutes. For the material with reduction ratio R=2.1, only the specimen that was deformed at 300°C is not fully recrystallized. Only an inner radius of approximately 3mm remains “as deformed”. From the annealing experiments that were performed at the material with reduction ratio R=1.4, an interesting conclusion is drawn: Changing the deformation temperature from 200°C to 250°C does not affect the amount of stored energy in the material significantly. The recrystallized microstructure reaches approximately 7 mm into the material from the surface for each specimen. When performing the deformation at 300°C, the amount of stored energy is significant lower, and only the outer 3.5mm of the material is recrystallized.

5.7 Texture evolution

Texture measurements in the form of ODFs are given in Figure 4.3.3 - 4.3.4, Figure 4.3.7 – 4.3.8 and Figure 4.4.4 – 4.4.5. It is very important to be aware of the limited number of grains that is the basis for the formation of the ODFs. The results given in the above-mentioned figures thus only acts as indications on the qualitative texture in each specimen.

As the deformation temperature is increased from 20°C to 200°C and further to 300°C, there are no observations that indicate an influence from temperature variations the texture development. This is evident for both alloys. With more accurate measurements, one might expect that an increase in temperature would lead to a stronger texture for the material. Also no observations indicate that increasing the true strain (ε) from 0.4 to 0.8 leads to a change in the texture.

One significant difference between the texture in the two alloys AA6082 and the Alloy R is observed. In the AA6082, the main texture components are cube-oriented grains that are rotated around the <100> direction and the <111> direction. These texture components are common in non-recrystallized extruded materials. Material deformed in this process has no well-defined transversal direction. In the Alloy R, the same texture components are not found to dominate the global texture. Only the <100> texture is found to dominate here. The only difference between the two alloys are the Mn-containing dispersoids and hence the recrystallized microstructure. The recrystallized material from the forward extrusion of the billet is deformed further through forward extrusion in this project. The reduction ratio is limited to a maximum of R=2.1, and it is not observed any significant changes in texture from this process. Therefore, the cause for the difference in texture between the AA6082 and the Alloy R is believed to be the nucleation of recrystallized grains on the microstructure that has been deformed through the forward extrusion of the billet. The nucleation process of recrystallized grains through the forward extrusion at approximately 530°C is complex- Vatne and Johansen have pointed out through their experimental investigations of deformation structures that the <100> texture component had a larger subgrain size and a lower amount of stored energy than the <111> component. This explains the <100> recrystallization texture

as this substructure configuration provides enhanced nucleation and growth of the <100> oriented grains into the <111> texture components during recrystallization.

5.8 Some Comments to the EBSP measurements.

EBSP is a powerful technique in order to investigate microstructures at large investigations. But even though the software offers a lot of analysing possibilities, care should be taken to avoid errors as a result of wrong settings.

Orientation: The specimen has been aligned parallel to particle traces in the electron microscope. As the specimen is heavily tilted (70°), it was sometimes difficult to align the specimen due to the traces of coarse particles. The orientation of traces on a very small scale may also be affected by grain boundaries. This leaves a possibility of a small misorientation of the cross-section in the longitudinal direction.

Statistics: Due to the limited number of grains, -especially of recrystallized structures, the results are only indications of the real grain size. All measurements are performed at several cross-sections, in order to eliminate this error.

Refining of the data: There are several options in order to perform refining of the results when using the software. There will always be spots and areas where the software has failed in determining the exact orientation. These spots are saved without any orientation data. There are many possible reasons for this: Particles, distorted areas surrounding the particles, preparation faults in the surface, other surface defects.
In this work, seven of the closest neighbouring spots, have been compared to give the spot in the centre an expected orientation. If the spot does not have as much as seven neighbouring spots with given orientation, it will not be given an orientation. The process has been repeated by using six neighbouring grains, then five and finally four neighbouring grains with a defined orientation. This has resulted in well-defined high angle and low angle grains to determine subgrain sizes and grain sizes in the investigations in this project.

6. CONCLUSIONS

The main conclusions that can be drawn from the investigations performed in this work are:

Stress-strain relationship found from compression testing experiments:

- None of the alloys AA6063 or Alloy "R" reaches a steady state condition as true strain approaches 0.8 for deformation temperatures between 200°C and 250°C. At compression test performed at 300°C, the alloy "R" reaches steady state condition at a true strain equal to 0.4.
- As true stress-true strain relationship is investigated for the "Alloy R" and the AA6063 at comparable deformation parameters, it is shown that the alloy "R" with the highest Si-content requires the highest true stress for a given true strain value (AA6063: 0.45wt%Si, Alloy "R": 0.87wt%Si).
- The effect from Mn on the true strain-true stress relationship in the AA6082 is determined by investigations performed on the AA6082 and the Alloy "R". At the same deformation temperature, the true stress for the two different alloys reaches the same value after a certain amount of deformation. As deformation temperature increases, this common value of true stress corresponds to a decrease in true strain.
- No significant effect from changing the ram speed during compression testing of the Alloy "R" at room –temperature or at 300°C was observed. The ram speed was in the range 1mm/s – 250mm/s.
- The alloy "R" has been investigated in order to study the effect of different heat treatment conditions. For every deformation temperature, the highest true stress is connected to the T4 temper, and the lowest true stress value is connected to the W-temper. For the test that was performed at room temperature, the difference is significant (almost 100 MPa), but for the higher deformation temperatures, there is only a small difference in the true stress value.

URN:NBN:no-2108

Stress-strain relationship determined from forward extrusion experiments:

The following conclusions are valid for the AA6082 and the Alloy "R".

- Both "the peak force" and the "final force" decrease with increasing deformation temperature. The difference in ram force is significant as the deformation temperature is increased from room temperature to 200°C. For testing at higher temperatures, only small reductions in ram force are observed compared to the data obtained for 200°C.
- The difference between "the peak force" and the "final force" is decreased at higher deformation temperatures. At room temperature testing there is a difference of almost 100kN. At 200°C the "final force" is slightly lower than the "peak force", and for testing at 250° and 300°C they are almost identical.
- When comparing the two alloys, one observes that for the same deformation temperature and for the same die diameters, the ram force is the identical. It is worth noting that these alloys did not show the same relationship during the compression testing at low values of true strain (<0.8). On a microscopic scale, one concludes that Mn has no significant effect on the stress strain relationship for the applied deformation parameters during deformation in the forward extrusion process.
- Hardness measurements indicate that the age hardening potential in the extruded test specimen decreases as the deformation temperature increases.
- The hardness data is similar for both the AA6082 and the Alloy R, thus indicating that the Mn content has no significant effect on the strength of the material.

Recrystallization of AA6082 and the alloy "R":

- Within each separate alloy, the test specimen with the smallest reduction ratio has slightly larger recrystallized grains than the one with the highest reduction ratio.
- The recrystallized grain size in the Alloy "R" is significant larger than in the AA6082 at comparable deformation parameters after

annealing at 530°C for 15 minutes. This result is due to the effect of Mn-containing dispersoids in the AA6082.

- The recrystallized grain size in the Alloy "R" seems to be unaffected by the deformation temperature after annealing for 15 minutes. The observation of the AA6082 is quite different. A small increase in grain size is observed for both reduction ratios as the deformation temperature is elevated from 20°C to 200°C and further to 250°C. At extrusion temperatures of 300°C the recrystallized grains are significant larger.
- Annealing performed at 530°C to a fully recrystallized microstructure in the forward extruded AA6082 leads to elongated recrystallized grains in the extrusion direction in the material deformed at the highest temperature.
- For all investigated specimen, the recrystallized grain size increases from the surface to the centre.
- Annealing experiments performed at 430°C on the AA6082, indicates that a change in the deformation temperature from 200°C to 250°C does not affect the amount of stored energy in the material significantly.

Numeric simulations performed in Forge2:

- The material behaviour during the forward extrusion process has been successfully simulated by the use of the Forge2 program.
- In the numeric simulations, the true strain values increases from the centre of the extruded test piece to the surface. This is a most likely variation.
- As the simulated true strain values are compared to the grain size in the annealed material, the recrystallized grain size is related to the simulated true strain (amount of stored energy) in the material in a very convincing way.
- It is also shown that the recrystallized grain diameter is related to the simulated true strain as the grain diameter is investigated in the radial and the extrusion direction separately.

URN:NBN:no-2108

7 REFERENCES

Altenpohl, D., *Aluminum and aluminum alloys*, Berlin/ Gøttingen/Heidelberg/New York, Springer 1965

Alloy Digest, Inc, FC:Al-320, AA6063, 1991

Ayres, R.A., Metallurgical transactions A, volume 10A, July 1979, p. 849-854.

Dieter, G.E.,Mechanical Metallurgy, 1988, p.287-292

Forge2® V2.4, User Manual

Furu, T., Ørsund, R., Nes, E.,Acta. Met. Mater., 43, (1995), p.2209-2232.

Hulley S.I. and Lorimer, G.W, *The effect of dispersoids on the recrystallization behavior of a series of Al-Mg-Si-alloys*, The 3rd International Conference on Aluminium Alloys, 1992.

Humphreys, F.J., Acta Metall, 25, 1977, p.1323.

Humphreys, F.J. and Hatherly, M. , *Recrystallization and related annealing phenomena*, Pergamon, Oxford, 1996.

Humphreys, J., *Evolution of deformation microstructure*, The 5th International Summer School on Aluminium Alloy Technology, Trondheim, Norway, Aug.16th –20th, 1999

Jacobs, M.H., *Precipitation hardening*, TALAT Lecture 1204, European Aluminium Association, 1999, p.24-35.

URN:NBN:no-2108

Jensrud, O., Pedersen, K., *Cold forging of high strength aluminium alloys and the development of new thermomechanical processing*, Journal of Materials Processing Technology 80-81, 1998, p.156-160

Lang, G. and Castle, A.F., *Influence of Copper, manganese and chromium additions on the extrudability of AlMgSi-Alloys*, BR, D61, p293-296

Lange, K., Handbook of metal forming, Hot Extrusion, Chpt.16, 1985

Latkowski, A. and Stec, Z., *The effect of extrusion temperature and manganese content on structure and properties of the AlMgSiMn alloy*, Aluminium, Jahrg.60, Vol.8, 1984, p.606-609

Laue, K., Extrusion –processes, machinery, tooling, American Society of Metals, Ohio, 1981, p.136

Lodgaard, L., *The precipitation of dispersoids containing Mn and/or Cr in Al-Mg-Si Alloys Lodgaard*, Part IIIa: Lodgaard, L. and Ryum, Thesis, NTNU, 2000, p. 37-54

Lohne, O. and Dons, A.L., *Quench sensitivity in AlMnSi-alloys containing Mn or Cr*, Scandinavian Journal of Metallurgy, Vol 12, 1983, p.34

Lorimer, G.C., *Precipitation in Aluminium Alloys, Precipitation Processes in solids*, Proceedings at the 1976 TMS Fall Meeting, New York, September 20-21, 1976, publication of AIME, p.107-109.

Marioara, C.D., Andersen, S.J. and Høier, R., *Overview of the precipitation sequence in a 6082 Aluminium alloy, A TEM study of the precipitates in a 6082 Al-Mg-Si Alloy System*, Thesis, NTNU, 2001

URN:NBN:no-2108

Marioara, C.D., Andersen, S.J., Jansen, J. and Zandbergen, H.W., *The influence of temperature and storage time at 200 on nucleation of ß''-phase in a 6082 Al-Mg-Si-alloy, A TEM study of the precipitates in a 6082 Al-Mg-Si Alloy System*, Thesis, NTNU, 2001

Metals Handbook, 8th edition, Vol.1, "*Properties and selection of metals*", The American Society For Metals, 1961, p. 888-889.

Nes, E., 8th international light metal congress, Leoben-Vienna, 1987

Nes, E. and Martinsen, K., *Modelling work hardening and stress saturation*, The 5th international summer school on aluminium alloy technology, Trondheim, 16th-20th august, 1999

Nes. E, Ryum, N. and Hunderi, O., *On the Zener drag*, Acta Metall., Vol.33, No.1, 1985, p.11-22

Nes, E., Dons, A.L., and Ryum, N., Proc. ISCMA6, 1982

Pedersen,K. and Ulseth, P., *Termomekaniske prosesser*, SINTEF report No. STF24 F98536, *Halvvarm forming*, 1997

Pettersen, T., Vatne H.E., Nes, E., *Modelling Recrystallization after different modes of deformation*, The 4th International Conf. on Recrystallization and related phenomena, The Japan Institute of metals, 1999.

Puchi et al., Int. Conference on thermomechanical processing of steels and other metals, Thermec-88, Vol. 2, Ed Imao Tamura, Iron Steel Inst., Japan, 1988, p. 572-579

Reiso, O., *Extrudability of high strength AlMgSi-alloys*, FSU report, 86-29/3-102, 1986

Sellars, C.M., *Annealing processes-recovery. recrystallization and grain growth*, Proc. 7th Risø National Laboratory, 1986, p. 167-187

Sellars, C.M., *Thermomechanical processing of aluminium alloys,* International summer school on aluminium alloy technology, Trondheim, July 1-5, 1991

Tundal, U., Brobak, T.J., Reiso, O., Hydro Aluminium Research Center, Sunndalsøra, Internal report, No.94-29/3-36, (1994)

Valle, R., *Conversion coatings as part of the lubrication system in cold forging of al-alloys,* NorFa Course, Aluminium Surface Technology- Surface Treatment and Corrosion, Semester Reports 1998-99, Dept. of Matr. Techn. and Electrochemistry, NTNU

Vatne, H.E. and Johansen, A., *Deformation and recrystallization textures in extruded cylindrical aluminium profiles.*

Vatne, H.E. and Hutchinson, B., *Evolution of textures during deformation and recrystallization,* The 5th international Summer school on Aluminium alloy technology, Trondheim, August 16th-20th, 1999

Wahl, D.V.d. and Dingley, D.J., Philips Electron Optics Bulletin 134, p. 19-25

Ørsund, R. and Nes, E., Scripta Met., Vol.22, 1988

URN:NBN:no-2108